VIRTUAL VIBRATION TESTING OF BODY AND POWER UNIT MOUNTED COMPONENTS (DIESEL ENGINE EGR COOLANT RAIL)

BY

SAMANEH ARABI



A thesis submitted to the College of Engineering and Physical Sciences of the University of Birmingham for the degree of

DOCTOR OF PHILOSOPHY

School of Mechanical Engineering

College of Engineering and Physical Sciences

The University of Birmingham

October 2015

UNIVERSITY OF
BIRMINGHAM

University of Birmingham Research Archive

e-theses repository

This unpublished thesis/dissertation is copyright of the author and/or third parties. The intellectual property rights of the author or third parties in respect of this work are as defined by The Copyright Designs and Patents Act 1988 or as modified by any successor legislation.

Any use made of information contained in this thesis/dissertation must be in accordance with that legislation and must be properly acknowledged. Further distribution or reproduction in any format is prohibited without the permission of the copyright holder.

VIRTUAL VIBRATION TESTING OF BODY AND POWER UNIT MOUNTED COMPONENTS (DIESEL ENGINE EGR COOLANT RAIL)

Samaneh Arabi

Supervised by

Dr Oluremi Olatunbosun

October 2015

UNIVERSITY OF BIRMINGHAM
Edgbaston, Birmingham, West Midlands B15 2TT, United Kingdom

Acknowledgement

In the first place, I would like to express my greatest gratitude to Dr Oluremi Olatunbosun for his supervision and guidance from the very early stage of this research as well as sharing his extraordinary experiences throughout the work. I would also like to give him my special thanks for trusting me and opening my eyes to the world of professionals and support me compassionately to grow up step-by-step in my educational and personal life.

Thanks to Dr Soo and professor Blundell who graciously agreed to be my examiners, and their feedback in the final stages of my degree were invaluable.

It is a pleasure to sincerely thank my senior colleagues, Dr Mohammad Behroozi, Dr Xiaoguang Yang , Dr Adebola Ogunoiki, and Shahriar for scientific discussions, giving valuable advices, and sharing brilliant ideas as well as being good friends in my personal life while living in Birmingham. I would like to extend my thanks to our technicians including Carl Hingley and Peter Thornton for their help during my experiment. Also, special thanks go to one of my best friends, Nasim , for helping me get through the difficult times, and for all the emotional support, camaraderie, entertainment, and caring she provided.

My parents and my sister deserve special mention for their continuous support and prayers. I thank my parents for their faith in me and allowing me to be as ambitious as I wanted. It was under their watchful eye that I gained so much drive and an ability to tackle challenges head on. Words fail me to express my appreciation to my husband Mohammad whose dedication, love and persistent confidence in me, has taken the load off my shoulder. I owe him for being unselfishly let his intelligence, passions, and ambitions collide with mine.

Abstract

As part of the development procedure for body and power unit mounted components, random vibration testing is carried out to original equipment manufacturer (OEM) specification which the components must survive without damage. With the current move to minimise design and development costs and time-scales in the development of new vehicles, the use of CAE to validate system design through the use of virtual testing is becoming ever more important. The availability of accurate CAE models will enable designs to be optimised before commitment to building prototypes. The desire is therefore to develop computer aided analysis/numerical techniques that will replicate the vibration testing of body and power unit mounted components.

The research demonstrates the development of numerical analysis to replicate the vibration testing of a Diesel Engine EGR (Exhaust Gas Recirculation) Coolant Rail. A Finite element (FE) model of the coolant rail was developed and validated. The CAE model shows less than 5% deviation of natural frequency from test results for all modes. Subsequently, detailed FE models of the rubber hoses were developed and added to the coolant rail model in order to perform a forced response analysis of the structure. The metal tube was characterised by its elasticity (Young's modulus) while the rubber material property was modelled using visco-hyperelastic constitutive equations. In order to check the validity of the simulation results, a test rig was designed and developed to replicate the rail's operating condition on the engine and a shaker was used to produce the unidirectional excitation from where the rail was mounted. Results from vibration tests of the structure indicated good agreement with the simulation results (less than 9% deviation in terms of natural frequency). A method was

proposed for estimating the elastic stiffness and damping introduced by the addition of the rubber hoses in the FE models of body and power unit mounted components using spring-dashpot elements. This was to avoid modelling the rubber hoses in detail with resultant significant savings in computational costs.

In this research, the influence of the fluid dynamics on the vibration of a mechanical structure is also presented. A Finite Element (FE) analysis was conducted to simulate the vibration behaviour of an EGR coolant rail consisting of a metal tube and rubber tubes at both ends of the metal tube with water inside it. The excitation was applied in the form of sine sweeps with progressive frequency in the range of 40 Hz to 800 Hz, which represents the frequency domain of the engine and road excitation. A precise dynamic implicit approach was used to implement a displacement-controlled analysis, applied from the engine mounted support. The correlation study suggests a close agreement (less than 10% of deviation of natural frequency for all the modes) between the test and simulation results in terms of the prediction of the natural frequencies. This analysis enables design engineers to extract the natural modes and frequencies of vibrating parts with flowing fluid in order to investigate the failure modes and redesign brackets, supports, and fittings for desired strength.

The ultimate aim of the virtual vibration testing is to enable engineers to predict the resonant frequencies and resonant modes of the structure in the presence of pressurised fluid which is flowing inside the coolant rail.

Table of Contents

Acknowledgement II
Abstract III
Table of Contents V
List of Figures VIII
List of Tables XI
List of Nomenclature XII
List of Abbreviations XIV
Chapter 1: Introduction 1
1.1. Introduction 2
1.2. Motivation 3
1.3. Research theme 4
1.4. Problem definition 7
1.5. Aims and objectives 9
1.6. Chapters summary 10
Chapter 2: Literature Review 12
2.1. Introduction 13
2.2. Vehicle noise and vibration 13
2.2.1 Source of vibration 14
2.2.2 Affected performance 17
2.2.3 Identification methods 18
2.3. Finite Element Modelling 20
2.4. Material modelling and testing 24
2.5. FSI co-simulation 25
2.6. Summary 26
Chapter 3: Material Modelling 28
3.1. Introduction 29
3.2. Material modelling of compounds 29
3.2.1 Steel Tube 30
3.2.1.1 Linear elasticity 30
3.2.1.2 Models for linear elasticity 31
3.2.2 Rubber hoses with reinforcement cords 32
3.2.2.1 Hyperelasticity 33

3.2.2.2 Viscoelasticity 47
3.3. Summary 58
Chapter 4: Vibration testing 60
4.1. Introduction 61
4.2. Forced vibration test 63
4.2.1 Test rig development 64
4.2.2 Excitation system 68
4.2.3 Sensing system 70
4.2.4 Data acquisition and analysis 74
4.2.4.1 Vibration parameters 76
4.2.4.2 The LABVIEW program 78
4.3. Free vibration test 81
4.4. Damping factor 83
4.5. Summary 84
Chapter 5: EGR Coolant Rail Finite Element Modelling 86
5.1. Introduction 87
5.2. Methodology development for FE modelling 89
5.2.1 Coolant rail geometry 89
5.2.2 Rubber Hose Reinforcement modelling 90
5.2.3 Vibration Analysis type 92
5.2.3.1 Eigenvalue extraction 92
5.2.3.2 Steady state dynamics-Modal 94
5.2.3.3 Base motions in modal-based procedures 97
5.2.4 Contact modelling 98
5.2.5 Meshing techniques 98
5.2.5.1 Linear Hexahedral Elements Results (C3D8, C3D8R, C3D8I) 102
5.2.5.2 Quadratic Hexahedral Elements Results (C3D20, C3D20R) 104
5.2.5.3 Tetrahedral Elements Results (C3D4, C3D10) 108
5.2.6 Boundary condition setup 110
5.3. Damping Simulation 110
5.3.1 Tube Damping: 110
5.3.2 Viscoelastic damping of rubber: 112
5.4. Simulation results and validation 112
5.4.1 Job solving strategy 113
5.4.2 Forced vibration analysis: Model#1 114

5.4.3 Forced vibration analysis: Model#2 118
5.4.4 Representation of rubber hoses (Model #3) 123
5.5. Summary 126
Chapter 6: Fluid Structural Interaction Vibration Analysis of the EGR Coolant Rail 128
6.1. Introduction 129
6.2. Methodology Definition 129
6.3. Theory and Terminology 130
6.3.1 Frequency Analysis approaches 130
6.3.2 Co-simulation 132
6.4. FE Simulation 132
6.5. Results and discussion 134
6.6. Summary 140
Chapter 7: Conclusion and Future Work 141
7.1. Conclusion 142
7.2. Future work 146
References 148
Appendix A: Scripts for FSI Analysis 166
A.1. Python script for generating the INP deck file 167
A.2. Python script for Post-Processing 167
A.3. Matlab Script to View/Export results 170
Appendix B: List of Publications 172

List of Figures

Figure 1.1. Engine Coolant rail system TDV6 3.oL Diesel (Jaguar Company, 2012).....2
Figure 1.2. EGR system 8
Figure 2.1. N&V category.....14
Figure 2.2. A meshed coolant rail with elements 21
Figure 3.1. Structure of a steel tube 30
Figure 3.2. Structure of a rubber hoses 32
Figure 3.3. Hyperelasticity in comparison with linear elasticity in tension and compression region 34
Figure 3.4. Tensile test machine to measure hyperelasticity 42
Figure 3.5. Rubber sample under tensile test.....43
Figure 3.6. rubber hose specimen 43
Figure 3.7. Uni-axial pre-conditioning test curves for rubber 44
Figure 3.8. Hyperelastic behaviour for rubber hoses 45
Figure 3.9. Prediction of hyperelastic behaviour using different models for rubber.....46
Figure 3.10. Viscoelasticity features of elastomers.....48
Figure 3.11. Instron Test Rig for Rubber Stress Relaxation Test 53
Figure 3.12. Normalized stress relaxation of rubber.....54
Figure 3.13. DMA test machine 56
Figure 3.14. Stress and strain vs. time t in dynamic loading of rubber 57
Figure 3.15.Rubber DMA test result.....58
Figure 4.1: Structure under test (Ole Dossing, 1988) 62
Figure 4.2: Schematic setup for forced vibration system.....64
Figure 4.3: Vibration test rigs and CAE models 66
Figure 4.4: The vibration test setup for model #1 67
Figure 4.5: The vibration test setup for model #2 68
Figure 4.6: A schematic of components in electromagnetic shaker (Lang & Snyder, 2001)...69
Figure 4.7: Ling Altec model 407 electromagnetic shaker 70
Figure 4.8: Impedance Head, Model 2110E.....71

Figure 4.9: Setup of sensors on the coolant rail 72
Figure 4.10: BERAN 700 series Amplifier 73
Figure 4.11: The schematic of data acquisition approach 75
Figure 4.12: An example of points of interest in EGR coolant rail 76
Figure 4.13: Block diagram of vibration test control/measurement 78
Figure 4.14: Flowchart of the data flow and procedure 79
Figure 4.15: Vibration test program 80
Figure 4.16: free- free vibration test set up 82
Figure 4.17: schematic setup for free- free vibration system 82
Figure 4.18: Half power bandwidth method 84
Figure 5.1: Procedures for FE simulation of EGR coolant rail 89
Figure 5.2. (a) Coolant rail without rubber hoses, model #1, (b) coolant rail with rubber hoses model #2 90
Figure 5.3: Rubber hose specimen 91
Figure 5.4: Frequency response of free test vibration 101
Figure 5.5 FE model of EGR coolant rail 101
Figure 5.6: Effect of mesh density with C3D8 elements 102
Figure 5.7: Influence of mesh density with C3D8R elements 103
Figure 5.8: Influence of mesh density with C3D8I elements 103
Figure 5.9: Effect of Increased C3D20 Mesh Density 104
Figure 5.10: Effect of Increased C3D20R Mesh Density 105
Figure 5.11: Mesh convergence for C3D20 106
Figure 5.12: Effect of mesh density on C3D10 and compare to C3D4 109
Figure 5.13: Comparison between hexagonal and tetragonal models 109
Figure 5.14: Boundary condition 110
Figure 5.15: Damping Ratio 112
Figure 5.16: Comparison between forced vibration simulation and test results of model #1 115
Figure 5.17: Comparison between forced vibration analysis and test results of model #1 (Transducer #B) 115
Figure 5.18: Comparison between forced vibration analysis and test results of model #1 (Transducer #C) 116

Figure 5.19: Mode shapes of forced vibration analysis of model #1 117
Figure 5.20: comparison between forced vibration simulation and test results of model #2 119
Figure 5.21: Comparison between forced vibration analysis and test results of model #2 (Transducer B).....119
Figure 5.22: Comparison between forced vibration analysis and test results of model #2 (Transducer A).....120
Figure 5.23: Mode shapes of forced vibration analysis of model #2 122
Figure 5.24: Maximum Von Mises stress of forced vibration analysis of model #2.....123
Figure 5.25: Schematic of SPRING-DASHPOT element.....124
Figure 5.26: Comparison between simulation and test results for coolant rail with rubber (Transducer A).....125
Figure 6.1: FSI vibration analysis process 133
Figure 6.2: Comparison between coolant rail FSI vibration analysis and test result at V~0 .135
Figure 6.3: Comparison between forced vibration simulation and test results.....136
Figure 6.4. Mode shapes of forced vibration analysis of FSI model.....137
Figure 6.5: A comparison between forced vibration analysis in model with water and without water.....138
Figure 6.6: A comparison between resonant frequencies in model with water and without water.....139
Figure 6.7: Effect of velocity of fluid flow on the first natural frequency of the coolant rail140

List of Tables

Table 3.1. Material Specification 32
Table 3.2. Hyperelastic models for incompressible rubber 38
Table 3.3. Tensile test machine specifications 42
Table 3.4. Yeoh model parameters 46
Table 3.5. Physical models of Viscoelasticity for rubber 50
Table 3.6. Viscoelastic Material Constants 54
Table 5.1: Reinforcement cord data 92
Table 5.2: FE Elements for vibration analysis 100
Table 5.3: The comparison between C3D20R model and experimental result 107
Table 5.4: Comparison between forced vibration simulation and test results of model #1.114
Table 5.5: Comparison between forced vibration simulation and test results of model #2.118
Table 6.1: Comparison between forced vibration analysis and test results 135

List of Nomenclature

a	Acceleration
m	Mass
n	chain density per unit of volume
δ	Phase shift
η	dashpot viscosity
η	Damping ratio
λ	stretch ratio
σ	Stress
σ	shift
ω	circular frequency
ϵ	Strain
ϵ	Engineering strain
φ	eigenvector
M_{jk}	Mobility function between point *j* and *k*
V_j	Velocity at point *j*
F_k	Driving input force at point *k*
λ_r^2	Eigenvalue of the r^{th} mode
${}_r\Phi_j$	j element of the r eigenvector $\{\Phi\}$
(α)	mass proportional damping
(β)	stiffness proportional damping
$K_s{}^{NM}$	imaginary stiffness proportional damping matrix
ζ_i	damping ratio
$[C]$	damping matrix
G'	storage module
G''	loss module
G_0	initial shear modulus
G_∞	long term shear modulus
I_1, I_2, and I_3	strain tensor invariants (first, second and third)
$[K]$	stiffness matrix
K_b	Boltzmann constant
L_0	initial length
$[M]$	mass matrix
P^N	external load vector
W_e	potential energy per unit volume
c_{ij}	Isochoric shear behaviour

c_m	modal damping
c_α	damping
k_m	modal stiffness
$m_{effective\ mass}$	Effective mass of shaker
m_m	modal mass
m_α	mass
q_α	amplitude of mode α,
$\dot{u}$	velocity
$\ddot{u}$	acceleration
α_β	complex modal amplitudes
$\dot{\varepsilon}$	time derivative of strain
λ_1, λ_2, and λ_3	principal stretch ratios
λ_i	principal stretches
λ_m	locking stretch
σ_0	constant applied stress
σ_∞	equilibrium stress term
σ_m	Maxwell stress
ϵ_0	constant applied strain
Δu	Deformation magnitude
A	Amplitude of the vibrational response
A_0	Amplitude of the vibrational input
D	loss factor value
E	Young's modulus
F	Force
G	Dynamic module
L	deformed length
n	Number of degrees of freedom
U_{max}	total stored reversible energy of the system
ΔU	energy loss per cycle
Δx	Deformation in spring
M, θ	eigenvalue
τ	Relaxation Time
ω	Frequency
ω_n	Natural Frequency
E	springiness constant
F	Generated force in spring
$F(t)$	relaxation function
$G(t)$	time-dependent shear modulus
$J(t)$	creep compliance
K	spring stiffness
T	absolute temperature

List of Abbreviations

CAE	Computer Aided Engineering
CFD	Computation Fluid Dynamics
DMA	Dynamic Mechanical Analysis
EGR	Exhaust Gas Recirculation
FDA	Frequency Domain Analysis
FE	Finite Element
FEA	Finite Element Analysis
FRA	Frequency Response Function
JLR	Jaguar Land Rover
N&V	Noise and Vibration
OEM	Original Equipment Manufacturer
VR	Viscoelastic Relaxation

Chapter 1: Introduction

1.1. Introduction

As a part of the sign-off procedure for vehicle body and power unit mounted components, vibration testing is carried out where the components must survive without damage. Vibration testing for power unit mounted components in a vehicle is essential during product development. In this type of testing, products are tested in their real or simulated operating environment to determine their vibration response, and assess their durability performance. A diesel engine EGR (Exhaust Gas Recirculation) coolant rail with rubber hoses shown in Figure 1.1 is the subject of this study. The EGR technique can noticeably reduce the Nitrogen Oxide (NOx) emission of diesel engines.



Figure 1.1. Engine Coolant rail system TDV6 3.oL Diesel (Jaguar Company, 2012)

With the current move to minimise design and development costs and time-scales in the development of new vehicles, the use of Computer Aided Engineering (CAE) tools to validate system design through the use of virtual testing is becoming ever more important. The availability of accurate CAE models will enable designs to be optimised before commitment to building prototypes. The desire is therefore to develop computer aided analysis/numerical techniques that will replicate the vibration testing of Diesel Engine EGR Coolant Rail.

This study aimed to develop an accurate FE model of the EGR coolant rail, including its connecting rubber hoses, to enable designs to be optimised before commitment to building prototypes. The aim was therefore to replicate the vibration testing of the coolant rail using FE simulation with a view to solving any durability problems quickly and efficiently.

1.2. Motivation

Frequency domain analysis (FDA) of vehicle components is a vital and mandatory stage in qualification inspection of designed components, particularly for those that are exposed to periodic loads with a wide range of frequency and amplitude excitation. Vibration analysis of these components in virtual environments has become fairly routine in the last few years. However, the analysis roadmaps are intentionally planned toward optimization of those virtual testing and modelling methods in order to increase the productivity in component design, speeding up product development, and implementation of virtual tools for durability checks and quality control.

Finite Element method is a powerful tool that has been extensively used for the analysis of vehicle parts in a wide range of applications. For FDA, FE tools are capable of predicting natural modes and mode shapes, as well as extraction of frequency response functions (FRFs)

when a component undergoes cyclic loads. The FE method has its own challenges on its path to predicting mechanical vibration behaviour of structures.

Understanding the impact of mechanical properties of materials used in the EGR coolant system, such as complex macro scale behaviour of rubbery materials in a structure and their viscoelastic behaviour, is a necessary step before performing design synthesis in frequency analysis of components for durability. Knowing this, the material testing contributes a major part of characterizing mechanical behaviour of parts under vibration. Being time-consuming is not the only drawback in FDA to characterize these phenomena, but it is expensive in terms of the required equipment as well as post-processing of outputs. Therefore, reduction in test equipment and optimization of test approaches can help engineers to save both time and effort spent for design synthesis in product development.

Having discussed about the potential benefits of an OEM of using virtual assessment tools, it is worth mentioning that this research is strongly motivated by JLR as a part of OEM's goal to develop reliable virtual sign-off/approval of engines soon future. The traditional approach is to closely work with supplier to develop a number of EGR coolant rail designs and evaluate them against the vibration metrics to check which design would hit the performance target and provides the least vibrational deficiencies. Replacing a trustable fine assessment would save more time and resources from the initial product development steps to the point where the sign-off/approval of engines are reviewed.

1.3. Research theme

In this research, a finite element model which is capable of accurately representing a vibration test of a Diesel Engine EGR Coolant Rail without rubber hoses attached has been initially

developed. In order to do this, the free and forced vibration analyses were carried out so that the tube model was verified in an initial validation study.

Initially in the validation study, the coolant rail was freely suspended from a noise isolated stand and an instrumented hammer test was performed for validation of free vibration natural frequencies. The dynamic physical vibration tests were then carried out on the coolant rail with/without rubber hoses and in the presence/absence of water as coolant fluid using the developed test rig. The physical test was purposely arranged in order to provide test data for the correlation study on mode shape and natural frequencies using predicted modal response functions such as transmissibility and mobility. The vibration test was conducted on the test rig using both force-controlled and displacement-controlled excitation in sine sweep forms as input to the coolant rail where it was attached to the engine. The frequency was varied between 40 Hz and 800 Hz. Acceleration of the coolant rail at selected positions was measured.

In the second phase of frequency analysis, a finite element model of the cooling rail was modified accordingly to include rubber hoses which were attached to the rail and also grounded. A natural mode extraction analysis was also carried out in the 40 to 800 Hz frequency range. The mode results were then used in carrying out a forced response analysis in the same frequency range. Detailed modelling of the rubber hoses included consideration of both the reinforcements and the rubber. The FE package Abaqus™ tools by Simulia was used for simulation in this research.

In order to prepare the FE models for vibration testing, material properties of the constituents of the hoses were measured as required. Rubber hose hyper-elasticity was needed for rubber physical behaviour modelling as an elastomeric material. Therefore, the material test was

carried out on three rubber specimens, cut from the provided hoses, so that the hyper-elastic and visco-elastic properties of the rubber hose could be obtained. The tensile test was repeatedly carried out on each specimen separately until identical graphs for last tests were achieved. Then the properties were calculated by averaging the three specimen graphs.

In this approach, the rubber was initially tested with extended elongation tensile test to determine its hyperelastic property. Dynamic Mechanical Analysis (DMA), and viscoelastic relaxation (VR) tests were also carried out in order to derive its mechanical behaviour. Then a methodology was adapted to avoid carrying out the DMA test and extracting viscous behaviour using only the viscoelastic relaxation test. The energy dissipation generated by DMA's and VR's viscoelasticity were cross-validated in order to eliminate the expensive DMA test and replace it with a simple VR test.

Finally, a simplified Maxwell model was developed to simulate the VR behaviour with only two parameters: dashpot and spring coefficients. This resulted in a much cheaper final simulation in terms of calculation and instrumentation. The equivalent Maxwell model replaced the complex rubber hose FE model in the model of EGR coolant rail and the simulation results were compared with the physical test and viscoelastic rubber hose-attached model.

Using the results obtained from material testing, FE analysis and vibration test, an attempt has been made to validate the FE model of the system. Modifications were made to the FE model to improve the correlation between FE results and measured responses to develop techniques for estimating the elastic stiffness and damping introduced after the rubber hoses are attached to the coolant rail system.

1.4. Problem definition

This research focuses on the 3.0L Lion V6 Diesel Engine EGR (Exhaust Gas Recirculation) Coolant Rail and aims to develop an extended FE model to replicate the vibration testing of the system, including the rubber hoses. It also proposed a method to consider the effect of the rubber hoses in the FE models of body and power unit mounted components without having to model the hoses in detail. In addition, this research proposes a method for including the effect of flowing fluid in the finite element models of body and power unit mounted components by modelling the Fluid-structure interaction (FSI) in detail.

The Diesel Engine EGR Coolant System as shown in Figure 1.2 is a water cooled circuit which is a combination of a heat exchanger, water pump, coolant rail, and connecting hoses. The functionality of this system is to reduce the temperature of recirculated exhaust gas before it is mixed with the intake of the filtered fresh air to enter the combustion chamber. This is to enable the cylinder intake gas to operate at a lower temperature, so that less Nitrogen Oxides are generated, resulting in a cooler chamber and lower oxygen content. The engine vibration causes a forced excitation of the components, specifically on the coolant rail because of its long structure, and the fact that it is filled by water resulting in a higher inertia in comparison with air-conveying tubes, so that the resonant modes occur at lower frequencies. Hence, it is important to discover where the rail resonant modes occur in order to determine a way to reduce the failure modes in the cooling system.

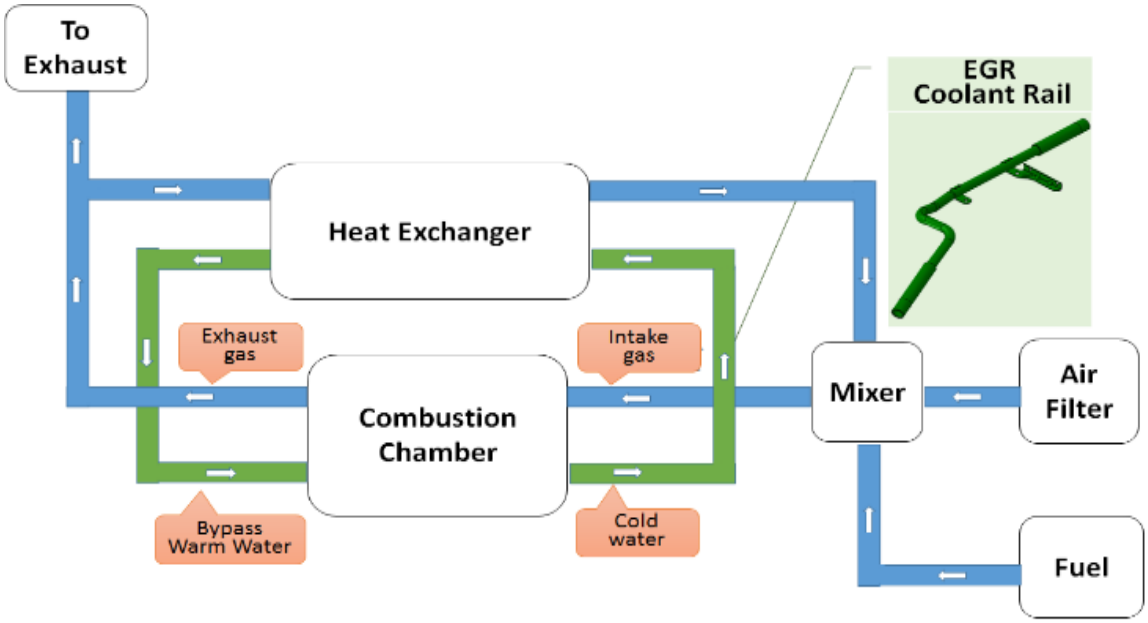


Figure 1.2. EGR system

The EGR coolant rail is composed of a steel tube attached to rubber hoses which connect it to the cooling system. It is mounted on the engine and exposed to engine vibrations as well as additional rotary components in all three principal directions over a wide range of excitation frequencies from 40 Hz to 800 Hz. Under such conditions, its durability performance needs to be determined particularly as there have been reported failures in the field. There is, therefore, a need to develop appropriate modelling techniques and validated FE models of the coolant rail and rubber hoses which can accurately describe the behaviour of the coolant rail. The Introduction of a simplified rubber model in terms of equivalent stiffness and damping characteristics as an alternative to the complex rubber hose FE model of the EGR Coolant Rail would further reduce the computational cost.

As described, the vibration of the structure may be heightened by the fluid flowing inside it which is then manifested as a potential problem during the sign-off process. The flowing fluid inside the structure does not only produce an additional mass in the vibration analysis, but its velocity, pressure, and viscosity can make a difference in the vibrational behaviour due to

dynamic interaction with the solid structure. In fact, the influence of fluid dynamics when exposed to a harmonic oscillation cannot be neglected. The fluid also experiences a pressure gradient phenomenon due to the flow, which can be modelled using the Navier-Stokes equations. Such vibration analysis presents a number of challenges namely:

- Geometrical complexities such that most analytical approaches are not capable of formulating the fluid-solid interaction behaviour,
- Nonlinear nature of both material and two-phase physical behaviours,
- Difficulties in modelling and implementation of the numerical integration problems for the fluid-solid interaction.

1.5. Aims and objectives

The aim of the research is to develop computer aided analysis capable of accurately representing the vibration testing of coolant rail, particularly those involving rubber hoses and therefore provide a virtual testing platform for such components in the early stages of system design and development. In order to validate the finite element model of the coolant rail by comparing with the measured mobility and acceleration, a number of vibration test rigs were designed and developed for various purposes. For doing this, the vibration testing was carried out by introducing a forcing function into a structure, usually with a shaker and using system analysis techniques to measure the ratio of the response to a measured input force. In this research, a general methodology for optimizing vibration test procedure was developed for simulation of structures with rubbery type material and this approach was examined on an exhaust gas recirculation (EGR) coolant rail with/without the presence of coolant fluid.

The ultimate aim of the virtual vibration testing is to enable engineers to predict the resonant frequencies and resonant modes of the structure in the presence of pressurised fluid flowing inside the coolant rail. Within the chapters of the thesis, the proposed methodology to cope with these challenges is explained.

1.6. Chapters summary

In chapter 2, a literature survey of previous work on vibration analysis is presented which describe up-to-date vibration testing and analysis of mechanical systems at low and high frequencies. A categorisation of Noise and Vibration (N&V) problems and a review of proposed methods to cope with the problem are presented. N&V problem in vehicles are classified based on the source of vibration: Road-excited vibration, Tyre vibration, Wind-excited vibration, and Engine-excited vibration; which are briefly explained in this chapter. The impact of N&V on components is generally identified using one of the experimental, analytical or numerical techniques which are briefly surveyed in this chapter.

As the first step in FE model preparation, chapter 3 presents the material property testing and modelling. This chapter starts with explaining how the materials specimens are obtained and in continuation, the viscoelastic and hyperelastic tests are performed and the required data for modelling is obtained. Within the last sections, the test data are used in modelling the material behaviour particularly in rubber and the models are implemented using the Abaqus™ Material Evaluation tools. Eventually, the fitted coefficients are used to generate the input deck files.

The vibration testing setup and test rig development are discussed in chapter 4. The free and forced vibration test setup is initially explained in the early section of this chapter and in continuation the LabView scripts for vibration testing development in forced mode are

presented. It is then described how the test is set up and implemented for four vibration cases in this chapter: Free vibration, forced vibration without attached rubber hoses, forced vibration with attached rubber hoses, forced vibration with attached rubber hoses when the coolant fluid is flowing inside.

In chapter 5, a benchmarking is initially performed on the virtual vibration testing methods to compare those methods for efficiency and accuracy simultaneously. The FE models are then developed for the above-mentioned test cases with/without rubber hose attachment except the FE model for coolant fluid which is separately discussed in chapter 6. At the end of this chapter, a simplified dashpot and spring model is presented to replicate the impact of rubber hoses on the vibration of EGR coolant rail.

As mentioned, the FE model development and vibration analysis of EGR coolant rail is presented in chapter 6. In this chapter, a co-simulation approach and analysis method is introduced to model the vibration of fluid-structure interaction system and the influence of water as the coolant fluid is discussed in depth.

The conclusion and future work are finally presented in chapter 7 to sum up the accomplishments within the current works and in continuation, this chapter proposes the future analyses as an extension to the proposed approach in this thesis.

Chapter 2: Literature Review

2.1. Introduction

Frequency Domain Analysis (FDA) of vehicle components is a vital and mandatory stage in qualification inspection of designed components, particularly for those that are exposed to periodic loads with a wide range of frequency and amplitude excitation. Vibration analysis of these components in virtual environments has become fairly routine in the last few years. However, the analysis roadmaps are purposely planned toward optimization of those virtual testing and modelling methods in order to increase the productivity in component design, speeding up product development, and implementation of quality control virtual tools.

In this chapter, a literature survey of the previous works on vibration analysis is presented which describe up-to-date vibration testing and analysis of vehicle systems at low and high frequencies.

2.2. Vehicle noise and vibration

Noise and Vibration (N&V) problem in vehicles are widely investigated as it became a routine work to tackle in everyday engineering world within various OEMs and their suppliers. Therefore, it is important to understand where the N&V analysis of a vehicle component like EGR cooling rail is standing. Categorisation on such comprehensive problem will assist to identify the most useful methods and analytical/testing tools for the problem of interest in this research. Succeeding this steam, a categorisation of N&V problems and the review of proposed methods to cope with the problem is presented in the following.

The N&V problem can be categorised based on various criteria, methods, and the nature of issues as classified in below chart (Figure 2.1).

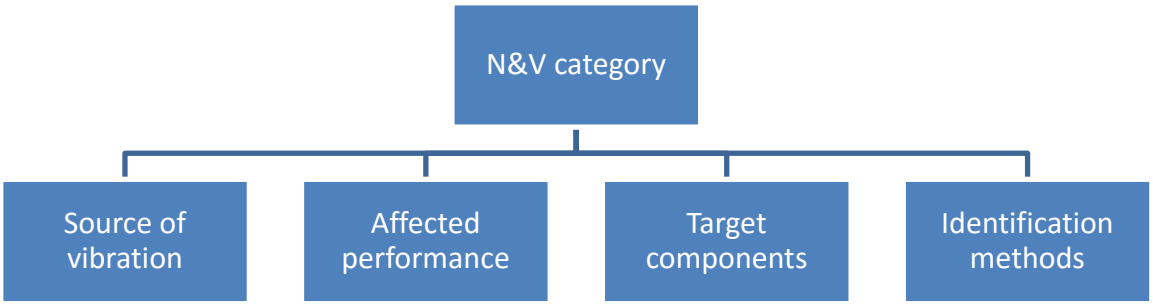


Figure 2.1. N&V category

These categories are discussed in the following sub-sections.

2.2.1 Source of vibration

N&V problem in vehicles can be classified based on the source of vibration. In this category, four sources of vibration are generally identified: Road-excited vibration, Tyre vibration, Wind-excited vibration, and Engine-excited vibration.

Road-excited vibration source: Road surface excited noise and vibration is the result of vehicle suspension vibration due to tyre/ road interaction mechanisms such as tread impact, stick/slip on the tire/road interface, and air-pumping of the tread, which is transmitted to the vehicle body to generate the vibration (Phillips, 1971). Kim et al. (Kim, et al., 2003) used the mobility technique to analyse the transfer functions of road noise between the suspension and the body structure for modelling the road noise phenomena. Gagliano and Tondra (Gagliano, et al., 2009) made significant improvement over the spindle force method to the tyre patch. They developed a tyre model derived from experimental data, along with three degree of freedom tyre contact patch input displacements. When coupled with a vehicle model, road noise can be predicted accurately up to a frequency of 300Hz, enabling virtual testing of the suspension and body design changes.

Tyre vibration: the non-uniform geometry and imbalance mass distribution in tyres produce an unwanted excitation which rather generates sensible and annoying disturbance to the driver in higher rolling speeds. This type of vibration has its main effect on the steering system as the high priority to investigate on and then the unwanted noise and durability problems at lower priority. Dunn (Dunn, 1972) (Dunn, 1972) (Mills, 1971) performed a wide-ranging review of tyre dynamics and developed an empirical model for predicting the behaviour of rolling tyres in the frequency range 5-300Hz, using measured tyre data from a test rig. Since the rolling tyre is the main source of vibration into the vehicle compartment through the suspension system, the tyre dynamic stiffness and damping coefficients have a great influence on the vehicle ride characteristics and therefore the interior noise of the motorcar. Yehya (Yehya, 1976) extended Dunn's work by investigating three-dimensional tyre vibration characteristics to calculate the stiffness coefficient and damping factor of radial tyres. Dunn and Olatunbosun (Dunn, 1988) (Dunn & Olatunbosun, 1989) (Olatunbosun & Dunn, 1991) extended previous work using a modified test rig which allows full tri-axial analysis of the tyre. The dynamic characteristics can be measured in the vertical, longitudinal and lateral directions. Burke (Bruke, 1998) extended the experimental work to numerical work to develop a tyre/ground contact model and dynamic models for finite element analysis. Yang (Yang, 2011) did an investigation of the relationships between the tyre strain feature and tyre operating conditions based on finite element analysis and experiments for the development of a strain-based intelligent tyre system. All these studies used the mechanical mobility techniques enabling a unified approach to the problems of noise and vibration to be adopted in the Automotive Engineering Centre at Birmingham University.

Wind-excited vibration source: Another vehicle's noise and vibration sources is wind noise and vibration, which is associated with turbulent pressure fluctuations exerted by the air flow on surface areas of the vehicle such as the windshield, A-pillar, side mirrors, and Underbody. They were investigated by many researchers. Oettle et al. (Oettle, et al., 2010) worked in assessing the relationship between the sound pressure level in the cabin and on-road flow conditions. They carried out the test on roads at typical highway speeds, where wind noise is very prominent, to collect the Flow data, Sound data and GPS data. They found that there is a good agreement between the variations of in-cabin sound pressure level with yaw in the wind tunnel with on-road data at low lateral turbulence intensities.

Kook et al (Kook, et al., 2011) developed an analytical model for the vehicle interior noise level based on a simple power law. Power-law-based models can estimate the wind noise component of the vehicle interior noise more directly over traditional methods.

Engine-excited vibration source: Engine noise and vibration includes intake/exhaust vibration as well as engine vibration itself transmitted through the mounts, the driveshaft, and airborne paths. Studies of the engine-excited vehicle vibration and noise have been conducted by many other researchers (Sacks & Brackett, 1989) (Stout, 2001) (Paul, 2004) (Hirate, et al., 2009). Zheng and Mao (Zheng, et al., 2015) developed a coupled model of an engine and a dash panel to analyse the relationship between the engine noise and interior noise of an automobile. Finite element analysis, flexible multi-body dynamics, and boundary element analysis were integrated to obtain the tetrahedron-element models, structural vibration response, and radiated noise, respectively to reveal that the interior noise is optimized due to the engine noise reduction. Sun and Steyer (Sun, et al., 2002) demonstrated the method of modelling axle systems by using the building block FEA approach, the procedure of model

correlation and how the model can be used to conduct NVH design study. The model can provide excellent predictions of the system dynamics up to at least 800 Hz.

The vibration techniques described in the researches reviewed above provide a basis for the development of techniques to be used in this research. It is clear that high frequency vibration (mechanical vibration above 40 Hz) from the engine-excited vibrations dominate the EGR coolant rail vibration and should therefore be the focus of this study.

2.2.2 Affected performance

The N&V can be categorised based on what performance of vehicle is affected. In this view, vehicle ride for passenger's comfort, handling for vehicle's dynamic performance, and component durability are those performances impacted by an uncontrolled N&V. In this thesis, the research theme is set to investigate the frequency domain analysis and mode shape formation in order to design the EGR coolant rail to survive and perform adequately stable in a wide range of frequencies.

Mr. Hong (Hong, 2008) used virtual analysis using FE methods in order to study the failure modes in the axle structure system. Swept sine and random excitation techniques were employed in a dynamic stress simulation and used the statistical the material life data in the form of well-known S-N fatigue curve to study the part durability and life prediction. The results of his research demonstrated that virtual CAE is capable to predict the potential weak areas in axle where fatigue damage can occur. This research along with similar examples such as (Auweraer & Janssens, 2007) (Rao , et al., 2015) (Carrera, et al., 2013) and (Duvigneau, et al., 2015) in which a CAE virtual analysis using the FE method are proposed encourages the research approach in this thesis to follow a similar path as it become more and more recognised within both industry and academia. However, the challenge here is to understand

how the complex two-phase physics can be modelled in FE for vibration analysis and mode shape extraction and which simulation is best suited to tackle the problem of solving the vibration analysis of EGR coolant rail with presence of fluid.

2.2.3 Identification methods

The impact of N&V on components is generally identified using one of the experimental, analytical or numerical techniques which are briefly surveyed in this section. In continuation of this section, the noise and vibration measurement and analysis is discussed and the challenges ahead of this research are explained.

The first ever developed technique from many long times ago is the intuitive perception and simplified visualisation of observable N&V. For instance, this perception was manifested in works by Da Vinci, Euler and Bernoulli on vibration analysis of a cantilever beam (Ballarini, 2006). The measurement of noise and vibration has been evolved within last decades by utilising advance technologies such as piezoelectric sensors (Phung-Van, et al., 2013), strain gauges (Jiang & Mao, 2014) , accelerometers (Safizadeh & Latifi, 2014), microphones (Minck, et al., 2012) , and last not the least, high-speed stereo-photogrammetry (Nedergaard, et al., 2014) (Berger, et al., 2012) with high precision and variable range of applicability and functionality. According to the researches and technical articles, the piezoelectric, strain gauges or accelerometers are the most commonly used measurement sensors due to the affordable price per unit that usually does not exceed more than hundreds of dollar (Measurement Specialties, Inc, 2001) (TMS , 2015).

On the other hand, more advanced sensing devices such as microphone or high-speed stereo-photogrammetry can cost thousands of dollars due to accuracy and added-value features which supports understanding of more complex phenomena. Microphone technology is

mainly used to detect the noise and acoustical vibration that is produced within the interactions between two solid materials or an internal noise generation. The theme of this research is focused on the vibration and durability analysis and noise generation is not a matter of interest here. Baqersad et. al. (Baqersad, et al., 2012) (Baqersad, et al., 2012) (Baqersad, et al., 2012) demonstrated the utilisation of high-speed stereo-photogrammetry and Digital Image correlation to visualise the natural frequencies and mode shapes of turbine blades. This technique can provide data in as many spots as required and not limited as the conventional sensing approaches such as accelerometer and strain gauges are limited to. The price of such sensing system is however expensive and requires initial calibration using strain gauges at a few points of interest.

Strain gauges and piezoelectric based sensing system are generally cheaper instruments and appropriate to measure field stress locally due to deformation at where it is installed. These sensors are not capable of directly measuring the acceleration, velocity, and motion in general term at the point where they are located. Accelerometer however provide access to the local motion information and cost-effective enough such that these sensors are widely used in many researches that the vibration of solid materials and structures are measured. These sensors are usually reliable and sense motion with acceptable accuracy specifically for using as the sensing system in this research. Like any other sensors, accelerometers has its own caution when used. First, the mass and size of these sensors are greater than the piezo-based sensor. This would be inappropriate if the mass or size of these sensors are considerable in comparison to the mas or size of the structure under study, so that the sensor mass/size becomes important. Second, these sensors are glued to the structure and solidity of the glue and support may influence of the sensor measurements.

In this thesis, accelerometers are used due their wide usage in measuring the vibration of structures. The disadvantages are acceptably minimal as the weight/size is not a big issue in comparison with the weight/size of the EGR coolant rail (1/120 in mass and 1/90 in size). The gluing was also done carefully in order to reduce its effects on the acceleration measurements.

In addition, the noise and vibration analysis can be studied analytically where the equation of motion or deformation of structure is derived and solved analytically/numerically. These methods are appropriate where the geometry of structure is simple enough to model. This method is not conveniently usable when the geometry is complex so that the equation and boundary condition are difficult to set and the interpretation of solution becomes more challenging as a unique response is hard to achieve. In numerical methods, the geometry is broken into the feasible region that the equation of motion/deformation is easier to derive and therefore a set of equations are formed to represent the vibration behaviour of structure at the points of interest. Finite Element approach is one of the most used approaches which is explained more in details with the next section and chapter 5.

2.3. Finite Element Modelling

Finite Element (FE) method is a well-known numerical approach to solve large-sized problems with complex physical problems. In this method, the geometry is discretised into elements interconnected at nodes as the elementary components of an FE model, as it can be seen in Figure 2.2. The full geometry of vehicle components can be usually imported into or created in FE codes, unlike the simplified geometry that is employed in other physical models. However, FE approach has the flexibility to model simplified models comparable with other

physical models. Therefore, FE models are available in different levels of complexity based on the desired functionality.

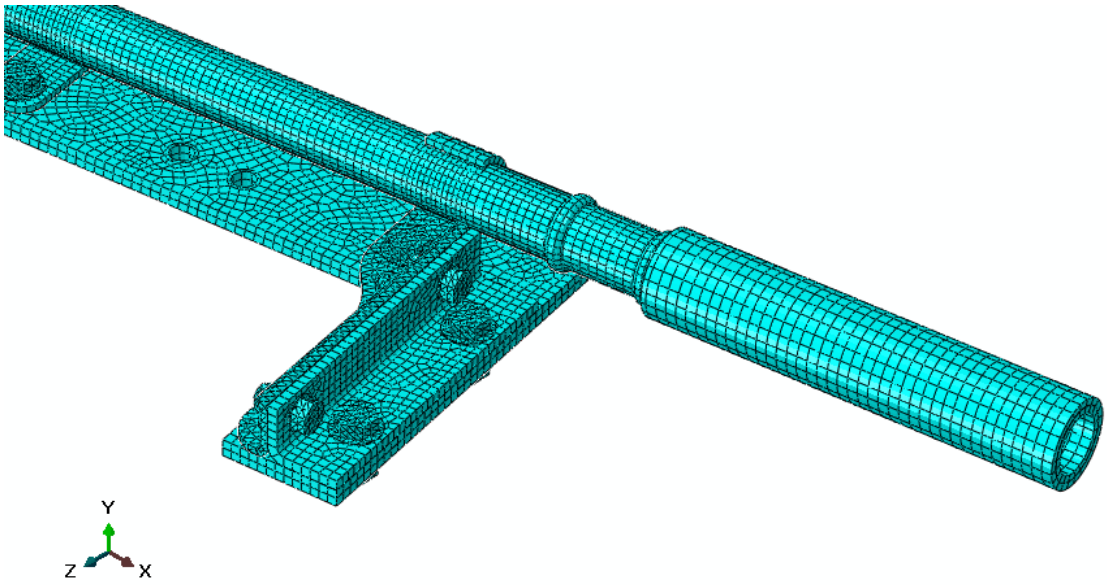


Figure 2.2. A meshed coolant rail with elements

This model delivers physical modelling with desirable technical features and has a great flexibility to add as much physics and analysis as required. For instance, fluid structural interaction effects can be added to the analysis and coupled with a dynamic analysis model. FE model can be implemented for a wide range of simulations from static, quasi-static, dynamic, steady state, and time based transient to linear perturbation procedures for frequency based analyses. Like other physical models, extrapolation can be reliably extended to nonlinear region in time and frequency based static, steady state, and transient analyses.

Pointing out the nonlinearity, generally three type of nonlinearities are identified on the problem of this research: the material nonlinearity in mechanical behaviour of the rubber hose, the geometrical nonlinearity in the contact problem, and the nonlinear interaction in physics between the solid structure and flowing fluid.

A number of researches have been carried out on the simulation of rubber mount to capture its mechanical behaviour (Ramachandran, et al., 2012) (Ooi & Ripin, 2011). Jung and Lee (Jung, et al., 2013) assessed a compound for improving the vibration insulation characteristics on the intercooler hose of the intake system and the heater hose of the heating system.

In the University of Birmingham, several researches were carried out by Behroozi, Bolarinwa and Yang, (Behroozi, et al., 2012) (Bolarinwa, 2004), (Bolarinwa & Olatunbosun, 2004), (Olatunbosun & Bolarinwa, 2004), (Bolarinwa, et al., 2004), (Yang, et al., 2009), (Yang, 2011), and (Yang & Olatunbosun, 2012), in order to bring the finite element method into simulation of tyre as a rubber-like material using Simulia/Abaqus. This FE package uses the "rebar element" concept to simulate the behaviour of the reinforcement embedded in the rubber. Rebar elements are used to define layers of uniaxial reinforcement in membrane, shell, and surface elements.

The FE model, with great advantages discussed above, has a couple of drawbacks that affects its functionality for a number of applications. Firstly, the FE model is computationally expensive mainly because of the number of variables created in association with model elements required to describe its physical state multiplied by the refinement level of geometry discretisation. This multiplication results in very large numbers of equations which have to be solved simultaneously. Matrix solvers are employed requiring considerable calculation cost, so that FE models are not usually appropriate for real-time simulations.

On the other hand, carefully measured material properties to describe the physical behaviour of rubbers and cords are required for accurate coolant rail modelling needs. The characterisation steps can be more challenging if the cords arrangement is unknown to the modeller and the rubber hoses needs to be cut in radial segments of cross section in order to

identify the cords orientation and density as well as the geometrical details. The specification of material properties also requires substantial time and efforts if the properties are not provided by the supplier. As a result, the coolant property characterisation may need destructive experiments that are sometimes not desirable in circumstances where a limited number of coolant rail are available for modelling in addition to the time and money costs and special cutting facilities.

It is common practice to utilize methods such as Frequency Analysis, or Steady State Dynamic Analysis to investigate the durability of parts under loads coming from the engine. These methods are usually fast and effective with linear models in the determination of resonance frequency that occur on the parts. A difficulty that arises with the complex parts particularly those involving rubber hoses, is that the nonlinear models and time dependent material property of rubber hoses may influence the convergence in solution. As a result, the final solution is somehow influenced by the quality of the numerical methods used and special arrangements should be made in tuning the effective convergence factor of numerical methods using the trial and error procedures.

The FE approach is picked as the virtual testing and analysis tool to study the vibration of EGR coolant rail system in this thesis because of all capabilities that were explained in this section. However, this method is complicated to employ due to different types of solvers, different types of elements, mesh density and their effects on accuracy and reliability of collected information from the structural vibration. Many research works have addressed and published quality research to study those parameters which is generally beneficial to consider as a guideline. However, every single problem due its physics and nature can have a refined set of parameters that would not necessary suites another problem. Specifically, a number of

modelling and solution techniques are used in this thesis which are appropriate at various mode of analysis. To understand the effect of these parameters, a deep study is arranged in chapter 5 to independently investigate the sensitivity of solver type, different types of elements and mesh density.

2.4. Material modelling and testing

FE model can produce good accuracy in virtual vibration testing and the steady state dynamic analysis for delivering the resonance frequency, mode shape and damping, depending on the material modelling precision provided in the model. The steel tube has linear behaviour in its elastic deformation region while the nonlinear hyperelastic behaviour is seen in rubber compound of the hose. This facts leads the analysis to a more complex one where the nonlinearity in materials should be involved in the simulation.

Identifying the influence of phenomena such as complex macro scale behaviour of rubbery materials in a structure and their viscoelastic behaviour should be considered as necessary steps before frequency analysis of components. Material testing contributes a major part of characterizing mechanical behaviour of parts under vibration. Being time-consuming is not the only drawback in Frequency Domain Analysis (FDA) to characterize these phenomena, but it is expensive in terms of the required equipment as well as post-processing of outputs. Therefore, reduction in test equipment requirements and optimization of test approaches can help designers to save both time and effort spent for development and qualification stages of a product.

Previous studies have reported the vibration analysis of structures mounted on rubber type materials (Ramachandran, et al., 2012) and (Ooi & Ripin, 2011) in which the rubber type material was modelled using FE analysis. Techniques were developed for determining

corresponding mass, effective stiffness and equivalent damping (Austrell & Olsson, 2012) for the attached rubber type material in order to effect a considerable reduction in problem size and complexity. The Kelvin-Voigt model (Lewandowski & Chorążyczewski, 2010), Standard Linear Solid (SLS) model (Wang Chung & Lindsay Buist, 2012), and Maxwell rheological model (Singh, et al., 2003) are well-known models for representing the viscoelastic behaviour of elastomeric materials. However, the Prony series method (Ghoreishy, 2012) and Dynamic Mechanical Analysis (DMA) (Roylance, 2001) are two of the most commonly used methods in FE analysis and were employed in this study and explained more in details in chapter 3.

2.5. FSI co-simulation

The lack of knowledge on how the vibration of EGR coolant rail in interaction with flowing fluid is affected leads researched to more comprehensive approaches. One possible option to perform such analysis is to consider the fluid as a solid element within the structure. In this case, the mass of fluid is artificially added to the solid structure. This method however ignores moment of inertia at different mode shapes as fluid shape changes due to the structure change. Also the momentum due to the fluid speed and pressure gradient is ignored. The other approach is to consider the flowing fluid as a separate element inside the solid structures where the physics of solid and fluid interactively talk to each other and exchange information about their vibration status to construct a more meaningful relationship.

The analysis of vibration for multi-phase structures has been a growing area of research interest during the past years (Tong, et al., 2007), (Xua, et al., 2010), (Chen, et al., 2011), (Park, et al., 2011), (Allahverdizadeh, et al., 2013), (Kumara, et al., 2014), (Nguyen-Thoi, et al., 2014). This analysis has been traditionally conducted by adding equivalent fluid mass into the structure and the fluid-solid interaction has been ignored. The CFD analysis of the flowing

fluid and the FE analysis of supported structure were done separately in older researches due to the computational efforts and immaturity of the coupled approaches. In this approach, the CFD analysis assumed the structure walls as rigid, which is not an accurate representation of what exactly happens in the coolant rail since rigidity is not a valid assumption for rubber compounds. Advances in recent years in both computer hardware and software has enabled researchers to tackle the coupled fluid-structure analysis problem by bringing the mechanics of both phases into a coupled integrated approach. However, the current available researches do not suggest a modal analysis in the frequency domain for complex and nonlinear geometry. Therefore, a time-domain method with implicit solution is proposed in this research work to indirectly compute the frequency response of the coolant rail in terms of its amplitude in the relevant frequency range which was explained in chapter 6.

2.6. Summary

In this chapter, the researches on the field of vibration testing and analysis were investigated. A categorisation of N&V problems and the review of proposed methods to cope with the problem were presented. N&V problem in vehicles was classified based on the source of vibration: Road-excited vibration, Tyre vibration, Wind-excited vibration, and Engine-excited vibration; which were briefly explained in this chapter. The vibration analysis techniques described in the section provided a basis for the development of techniques to be used in this research. It is clear that high frequency vibration (mechanical vibration above 40 Hz) from the engine-excited vibrations dominate the EGR coolant rail vibration and should therefore be the focus of this study.

The impact of N&V on components is generally identified using one of the experimental, analytical or numerical techniques which were briefly surveyed in section 2. In continuation

of this section, the noise and vibration measurement and analysis was discussed and the challenges ahead of this research were explained.

The FE approach is picked as the virtual testing and analysis tool to study the vibration of EGR coolant rail system in this thesis because of all capabilities that were explained in section 2.3. However, this method is complicated to employ due to different types of solvers, different types of elements, mesh density and their effects on accuracy and reliability of collected information from the structural vibration. A deep study is arranged in chapter 5 to independently investigate the sensitivity of solver type, different types of elements and mesh density. One of the challenges of this research is bringing the effect of three major nonlinearity parameters in the FE vibration analysis: the material nonlinearity in mechanical behaviour of the rubber hose, the geometrical nonlinearity in the contact problem, and the nonlinear interaction in physics between the solid structure and fluid.

The literature of material modelling and testing is reviewed and explained more in details with the next chapter (chapter 3) and appropriate material models for use in FE models are selected based on the accuracy and ease of material testing.

Chapter 3: Material Modelling

3.1. Introduction

Material modelling is one of the most significant aspects in vibration analysis using the Finite Element method. In fact, the essential modal parameters such as mass, stiffness and damping are introduced to the analysis through material behaviour modelling. In the analysis carried out in this research, material properties are used to describe the dynamic response and mechanical characteristics in automotive engine parts. In this chapter, testing scenarios for characterisation of material property in EGR coolant rail with rubber hoses are discussed and essential prerequisites for the FE modelling and vibration analysis of parts in terms of their material behaviour are obtained.

As mentioned in chapter one, the 3.0L Lion V6 Diesel Engine EGR Coolant Rail on a large saloon car was taken for the case study. The cross-section drawing of rubber hoses including data related to material geometries such as the cord orientation inside the rubber hose, cord spacing and diameter beside the material properties were obtained using University of Birmingham facility.

In section 2, available material models for coolant rail and rubber hoses with reinforcement are discussed and evaluated in order to investigate requirements of an FE modelling and vibration analysis method. Later in this chapter, based on the selected modelling method, the obtained material properties are assessed and characterised.

3.2. Material modelling of compounds

Mechanical behaviour of the EGR coolant rail is generically comprised of various structural deformations resulting from the loads to which its composing components are exposed. EGR coolant rail structure is typically constructed from three main materials: steel tube, cured rubber hoses and Para-Aramid cords. In this section, the behaviour of the coolant rail along

with rubber hoses in terms of elasticity, hyperelasticity and viscoelasticity are discussed. In addition, the standard procedures for collecting the experimental data for material property of rubber are presented. Later in this section, the material properties obtained are assessed to check for their behaviour under operating conditions in terms of properties such as exposed strains. Finally, the material models are characterised and the best method of modelling of material property is picked using the selection criteria set for the preferred model.

3.2.1 Steel Tube

The coolant rail is constructed of high strength steel tube with 9 mm diameter and 1 mm wall thickness as shown in Figure 3.1, with minimum elongation desired under high loading condition. The linearity in stress versus strain is the main behaviour of the steel tube owing to its mechanical design where the yield and plastic regions are prohibited. Hence, linear elasticity is expected to be the main behaviour of steel tube.



Figure 3.1. Structure of a steel tube

3.2.1.1 Linear elasticity

Elasticity is a macroscopic mechanical behaviour in solid mechanics which describes the return of material from its deformed form under external loading to its original shape before the load applied. For small elastic strains normally less than 5% of material deformation, a linear behaviour of elasticity in the process of the applied force and generated displacement

(or vice versa) is defined, specifically for metals when the stress and strain are correlated with a linear relation. The directional linear elastic behaviour in a material can be characterised by orthotropic (orthogonal direction dependency), isotropic (non-directional dependency), or fully anisotropic (full-directional dependency) behaviour. Steel shows isotropic behaviour in its elongation behaviour (Bhadeshia & Honeycombe, 2006). It is also worth mentioning that the linear elasticity is usually dependent on its temperature.

3.2.1.2 Models for linear elasticity

As previously explained, the tube's mechanical response is isotropic and linear elastic due to small deformations. The reinforcing cords in the rubber hoses were also considered in the same category, but not necessarily isotropic since the cords do not resist in compression. The most common model that is used to describe the springiness is the Hooke's law (Hooke, 1676), expressed as:

$$F = -K.\Delta x \qquad \text{Equation 3.1}$$

where F is the force generated, Δx is one dimensional deformation, , and K is the stiffness in the spring. In order to represent the relation between stress and strain in material, by re-arranging the equation 3.1, The Hooke's law can be generalised to linear elasticity in materials, and thus can be written as:

$$\sigma = E\epsilon \qquad \text{Equation 3.2}$$

where σ indicates the stress, ϵ denotes strain and E represents as Young's modulus or Elastic modulus.

Material characteristics of the tube and brackets are listed in Table 3.1 according to the data obtained from JLR.

Table 3.1. Material Specification

Part Name	Material	Density [kg/m^3]	Young's Modulus [MPa]	Poisson's Ratio
Tube	EN10305-3 E195+N	7.87E3	207,000	0.3
Brackets	EN10130 DC01	7.87E3	207,000	0.3

3.2.2 Rubber hoses with reinforcement cords

The rubber hoses, as parts with composite structure, have unconventional characteristics owing to their varied material properties and complex structure made by high modulus cord and low modulus rubber. The cord reinforcement acts as the main load bearing component of the composite and assists it to endure the diversity of loads that it is subjected to in its service life. Rubber hoses in EGR coolant rail are reinforced with Para-Aramid fibres with high strength specifications which provide benefits in terms of durability, and resistance to failure and large elongation. Aramid fibres are aromatic polyamides made from an aromatic acid for instance terephthalic acid or an aromatic dichloride like terephthaloyl dichloride and para-phenylene diamine (Visakh, et al., 2013). The reinforcing cords in the rubber hose are made by twisting threads of Para-Aramid fibres. A number of layers of cord spaced in the rubber play the reinforcing frame of the hoses as shown in Figure 3.2.

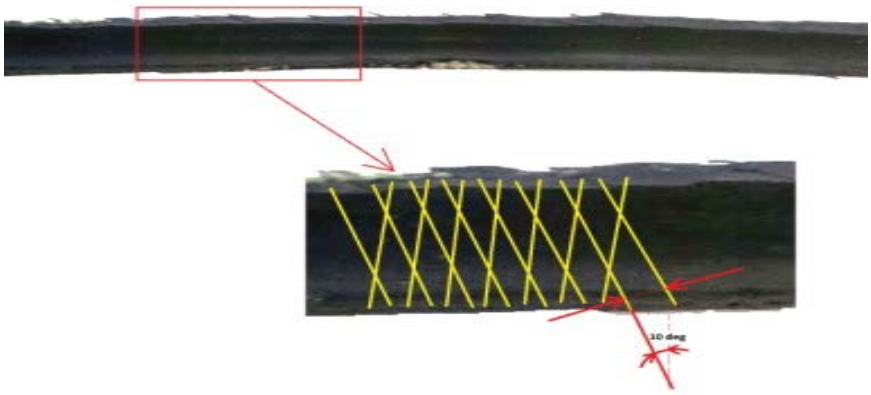


Figure 3.2. Structure of a rubber hoses

The rubber hose under engine vibration and dynamic loads undergo small deformation so that the elasticity is enough to represent the mechanical behaviour of the Para-Aramid cords. Since these cords have negligible size in comparison to the rubber in hose construction and therefore low volume, the viscoelastic effect is not noticeable in overall behaviour of hose and will be ignored for the cords in this research.

The rubber hose exhibits nonlinear deformation behaviour which can be represented as hyperelasticity mainly in steady quasi-static events, where no return cycle is practiced for modelling and the strain rate is lightly retained under an acceptable level. Moreover, the hysteresis loop is made by cyclic load. The latter behaviour is linked to the viscoelastic properties in elastomers and simulates the viscous behaviour in dynamic excitation.

The rubber compound used in the EGR coolant rail system is exposed to a small deformation under vibration loads, and consequently, the change in rubber volume is not considerable enough to account for compressibility to such an extent that rubber is nearly supposed incompressible for simplification (Hughes, 2000). The volumetric change is measured using the Poisson's ratio when multi axial loading is exerted and the Poisson's ratio magnitude reaches its maximum which is 0.5 for incompressible material.

3.2.2.1 Hyperelasticity

Rubbers as a class of polymers are amorphous and included long molecular chains. The molecular chains are highly twisted and coiled. Under a tensile load, these chains turn into partially straightened and untwisted. The chains return back to their original configuration upon elimination of the generated tension. Forming crosslinks between molecular chains through a vulcanization process results in strengthening of the rubber (Visakh, et al., 2013).

Owing to the untwisting of cross-linked molecular chains, rubbers can experience large elastic deformation. Since the deformation is relevant to straightening of chains, little volume change can occur under applied tension. Therefore, elastomers are approximately incompressible. Their stress-strain relationship can be highly nonlinear. Generally the material is firstly softened in tension and then becomes stiffer at higher strain. On the other hand, the response in compression becomes quite stiff in comparison with the behaviour in tension as the compression of twisted chains needs more effort than untwisting them.

According to abovementioned intermolecular physics, the hyperelasticity is determined as an isotropic property which demonstrates the nonlinear time-independent behaviour of elastomers or rubber-like materials subjected to the tensile test. The hyperelastic trend of a sample rubber and comparison with the linear elastic trend is presented in Figure 3.3.

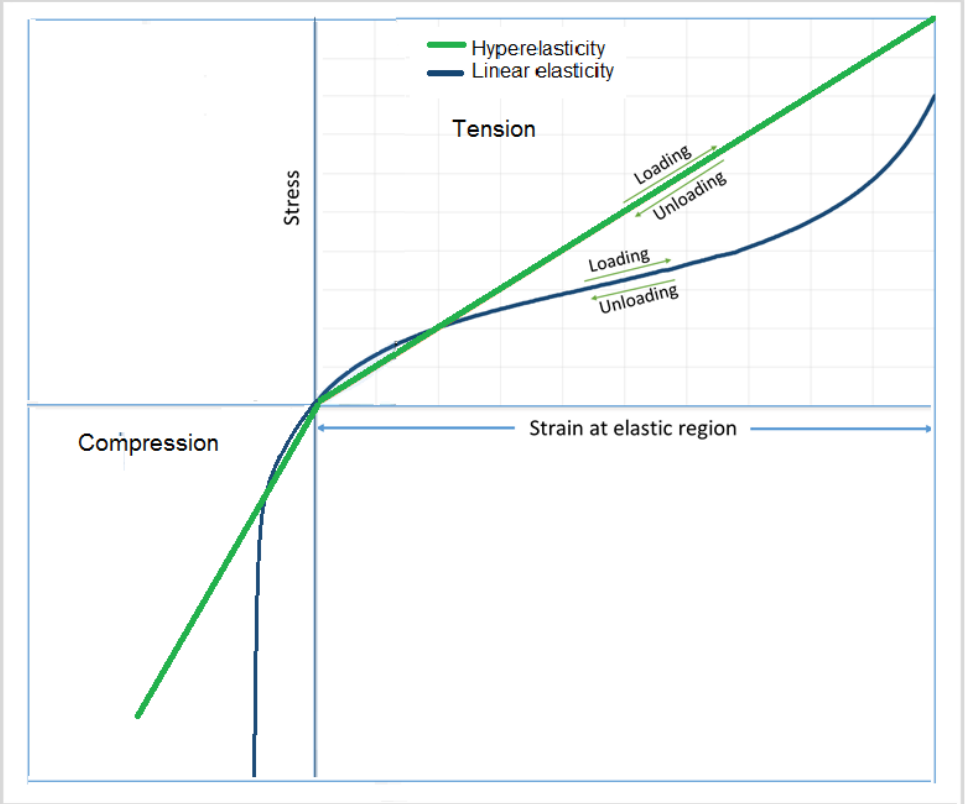


Figure 3.3. Hyperelasticity in comparison with linear elasticity in tension and compression region

Phenomenological and physical-based are two approaches to predict the hyperelastic behaviour in elastomers. Phenomenological constitutive models provide a definition of the material behaviour based on the empirical observations, and usually consist of polynomial mathematical functions. In this regard, direct polynomial formulations are used to represent the material behaviour with low calculation cost. Reducing the noise over-crossing, reducing the fitting error and maximising the correlation factor R^2 between the test data and model results are the most important factors to find the best fitting functions. Although the phenomenological is an appropriate method for modelling rubber hyperelasticity in the range where data is measured, the extrapolation is difficult in the area with no experimental data.

The physical-based models are derived from micromechanical studies of the response of polymer chains in the network. These models lead to hyperelastic potentials depending on micromechanical deformation mechanisms observed in the elastomer. Since the relation of stress and strain in material in these models, is instantly resulting from the inter-molecular structure and the general mechanical behaviour is assessed through the solution of the main equations, the mathematical formulation of these models is quite complicated with high computational cost.

Models for hyperelasticity

The hyperelastic constitutive models are defined through a strain energy density function or strain energy potential W_e (potential energy per unit volume). Before proceeding to a detailed discussion on different forms of strain energy and constitutive models of hyperelasticity, basic terms are defined.

The stretch ratio for uniaxial tension of a rubber specimen is defined as:

$$\boldsymbol{\lambda = \frac{L}{L_0} = \frac{L_0 + \Delta u}{L_0} = 1 + \epsilon} \qquad \text{Equation 3.3}$$

where:

- L_0: initial length
- L: deformed length
- Δu: deformation magnitude
- ϵ: engineering strain
- λ: stretch ratio

The principal stretch ratios λ_1, λ_2, and λ_3 provide a measure of the deformation and they are commonly used to define the strain tensor invariants (I_1, I_2, and I_3) as shown below (Chang, et al., 1991):

$$\begin{cases} I_1 = {\lambda_1}^2 + {\lambda_2}^2 + {\lambda_3}^2 \\ I_2 = \lambda_1\lambda_2 + \lambda_2\lambda_3 + \lambda_1\lambda_3 \\ I_3 = {\lambda_1}^2{\lambda_2}^2{\lambda_3}^2 \end{cases}$$ Equation 3.4

Moreover, if the material is supposed to be fully incompressible, then $\lambda_1\lambda_2\lambda_3 = 1$, and as a result, the $I_3 = 1$.

The strain energy potential W_e can either be a direct function of the principal stretch ratios(λ_1, λ_2, and λ_3) or a function of the strain invariants (I_1, I_2, and I_3). The mathematical backgrounds of these relations are regularly stated in references for instance (Treloar, 1975), (Chen & Saleeb, 1982), (Haupt, 2000), and (Muhr, 2005). This relation can be stated as presented below:

$$W_e = f(I_1, I_2, I_3)$$ Equation 3.5

$$W_e = f(\lambda_1, \lambda_2, \lambda_3)$$ Equation 3.6

An overall form of the strain energy potential function in equation 3.5 can be denoted for an isotropic incompressible elastomer as equation 3.7 (Holzapfel, 2000):

$$W_e = \sum_{i+j+k=1}^{\infty} c_{ijk}(I_1 - 3)^i (I_2 - 3)^j \qquad \text{Equation 3.7}$$

where c_{ijk}, i, j, and k are the model parameters which have unlike configurations in different hyperelastic models and possibly will be stated using the experimental data.

A collection of famous and general phenomenological and physical methods are presented in Table 3.1. most of the fundamental models for hyperelasticity are characteristically identified based on the type of specific function used to denote a relationship between the strain energy density function and either stain invariants or the principal stretch ratios directly. The strain energy potential W_e requires specified types of parameters input as material constants.

The constitutive models of hyperelasticity are categorised based on their origin as demonstrated in Table 3.2 according to the following literatures: (Gent, 2001), (Gent, 1996), (Gent & Thomas, 1958).

Table 3.2. Hyperelastic models for incompressible rubber

HYPERELASTIC MODELS FOR RUBBER		STRAIN ENERGY POTENTIAL (INCOMPRESSIBLE MODEL)	FEATURE'S
PHENOMENOLOGICAL MODEL	Polynomial	$W_e = \sum_{i+j=1}^{N} c_{ij}(I_1 - 3)^i (I_2 - 3)^j$ (Dostal, 1939), (Isihara, et al., 1951), (Kaliske & Rothert, 1997) (Miehe, et al., 2004), and (Göktepe & Miehe, 2005)	- Less dependency of the strain energy potential on lesser independent variables and coefficients. - Established a fundamental basis to develop reduced versions of itself to achieve efficiency in computation. - High number of coefficients. - High complexity of the material model. - More expensive numerical costs in the parameterisation procedure for characterisation of the model in order to be calibrated using experimental data. - The dependency of polynomial models on a comprehensive set of test data. - Three directional experimental stress-strain data should be used for characterisation. - It may be applicable for strains up to 300%
	Mooney-Rivlin	$W_e = c_{10}(I_1 - 3) + c_{01}(I_2 - 3)$ (Swanson, 1985), (Carroll, 2011), (Miehe, et al., 2004) (Rivlin, 1992), , (Mooney, 1940)	- The model accuracy in large deformation is an issue when this reduced order Mooney-Rivlin is employed for prediction of stress-strain behaviour. - Mooney-Rivlin model is empirical phenomenological models and physical parameters are not inherently used in their formulation, a characterisation procedure is required to obtain the parameters and coefficients based on experimental. - This model is widely used for rubber application, specifically when subjected to bi-directional loading condition and the model is valid for lower than 200% deformation.
	Reduced polynomial	$W_e = \sum_{i=1}^{N} c_{ij}(I_1 - 3)^i$ (James & Guth, 1943), (Wang & Guth, 1952), (Nah, et al., 2010)	- Simplified structure in formulation and an acceptable accuracy for the unidirectional load cases. - Many coefficients to be parameterised using the load-deflection experimental data. - Bi-directional loading may enable the prediction in extrapolation modes that may not provide consistent result in the direction that the model is not tuned for and experimental data is not available.

Yeoh (reduced polynomial)	$W_e = \sum_{i=1}^{3} c_{i0}(I_1 - 3)^i$ (Yeoh, 1990), (Yeoh & Fleming, 1998)	- The coefficients can be characterised with minimum unidirectional data where the lack of data and test facility is an issue. - The model is consistent enough in prediction of stress-strain behaviour under alternative loading modes particularly in large deformation condition. - The model requires fewer coefficients for parameterisation, so that the fitting procedure requires less calculation efforts in comparison with models with more parameters. - The FE models demand less expensive computational resources and the solution convergence is faster.
Arruda-Boyce (Eight-Chain)	$W_e = G_0 \sum_{i=1}^{5} \frac{c_i}{\lambda_m^{2i-2}} \left({I_1}^i - 3^i\right)$ - $[c_1, c_2, c_3, c_4, c_5] = [\frac{1}{2}, \frac{1}{20}, \frac{11}{1050}, \frac{19}{7000}, \frac{519}{673750}]$ - G_0 : initial shear modulus - λ_m: locking stretch, i.e. the point in stress-strain curve where the stiffness changes significantly. (Boyce & Arruda, 2000) (Arruda & Boyce, 1993) (Bergstrom & Boyce, 2001)	- Less parameters to be determined in comparison with the phenomenological models. - Less experimental data is needed to be collected for the characterisation of the model. - These models exhibit no common instabilities such as singularity or negative inclination in stress-strain curves as long as the configuration parameters are obtained from the physical properties of the material. - Low Inaccuracy in highly nonlinear deformation region. - Generally limited to 300% strain at most.
Ogden	$W_e = \sum_{i=1}^{N} \frac{2\mu_i}{{\alpha_i}^2} ({\lambda_1}^{\alpha_i} + {\lambda_2}^{\alpha_i} + {\lambda_3}^{\alpha_i} - 3)$ α_i and μ_i describe the shear behaviour of material	- The high number of constants and coefficients to be parameterised, which brings complexity and computational costs for a fitting programme and reduces the efficiency of the modelling in the characterisation procedure. - The necessity for comprehensive experimental data in three directions which is not easily obtainable for a number of applications and which requires more time and results in more destructive test procedures.

PHYSICAL BASED MODEL		(Ogden, 1997), (Ogden, 1972), (Ogden, et al., 2004), (Ogden, et al., 2006), (Ogden & Roxburgh, 1999)	- A model that is being developed based on the Ogden model is capable of predicting the elongation behaviour in different directions and deformation modes. Consequently, Ogden model is popular and well-developed for biomedical application where a high level of precision is required.
	Marlow	$W_e(I) = \int_0^{\lambda(I)-1} \sigma(\epsilon) d\epsilon$ σ : nominal stress ϵ : nominal strain of unidirectional tension, which are directly obtained from the experimental data (Marlow, 2003)	- The strain energy potential is obtained through unidirectional equations by resemblance of material deformation in three-dimensional mode. - Simplified shape for the strain energy density function
	Neo-Hookean	$W_e = c_{10}(I_1 - 3)$ $c_{10} = \frac{1}{2} n K_b T$ - n: chain density per unit of volume - K_b: Boltzmann constant - T: absolute temperature (Guo & Sluys, 2006), (Meuniera, et al., 2008), (Bechira, et al., 2006), , (Sasso, et al., 2008)	- This model does not require load-deflection experimental data - The low accuracy at large deformation mode due to the simple first order equations of elongation. - Weak prediction of hyperelastic behaviour under different loading modes

Van der Waals	$W_e = \mu\left\{-(\lambda_m^2 - 3)[\ln(1-\eta)+\eta] - \frac{2}{3}a\left(\frac{\tilde{I}-3}{2}\right)^{\frac{3}{2}}\right\}$ $\tilde{I} = (1-\beta)I_1 + \beta I_2 \quad \beta = \sqrt{\frac{\tilde{I}-3}{\lambda_m^2-3}}$ - μ : shear modulus λ_m: locking stretch (Kuhn & Grün, 2003), (Flory, 1967), (Flory & Erman, 1982), (Flory, 1977)	- Limitation in the model validity to predict very large strain due to large deformation under tensile load.

Rubber tensile testing

In this section, the instrumentation, rubber sample preparation and standard techniques to get the experimental data for hyperelastic property of rubber are presented.

Material tests were carried out on three rubber specimens, cut from the provided hoses, so that the hyperelastic property of rubber hose could be obtained. The test facility, “Lloyd” test rig, which is located in University of Birmingham, UK is shown in Figure 3.4. The specification of this material testing machine is presented in Table 3.3.



Figure 3.4. Tensile test machine to measure hyperelasticity

Table 3.3. Tensile test machine specifications

Force Capacity	100 kN
Speed Range	0.001 to 508 mm/min
Speed Accuracy	<0.2% at steady state
Load Cell Accuracy:	<0.5%
Extension resolution	<0.05 microns

A uni-axial test procedure was carried out on each rubber specimen in tension as shown in Figure 3.5. The dimension requirement of the specimen is that the length of the specimen is at least 10 times longer than its width or thickness. According to (Wan-Doo, et al., 2004), if the sample length in elongation is more than 10 times of its width, the strip sample can produce the same reliable test data as a dumbbell sample.



Figure 3.5. Rubber sample under tensile test

Figure 3.6 shows a rubber hose specimen that was used for material testing. The cord has not been removed, but it has a negligible contribution in rubber strength because of the direction where the specimen was cut so that there are no connected cords in the tensile test specimen from both sides of the test grip. As it can be seen, the yellow lines represent cords embedded into the rubber region, so the cords are inactive (not stretched) in this test. The length of samples (L_0) is 120mm with ± 0.5 tolerance, the 2mm size is set for thickness with ± 0.1 mm tolerance, and the width (b) is 15mm with ± 0.2 tolerance.

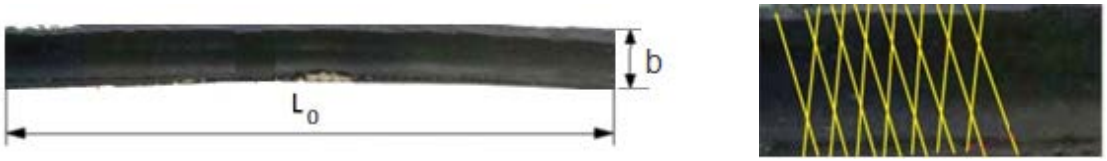


Figure 3.6. rubber hose specimen

Both end tabs of the specimens are symmetrically gripped and inserted into the tensile test machine, so that the tension is distributed homogeneously over the rubber sample. In the uni-axial test of the rubber, the samples are pre-conditioned at the speed of 50 mm/min up to 100% strain for 10 cycles. The result of pre-conditioning is to remove the stress softening effect.

Experimental data

The tensile test was repeatedly carried out on three specimens separately until identical graphs are achieved for the last consecutive tests (Yang, et al., 2010). Then the properties are calculated by averaging the graphs for the three specimens. The pre-conditioning state and stabilized curves are shown in Figure 3.7.

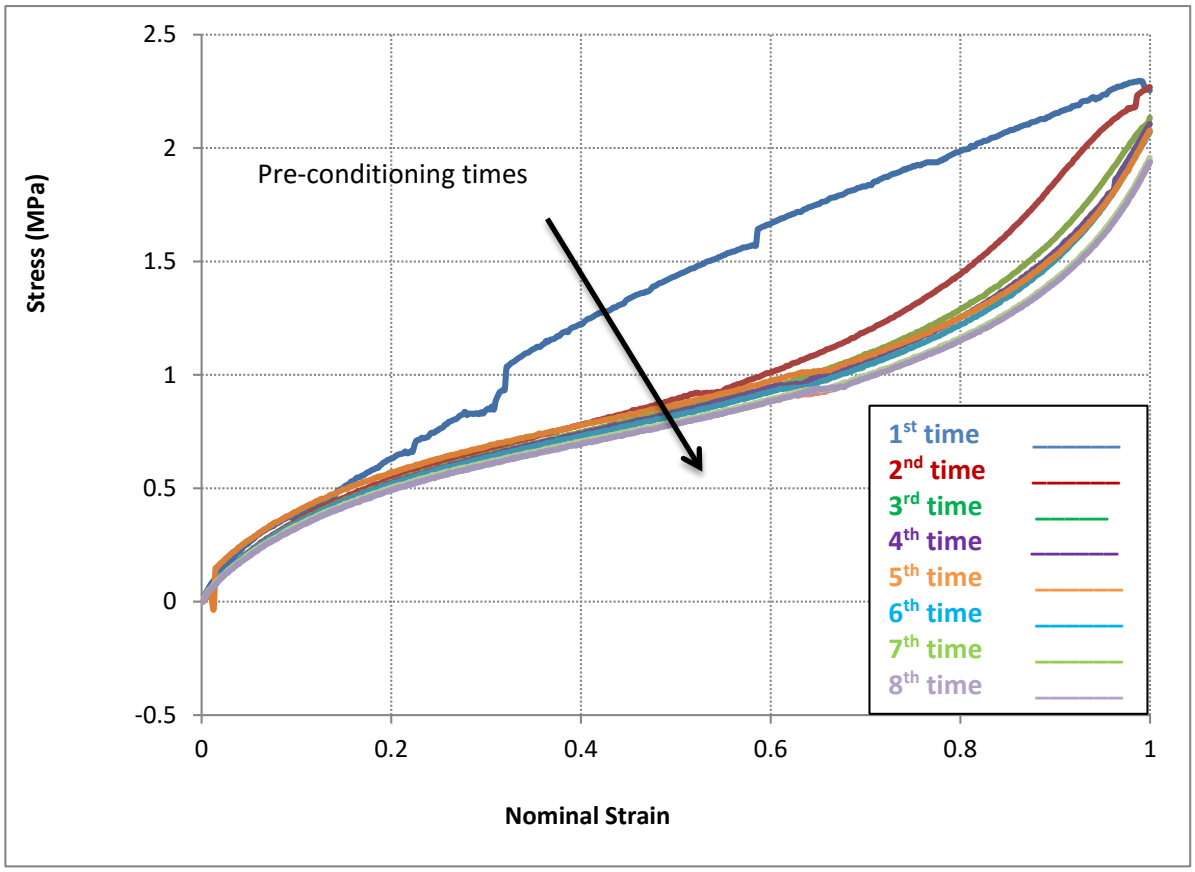


Figure 3.7. Uni-axial pre-conditioning test curves for rubber

The rubber hyperelastic property of coolant rail for the three specimens were demonstrated in Figures 3.8 in terms of nominal strain and stress in MPa. The results of applied stress versus the generated strain for selected samples indicate an acceptable repeatable process of tensile test for these materials.

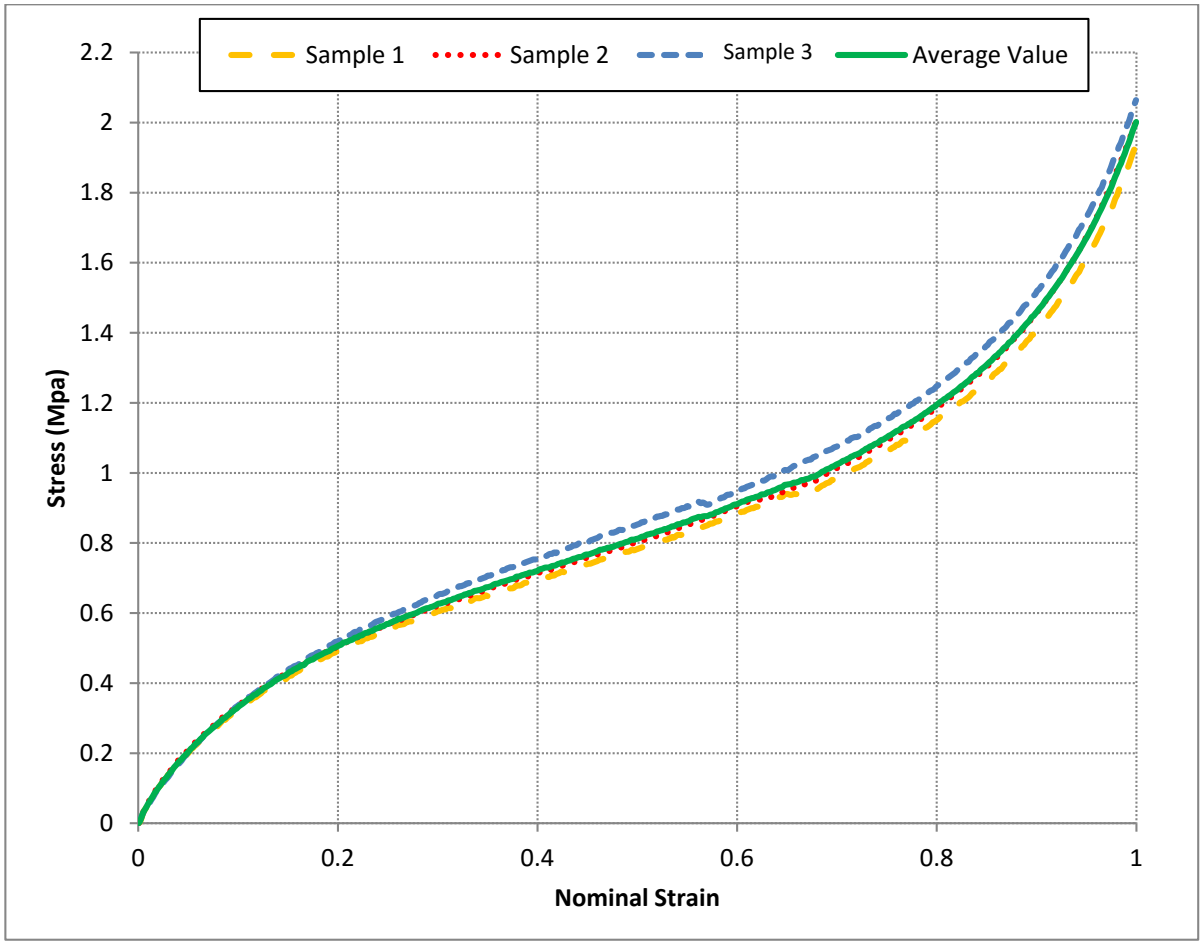


Figure 3.8. Hyperelastic behaviour for rubber hoses

Material model selection

Several particular forms of the strain energy potential are available in Abaqus™ to predict the hyperelastic behaviour. In Figure 3.9, the eight hyperelastic material models are compared with the test data in uniaxial loading conditions to find the accurate model.

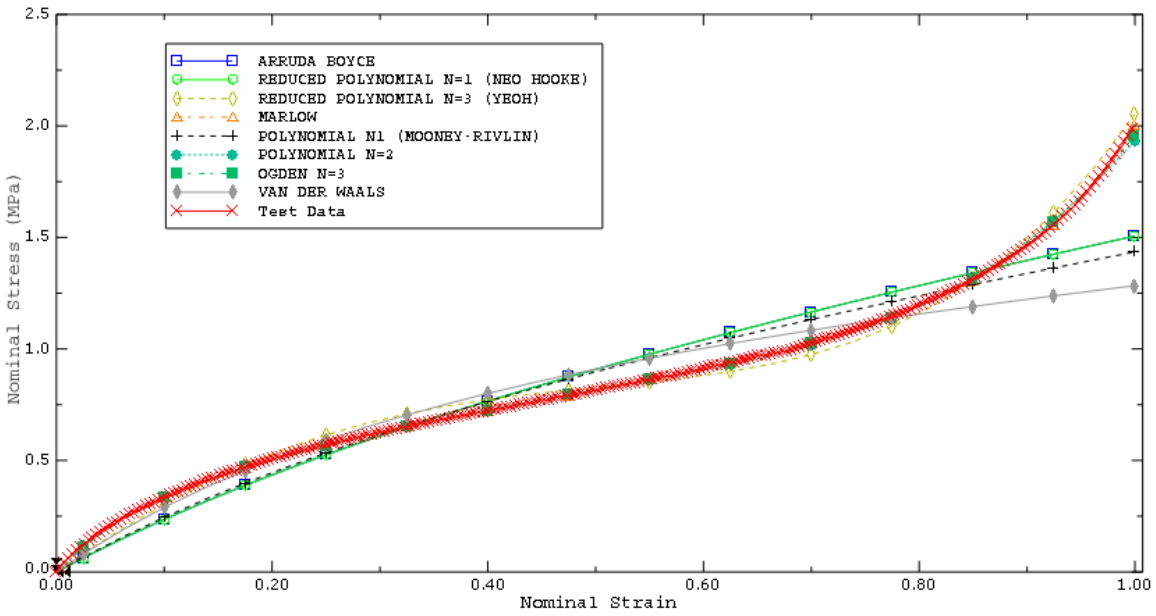


Figure 3.9. Prediction of hyperelastic behaviour using different models for rubber

The Yeoh material model is widely accepted as appropriate for representing rubber material behaviour in a uniaxial tension test (Behroozi, et al., 2012) (Kupchella, et al., 2009). In addition to the presented accuracy as shown in Figure 3.9, this model needs fewer coefficients for parameterisation, therefore the FE models require less expensive computational resources and the solution convergence is faster in comparison with Marlow and Polynomial models.

Considering its accuracy in representing the test data and the cost of implementing it in FE, the Yeoh model was adopted for modelling hyperelastic property of the rubber hoses in Abaqus™ solver and its coefficients are listed in the Table 3.4 according to Yeoh equation from Table 3.3.

Table 3.4. Yeoh model parameters

Yeoh model coefficients								
C_{01}	C_{10}	C_{02}	C_{20}	C_{11}	C_{30}	C_{21}	C_{12}	C_{03}
0	0.5674	0	-0.214	0	7.295e-2	0	0	0

3.2.2.2 Viscoelasticity

Viscoelastic behaviour of rubber-like materials distinguish them from other types of materials. Elasticity and viscosity are two characteristics which can be exhibited by viscoelasticity behaviour in polymers. This behaviour is normally discussed as the linear or non-linear time-dependent performance of the relationship between stress and strain in elastomers when they are under loading/unloading conditions (Ferry, 1980).

Viscoelasticity has the following features in relation to the mechanical properties of materials as presented in Figure 3.10:

- *Relaxation:* if the strain is retained constant, the stress decreases with time.
- *Creep:* the strain increases with time if the stress is held constant.
- *Hysteresis*: if cyclic loading is applied, a time delay or phase lag between the applied stress and resulting strain happens, resulting in a dissipation of mechanical energy. Internal friction of molecules in the viscous flow causes the generation of hysteresis effect for elastomers and the energy is dissipated in the form of heat. Dynamic modulus G can be used to denote the relations between the strain and oscillating stress:

$$G = \acute{G} + iG'' \qquad \text{Equation 3.8}$$

where $\acute{G}$ denote the storage modulus and G''refers to the loss modulus:

$$\acute{G} = \frac{\sigma_0}{\varepsilon_0} cos\,\delta \qquad \text{Equation 3.9}$$

$$G'' = \frac{\sigma_0}{\varepsilon_0} sin\,\delta \qquad \text{Equation 3.10}$$

where σ_0 is the amplitude of stress, ε_0 is the amplitudes of strain and δ is the phase shift between stress and strain.

Figure 3.10 presents the abovementioned features for viscoelasticity using time domain strain and stress plots and their corresponding fundamental viscoelastic material functions.

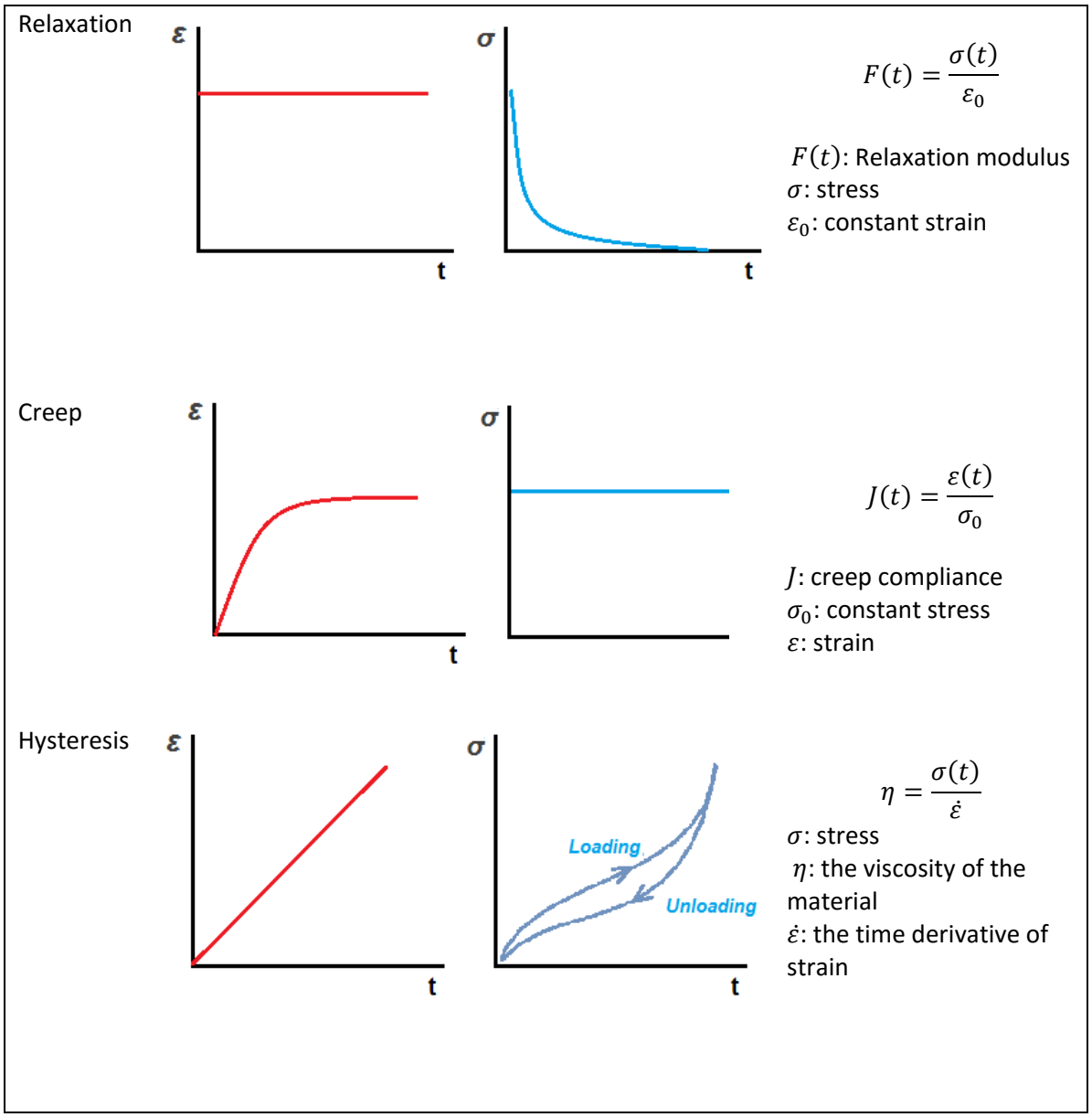


Figure 3.10. Viscoelasticity features of elastomers

One of the distinctive characteristics of viscoelastic materials is that their properties are affected by many parameters such as temperature, frequency, dynamic strain rate, static pre-load, and time effects such as relaxation and creep. The test methods adopted for characterising the viscoelastic material property model are strain creep test stress and

relaxation test in the time domain and the dynamic mechanical analysis (DMA) in the frequency domain.

Mathematical Models of Viscoelastic Material Property

In mathematical modelling of viscoelastic behaviour, in order to simulate the elastic and viscous components of the stress/stain response, the springs and dashpots with different configuration are used to simulate. The spring and dashpot obey the relations for tensile and shear stress as shown in equations below:

$$\sigma = E \times \varepsilon \qquad \text{Equation 3.11}$$

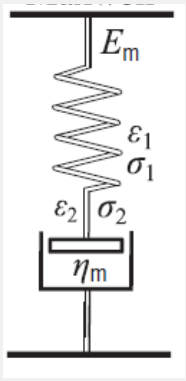
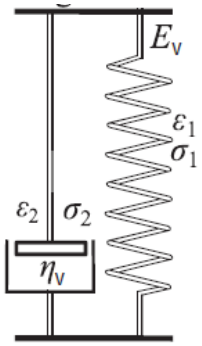
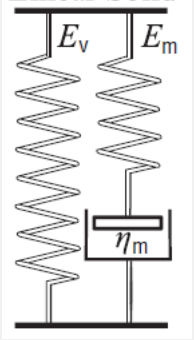
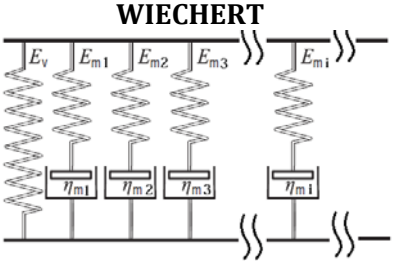
$$\sigma = \eta \times \dot{\varepsilon} \qquad \text{Equation 3.12}$$

where η and E represent the dashpot viscosity and spring stiffness respectively.

Since in the vibration of the EGR coolant rail, large elongation of the hoses doesn't happen, the behaviour of rubber under different conditions for instance creep, relaxation, and cyclic loading can be simulated through a linear viscoelastic model.

Various configurations of physical linear viscoelastic models are described in Table 3.5.

Table 3.5. Physical models of Viscoelasticity for rubber

VISCOLEASTIC MODELS FOR RUBBER	STRAIN ENERGY POTENTIAL (INCOMPRESSIBLE MODEL)	FEATURE'S
MAXWELL 	$\dot{\varepsilon}(t) = \frac{\dot{\sigma}(t)}{E_m} + \frac{\sigma(t)}{\eta}$ η: dashpot viscosity E: spring stiffness	- **Creep:** $\varepsilon(t) = \frac{\sigma_0}{\eta}t + \frac{\sigma_0}{E_m}$ the strain increases linearly with time - **Relaxation**: $\sigma(t) = \sigma_0 \exp(\frac{-E_m}{\eta}t)$ This model is acceptable as a first approximation to relaxation behaviour, but is inadequate for prediction of creep.
KELVIN-VOIGT 	$\sigma(t) = E_v\varepsilon(t) + \eta\dot{\varepsilon}(t)$	- **Creep:** - $\varepsilon(t) = \frac{\sigma_0}{E_v}\left(1 - \exp\left(-\frac{E_v}{\eta}t\right)\right)$ - **Relaxation:** $\sigma(t) = E \times \varepsilon$ - This model is acceptable as a first approximation to creep behaviour, but is inadequate for prediction of relaxation.
STANDARD LINEAR SOLID 	$\dot{\varepsilon}(t) = \frac{\dot{\sigma}(t) + \frac{E_m}{\eta}\sigma(t) - \frac{E_m E_v}{\eta}}{E_m + E_v}$	- This model represents the most accurate prediction of viscoelastic behaviour among simple models.
GENERALIZED MAXWELL-WIECHERT 	$\sigma(t) = \sigma_v(t) + \sum_{i=1}^{N}\sigma_m(t)$ $\sigma_v = E_v\varepsilon$ σ_m: Maxwell stress	

The most popular modelling for viscoelastic material models is Prony series model due to its integrity, accuracy, and computational efficiency which is described within the next section.

Prony series model

The Prony series is a pure numerical method unlike the previous viscoelastic models. The Prony series constants are calibrated using gradient-based fitting methods for stress-strain experimental data under stress relaxation, cyclic loading or creep.

The complete Prony series models originally begin with the standard illustration of the applied stress or strain in terms of the induced strain and stress as follow:

$$[\sigma(t)] = [E(t)][\epsilon(t)] \qquad \text{Equation 3.13}$$

where the $E(t)$ is generally the elastic modulus, while $\sigma(t)\ and\ \epsilon(t)$ denote the stress and strain respectively.

The ordinary point in these equations is the time-dependent elastic modulus $E(t)$. By the Prony expansion method, the time-dependent elastic modulus $E(t)$ can be extended to finite terms of exponential forms. The rubber model is presumed to perform like a general Maxwell solid for this application, as the stress eventually relaxes to a fixed value at infinite time. The Prony series equation for the shear relaxation is:

$$G(t) = G_\infty + \sum_{i=1}^{N} G_i\, e^{-t/\tau_i} \qquad \text{Equation 3.14}$$

where $G(t)$ expresses the time-dependent shear modulus and G_∞ is the long term modulus when the material is entirely relaxed. The parameters τ_i and G_i represent the relaxation time constant and Prony series factors for each term which are distinguished through the minimisation of fitting error.

An another form is achieved stating that the elastic modulus is related to the long term modulus in below equation:

$$G(t=0) = G_0 = G_\infty + \sum_{i=1}^{N} G_i \qquad \text{Equation 3.15}$$

Therefore,

$$G(t) = G_0 - \sum_{i=1}^{N} G_i \left[1 - e^{-t/\tau_i}\right] \qquad \text{Equation 3.16}$$

This form is appropriate when the elastic shear modulus G_0 is gained from data independent from the relaxation data, then for decreasing convergence time in computer implementation.

The equation 3.16 is normalised in order to distribute the usage of Prony series in relaxation mode to general deformation modes, as demonstrated in equations 3.17:

$$g(t) = 1 - \sum_{i=1}^{N} g_i \left[1 - e^{-t/\tau_i}\right] \qquad \text{Equation 3.17}$$

where $g(t) = \frac{G(t)}{G_0}$, and $g_i = \frac{G_i}{G_0}$.

To obtain experimental data for characterisation of Prony series coefficients, numerous techniques are proposed for instance creep test and relaxation test in time domain, and Dynamic Mechanical Analysis (DMA) test in frequency domain. In this research both DMA and relaxation test are performed and described in the next sections.

Rubber relaxation testing

The stress relaxation method is known as the most popular representation of stress-strain data for viscoelasticity due to the simplicity in implementation of relaxation test and its application in shorter timeframe, (Abu-Abdeen, 2010).

A stress relaxation test was carried out to extract the rubber viscoelastic properties. The rubber stress relaxation test measured the decreasing force which maintained the constant strain applied to the rubber sample.

The specimen samples and the test procedures were selected based on the standards such as ISO 6914 describing the stress relaxation test in tension. In the viscoelastic material property test, the same samples were used as those in the hyperelastic material property test as shown in Figure 3.6. The Instron test machine under remote computer control was used for the stress relaxation test as shown in Figure 3.11. After pre-conditioning test with load speed of 100mm/min and one hour relaxation time, the samples were stretched to 10%, 20%, 50% strain levels respectively and kept for 960 seconds at each level.

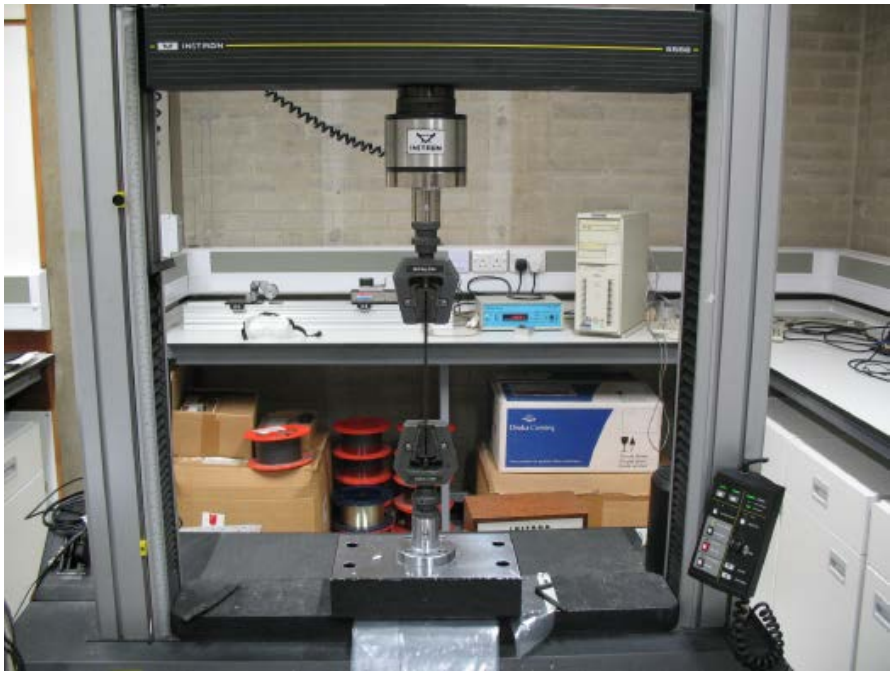


Figure 3.11. Instron Test Rig for Rubber Stress Relaxation Test

Stress values at various time intervals were recorded. The stress relaxation data were then normalised for use in Abaqus™ evaluation toolbox as shown in Figure 3.12. This toolbox formulates different material models in its library and provides parameterization of the fitted coefficients through the Abaqus solver.

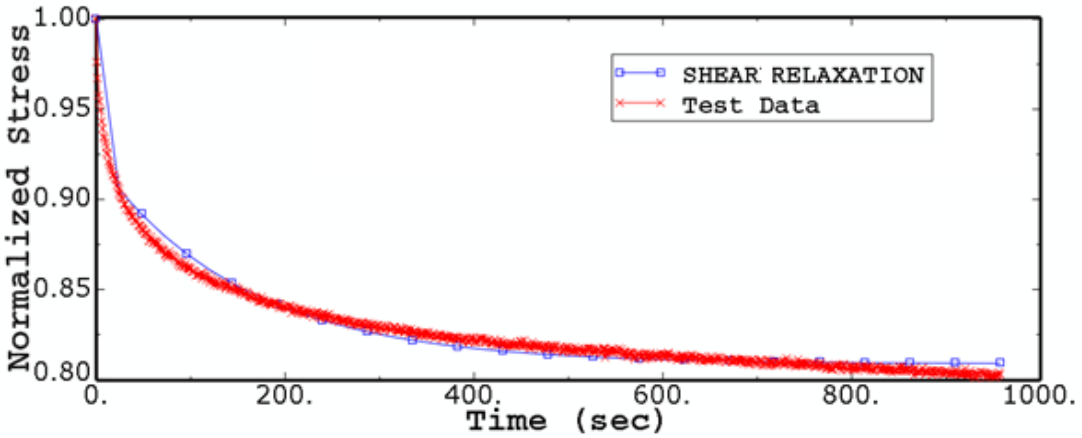


Figure 3.12. Normalized stress relaxation of rubber

Then, the Prony series parameters for viscoelastic materials were evaluated in Abaqus™ and reported in Table 3.6.

Table 3.6. Viscoelastic Material Constants

PRONY SERIES DEFINITION			
Relaxation Time (τ), sec		Relaxation Modulus (g)	
τ_1	τ_2	G_1	G_2
6.76033E-02	155.17	7.82057E-02	0.11306

Rubber Dynamic Mechanical Analysis testing

Dynamic Mechanical Analysis (DMA) is a method to investigate material property by applying small deformation to a sample in a cyclic manner, and can be used to determine the storage modulus (Elastic modulus E'), loss modulus (Viscous modulus E'') and Tan Delta (Damping coefficient ζ) as a function of frequency. The storage modulus is the measurement of the stored energy in viscoelastic material, representing the elastic portion. The loss modulus is a damping factor describing the dissipation of energy into heat under deformation. The Tan Delta is the ratio of loss modulus to storage modulus, which illustrates how efficiently a material loses energy owing to molecular movements and internal friction.

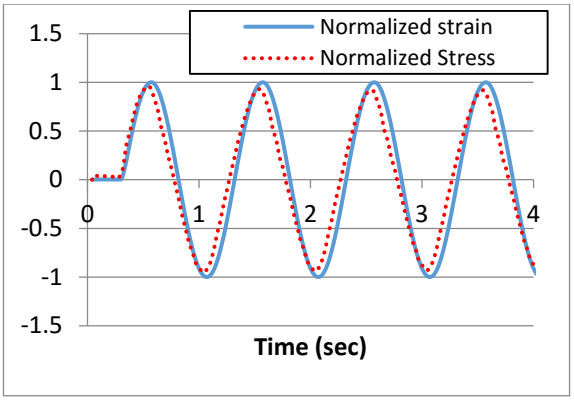
The MTS Landmark machine, which is located in University of Birmingham, UK, which is shown in Figure 3.13 was used for the DMA test to accurately measure properties such as tan(δ) and damping coefficient ζ for rubber. The MTS Landmark 200 Hz Elastomer Test System is constructed specially for distinguishing the dynamic properties of elastomeric materials and components. The system is optimized for different frequencies and available with maximum force capacities of 25KN and maximum pressure of 21 MPa.

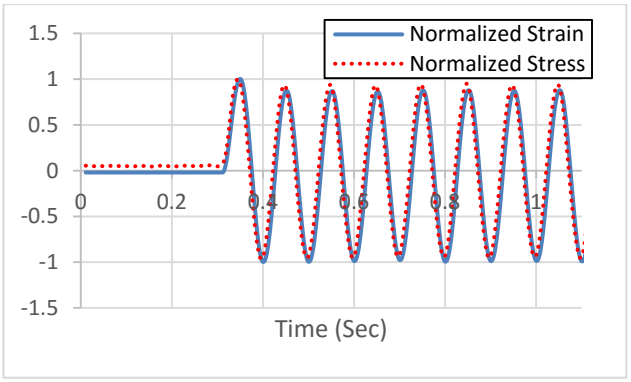
The test was performed in the low frequency range from 1Hz to 20Hz. In order to eliminate the buckling effect when the specimen is in compression, the specimens were stretched to pre-strain level and then sinusoidal strain was applied on the specimen at different frequencies. Normalized stress and strain values at each cyclic test were recorded.



Figure 3.13. DMA test machine

In order to reduce noise in DMA stress results, Wavelet denoising technique in Matlab software was used. Stress and strain vs. time in dynamic loading of rubber at frequency 1 Hz and 10 Hz are shown in Figure 3.14.





(Frequency= 1Hz, strain=50%) ***(Frequency= 10Hz, strain=50%)***

Figure 3.14. Stress and strain vs. time t in dynamic loading of rubber

When a viscoelastic material is subjected to a sinusoidally varing stress, finally a steady state will be achieved in which the resulting strain is also sinusoidal with the same angular frequency but phase angle;

$$Stress: \sigma(t) = \sigma_0 sin(2\pi f t) \qquad \text{Equation 3.18}$$

$$\text{Strain: } \varepsilon(t) = \varepsilon_0 sin(2\pi f t - \delta) \qquad \text{Equation 3.19}$$

where

f is frequency of strain oscillation,
t is time,
δ is phase lag between stress and strain.

The tensile storage and loss moduli are described as follows:

$$E' = \frac{\sigma_0}{\varepsilon_0}\cos\delta\ \varepsilon(t) = \varepsilon_0 \sin(2\pi ft\text{-}\delta) \qquad \text{Equation 3.20}$$

$$E'' = \frac{\sigma_0}{\varepsilon_0} sin\,\delta\ \varepsilon(t) = \varepsilon_0 \sin(2\pi ft\text{-}\delta) \qquad \text{Equation 3.21}$$

The period T of the waveform is the time required for one cycle:

$$T = 1/f \quad \mathrm{T} = 1/\mathrm{f} \qquad \text{Equation 3.22}$$

The phase angle is related to the time lag Δt between the sinusoids by

$$\delta = 2\pi\ (\Delta t)/T\ \delta = 2\pi(\Delta t)/T \qquad \text{Equation 3.23}$$

Tan $\boldsymbol{\delta}$ is a dimensionless number named loss factor and defined as the ratio of loss modulus to storage modulus. It is a kind of energy lost measuring which stated in terms of the recoverable energy, and indicates mechanical damping or internal friction in a viscoelastic system. The test data are shown in Figure 3.15.

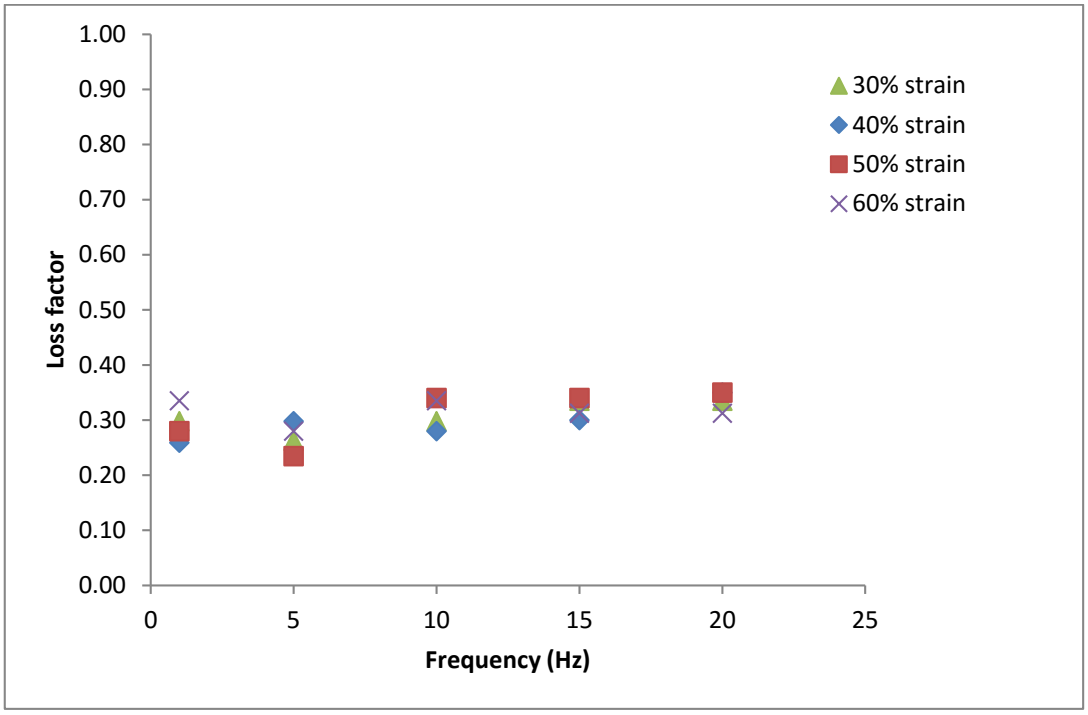


Figure 3.15.Rubber DMA test result

3.3. Summary

In this chapter, the material properties of EGR coolant rail were investigated and available models for elasticity, hyperelasticity, and viscoelasticity were explained. The steel tube, brackets and reinforcement cord material property were considered as linear elastic due to their small strain during normal EGR coolant rail operation. Hyperelasticity was selected to characterise the behaviour of rubber.

Practicable and standard material test procedures for hyperelasticity and viscoelasticity behaviour of rubber were developed. The specimens of rubber were obtained by cutting an EGR coolant rail provided by JLR. Uniaxial test was carried out to obtain the rubber hyperelastic material properties. Then, the material properties were parameterised using the material characterisation tests, then Yeoh model which is the model with minimum parameters was used to simulate the hyperelastic material behaviour of rubber hoses.

Moreover, the viscoelastic material properties of rubber were identified by stress relaxation test and DMA test. The constants of rubber material model were determined using the evaluation function in ABAQUS™.

Chapter 4: Vibration testing

4.1. Introduction

Excitation by dynamic forces causes vibration in structures. The effects of vibration range from reduced performance and any degree of permanent damage, fatigue, reduced comfort, to safety and even health hazards.

Most vibration problems are related to resonance phenomena. When the dynamic forces in an action excite modes of vibration or the natural frequencies in a structure, resonance occurs. Moreover, the dynamics of a structure can be described through its vibration modes, so these are some reasons for the importance of studying resonant modes and conducting vibration tests.

As mentioned in the first chapter, the aim of this project is to develop computer aided analysis models capable of accurately representing the vibration testing of the coolant rail, particularly when including rubber hoses and therefore provide a virtual testing platform for such components in the initial phases of system design and development. In order to validate the finite element model of the coolant rail through comparison with the measured mobility and transmissibility, a vibration test rig was designed and developed.

Vibration testing can be classified in two categories: free vibration and forced vibration. Free vibration means the system after an initial perturbation is left to vibrate on its own. In other words, external force doesn't act on the system. If a system is subjected to an external force, the ensuing vibration is identified as forced vibration. The vibration setup for free and forced vibration is shown in Figure 4.1. The sensors attached to the structure measure the directional motion of the point of attachment and this data is then transferred to the analysis software for characterization.

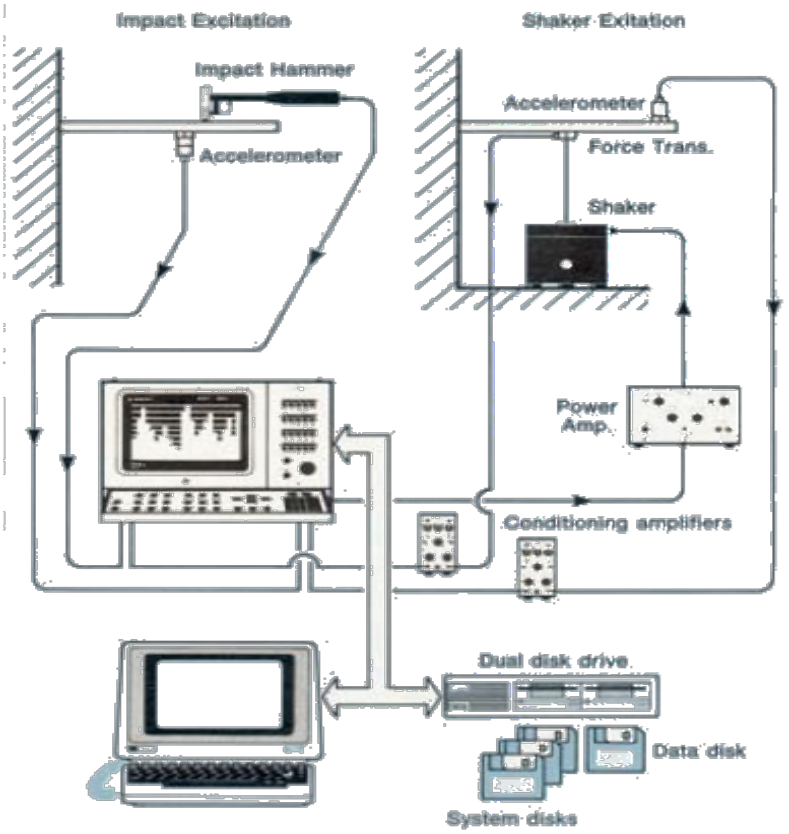


Figure 4.1: Structure under test (Ole Dossing, 1988)

The purpose of the test, time constraint, accuracy requirement, and physical constraint of the test structure are important factors in choosing both free and forced vibration test in this research. The free vibration is used for characterization when the free-free modes are of interest, while the forced vibration is carried out when the effect of boundary conditions is desired. In free vibration testing, the access to high frequency content is usually limited due to the restriction in testing methods while the forced vibration can be controlled to implement the test under desired frequencies.

Designing and building of a vibration test rig is a bottom-up process. First of all, the operating conditions and boundary settings of the structure under study was identified. Based on the information to be collected, the vibration rig was designed and built for free and forced vibration testing. The excitation and sensing system were then installed to obtain the test data. In the next step, the testing interface was developed. In this case LabVIEW software by

National Instruments™ was used for customized input functions and data acquisition system. The recorded data was then taken into the Matlab™ environment to plot the mobility and transmissibility in the frequency domain in order to calculate the structural damping and resonance frequencies.

In this chapter, the test equipment and setup for vibration analysis of EGR coolant rail are introduced. The target is to ensure the real-world operating condition and input excitation from the engine and other vibration sources are mimicked. The free and forced vibration tests are generally designed to get the natural frequencies and damping factor of the EGR coolant rail under engine induced excitation, the most likely cause of potential failure, and characterise its vibrational behaviour.

4.2. Forced vibration test

The various vibration tests can be used to obtain the dynamic property of a structure, in terms of the natural frequency and damping ratio. Those properties are able to be extracted from the mobility and transmissibility characteristics, which are obtained by taking the ratio between the response and excitation in the frequency domain; by designing a forced vibration test that enables both excitation and response to be measured simultaneously. Figure 4.2 illustrates the developed experimental setup used for forced vibration test in this research.

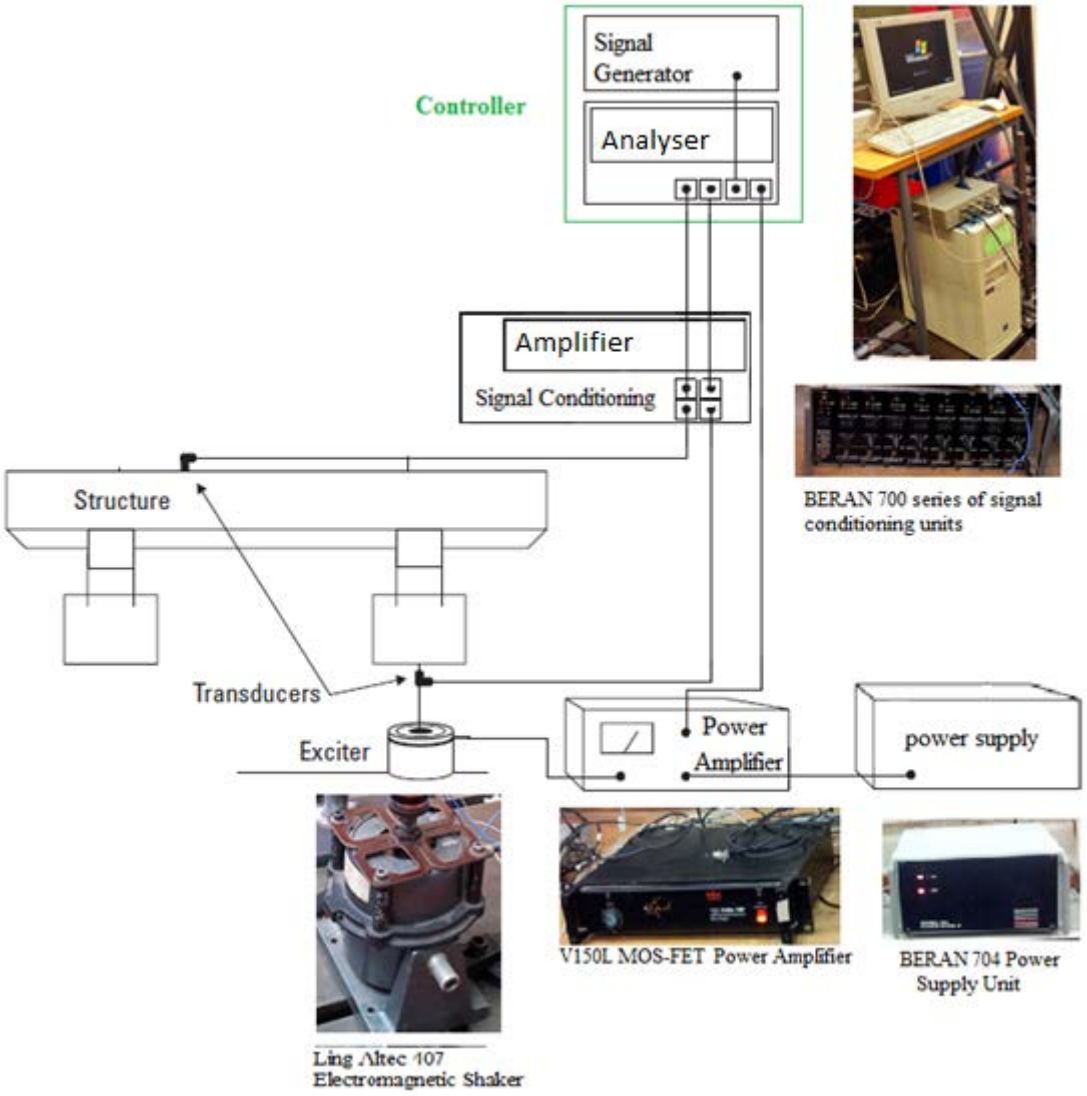


Figure 4.2: Schematic setup for forced vibration system

During a forced vibration test, the structure is connected to a shaker to provide a force/displacement to the structure. The force is proportionally changed by a specific command input voltage sent from controlling device (Personal Computer). It is important how the shaker is attached to the structure, since this connection can change the structure's boundary condition such that the results would not reflect the desired real-world conditions.

4.2.1 Test rig development

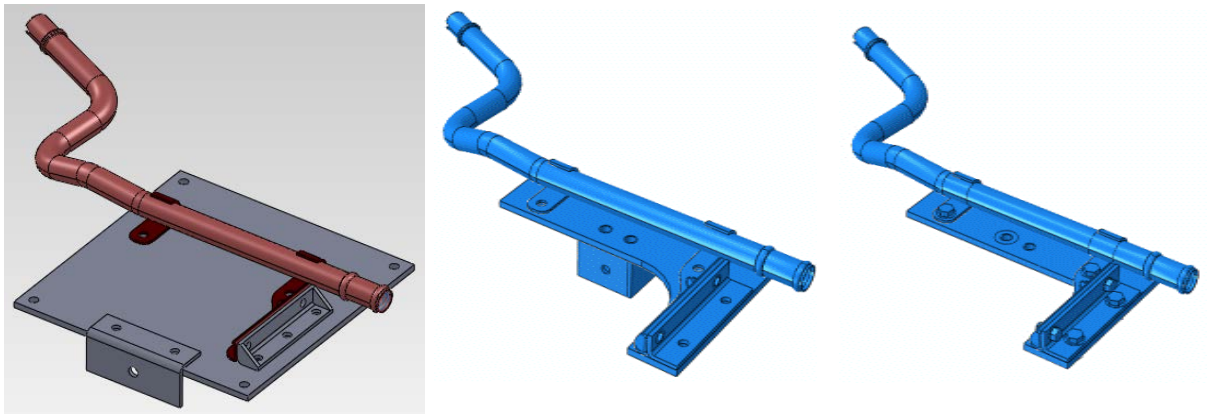
Designing a fixture mechanism in order to get the desired constraints (boundary conditions) is the first step in development a structure for frequency response measurements. Fixturing

is a vital stage in the test facility development as it directly has the effect on the general structural characteristics, particularly for subsequent analyses like structural modification, substructure coupling and finite element correlation (Agilent Technologies, 2000). The key in design of the fixture is to ensure the mounts are solid enough to avoid any extra motion induced into the rail. Furthermore, the mode shapes and natural frequencies of the fixture are identified within the frequency range of interest in the vibration test.

A number of criteria are important for designing a test rig plate for the coolant rail. The most important criterion is its own resonant frequency. The plate's own vibration should not influence the resonant frequencies/modes of the tube in order to certainly relate corresponding resonant modes of the tube to its simulation mode in FE code. On the other hand, the plate should be robust enough to work as a fixture for replicating the boundary conditions.

Three different designs were developed and evaluated for the support plate and brackets in order to find one with the least impact at the frequency range of interest in vibration of coolant rail system, as shown in Figure 4.3. Forced vibration test was carried out with these test fixtures in different directions and comparing the results indicated that most of the modes were excited by carrying out the test in the Y direction. The (a) design was a rectangular aluminium plate that demonstrated a number of high amplitude and frequency modes at the operating frequency range of the EGR coolant rail system. For a better isolation, the generic approach is to increase the stiffness and reduce the mass to allow a lower amplitude and less modes at the operating frequency. Therefore, the design (b) with an L-shape steel design and smaller size (higher rigidity) was developed and was mounted on a cubic support to allow three directional testing. The cube later found to add a number of

structural modes at the operating frequency which made it difficult to isolate the fixture modes from the coolant rail ones. Based on the above reasons, the design (c) of test fixture (Figure 4.3.c) which demonstrated a stronger fixture to reduce the influence of plate bending mode shapes in forced response analysis was eventually used for forced vibration test.





(a) ***(b)*** ***(c)***

Figure 4.3: Vibration test rigs and CAE models

The vibration testing was divided into three steps: setting up the rail-fixture-shaker-sensor measurements, building the control strategy and data acquisition system using LabVIEW software, and planning the run procedure. In the first step, the fixture was bolted to the

shaker while the shaker was strongly secured to the ground by several metal clips. The rail was fitted over the fixture plate by four bolts and after the rail was filled with water, the rubber hose ends were secured in position according to their location on the engine. Sensors were glued to the different points where the initial FE frequency analysis predicted considerable vibration amplitude and also to ensure the nodes were avoided. After the test was completed, the parameter estimation was carried out using a Matlab script in order to obtain the vibration characteristics such as mobility and transmissibility.

The final experimental setup for coolant rail without rubber hoses (model #1) is shown in Figure 4.4 and with rubber hoses (model #2) is presented in Figure 4.5. The new test rig for the coolant rails with rubber hoses was designed and built in order to adapt fixtures with the rubber hose additions to both ends of the tube. Each rubber hose was consequently attached to a fixture on either end of the tube.



Figure 4.4: The vibration test setup for model #1

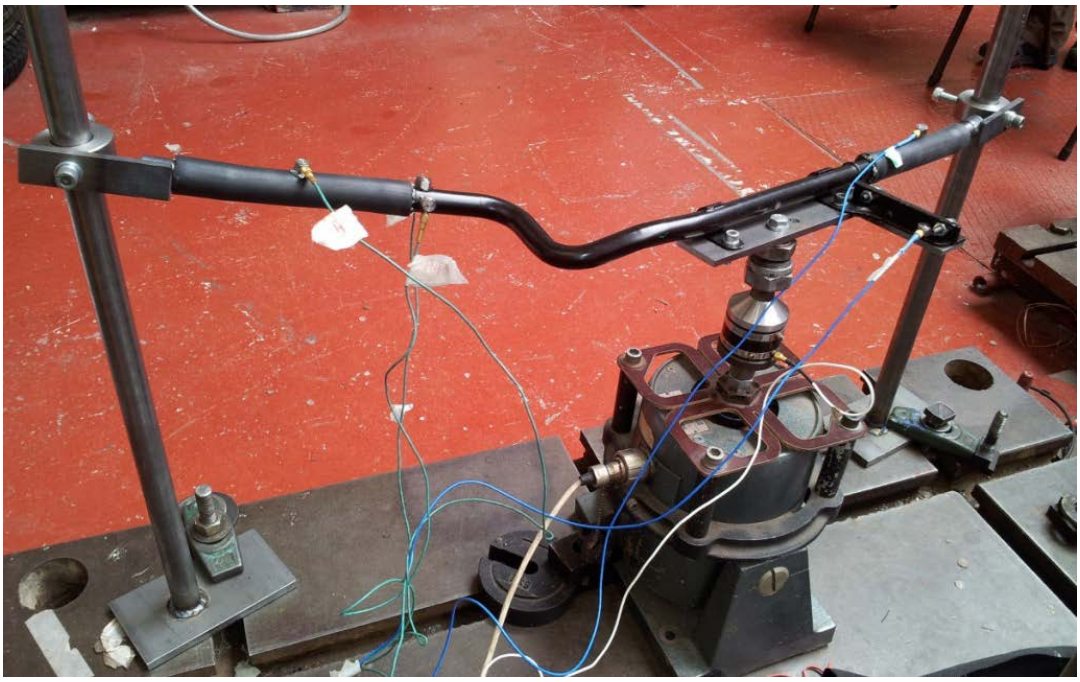


Figure 4.5: The vibration test setup for model #2

4.2.2 Excitation system

By applying excitation sources, kinetic energy can be injected into the test structure, then frequency response function can be measured by observing the behaviour of the structure. Several types of excitation schemes are employed in vibration testing such as (McConnell, 1995): a sudden release of a static load; mechanical vibration exciter based on either multi piston pumps or rotating unbalances; an impact force; electrohydraulic exciter and electromagnetic exciter, commonly known as a shaker. In this chapter, the characteristics of the two excitation methods used in this thesis' experimental work which are impact hammer for free vibration test, and shaker for forced vibration test, are described.

The electromagnetic shaker (Figure 4.6) was built from a moving cylindrical piece which was wrapped by a coil of wires (armature) coil and supported by a flexible bending membrane (flexure). The magnetic flux was proportionally generated with the current change in coil

which produces an electromagnetic field with north and south poles. The armature was located inside an inner permanent magnet or electromagnet which was rigidly mounted to the shaker's chamber and produces an axial force proportional to the coil current. When the applied current is sinusoidal, a periodic force is generated as a result and pushes the supported armature up and down with a sinusoidal waveform desired for vibration testing (Lang & Snyder, 2001).

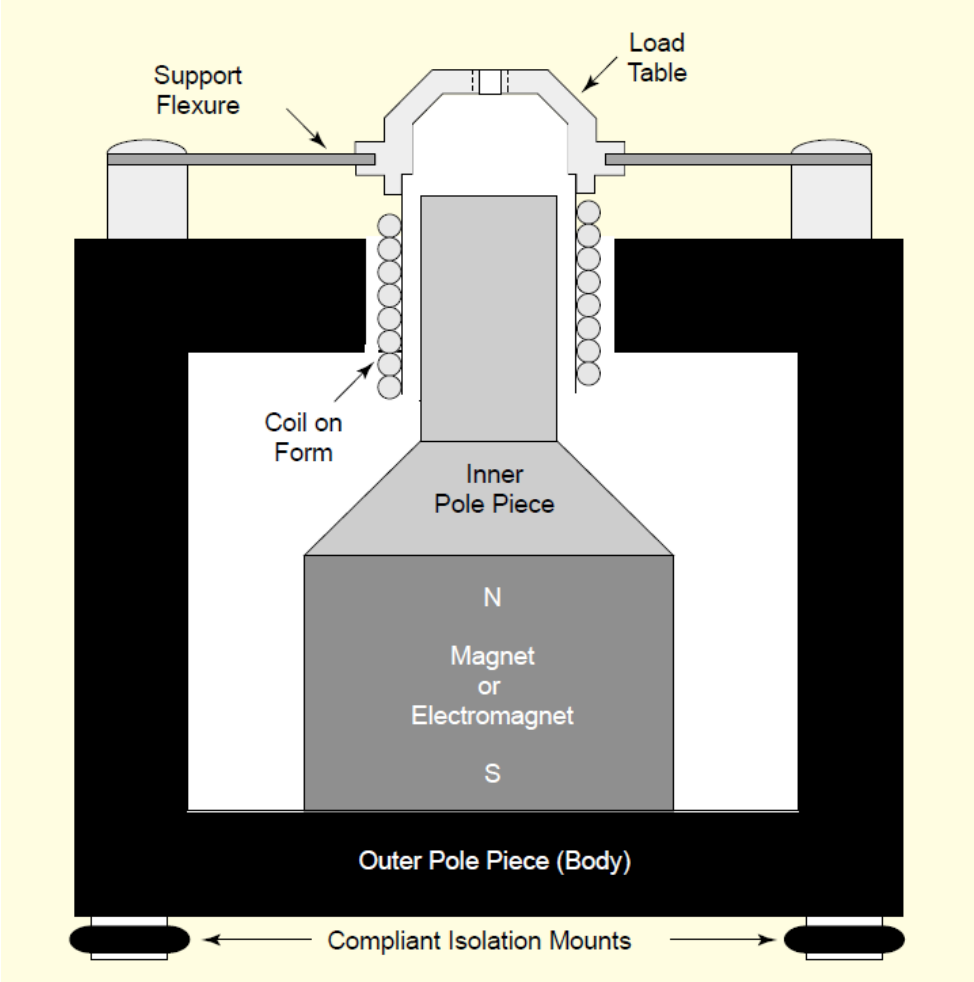


Figure 4.6: A schematic of components in electromagnetic shaker (Lang & Snyder, 2001)

Although the sinusoidal form of excitation is usually favourable to most vibration testing, the electromagnetic shaker is capable of any vibration pattern on demand corresponding to the input current and induced voltage. In comparison to the hammer test, these shakers can

provide controlled excitation in a wide frequency range and amplitudes with customized excitation pattern. `

Excitation in the form of sine functions at varying frequencies was introduced to the coolant rail by an electro-magnetic shaker as shown in Figure 4.7. The Ling Altec model 407 electromagnetic shaker is connected through a shaft to the plate where the coolant rail was mounted.

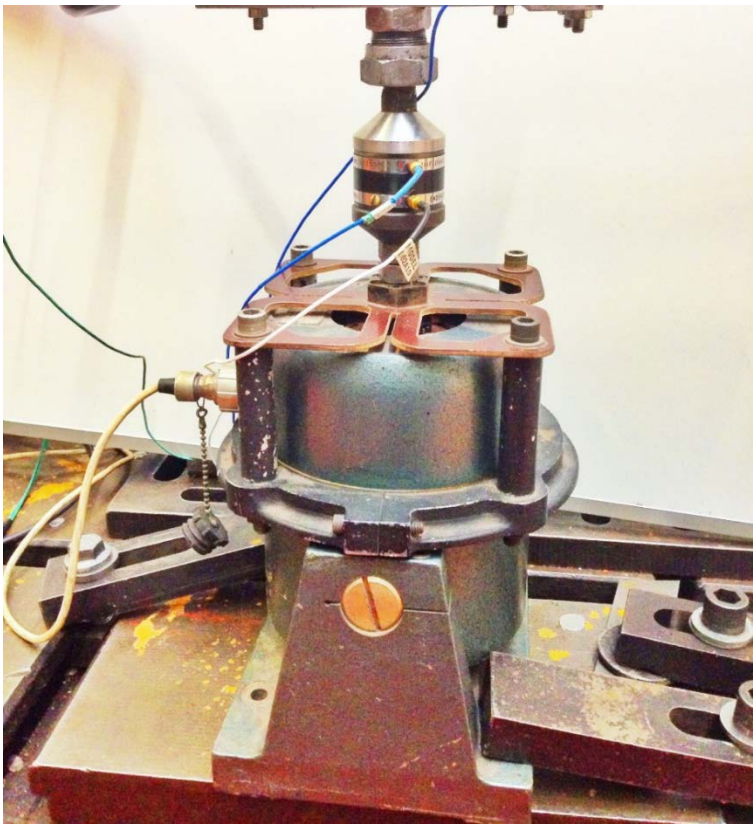


Figure 4.7: Ling Altec model 407 electromagnetic shaker

4.2.3 Sensing system

The frequency response function was derived to replicate the vibration behaviour in structures and consists of input and output signals which should be measured from the shaker and points of interests. The mechanical vibration dynamics can be observed in terms of ratio of input in the form of force, displacement, velocity or acceleration and the output in terms of displacement, velocity or acceleration. The force was usually captured by load cells and

acceleration was measured by piezoelectric accelerometers. The acceleration signals are integrated to derive the velocity and displacement signals.

The shaker shaft was equipped with an Endevco Impedance Head, Model 2110E. This mechanical impedance head includedd a force transducer (Load cell) and an accelerometer in one case which simplified the measurement of mechanical impedance as shown in Figure 4.8 It measures the input acceleration and input force to the rig plate through the shaft. Its wide frequency response, 2Hz to 5000Hz, and wide dynamic range to 500 g and 5000 Ibs, makes it useful in almost any application (R.R.Bouche, 1965). The compact and rigid design results in easy mechanical attachment to the structure. There was not any phase shift between acceleration and force over the useful frequency range.

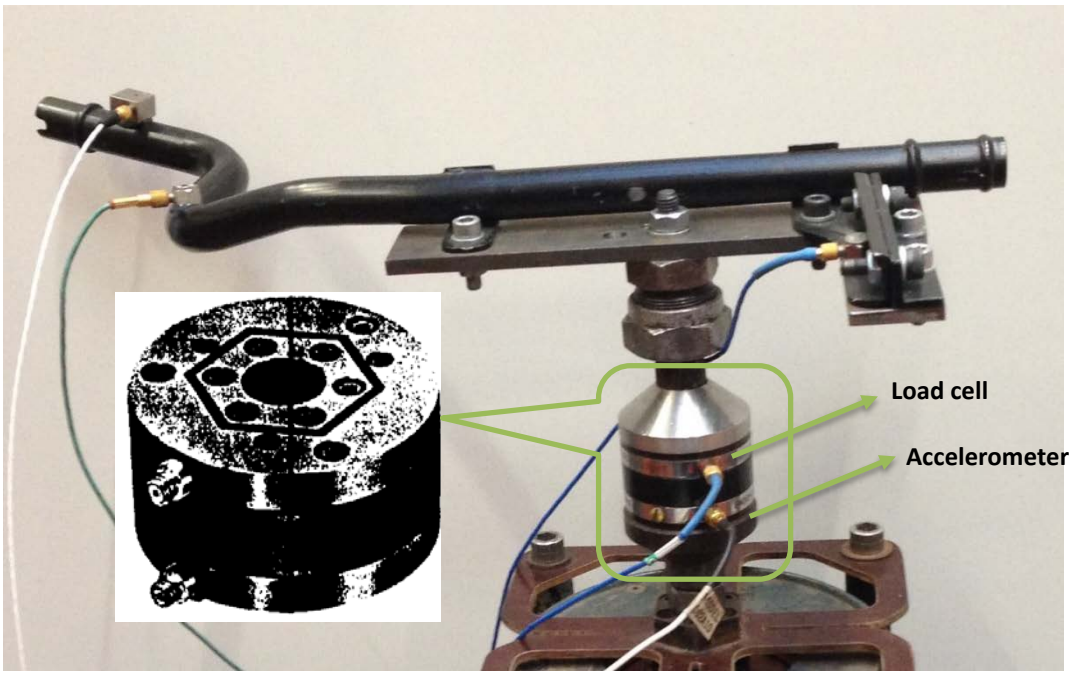


Figure 4.8: Impedance Head, Model 2110E

Moreover, a number of acceleration sensors were installed along the coolant rail in order to measure the induced acceleration by the shaker at the points of interest as shown in Figure 4.9. Two types of accelerometers, DJB Piezoelectric accelerometer, monoaxial model A/23 and triaxial model AT/04 were used in this research. The A/23 Piezoelectric accelerometer is

based on KONIC shear design sensing element, in which, lightweight (4.2gram), high resonant frequency (50 KHz) and wide operation temperature range (-50°C /+250°C) characteristics are suitable for EGR Coolant Rail test (DJB Instruments, 2008). Model AT/04 is a lightweight (12 gram) triaxial vibration sensor comprising of three charge output piezo-electric Konic Shear sensing elements mounted orthogonally within a titanium block, and welded construction, and with high resonant frequency characteristic (33 kHz in Z axis, 20 kHz in X/ Y axis) (DJB Instruments, 2008).

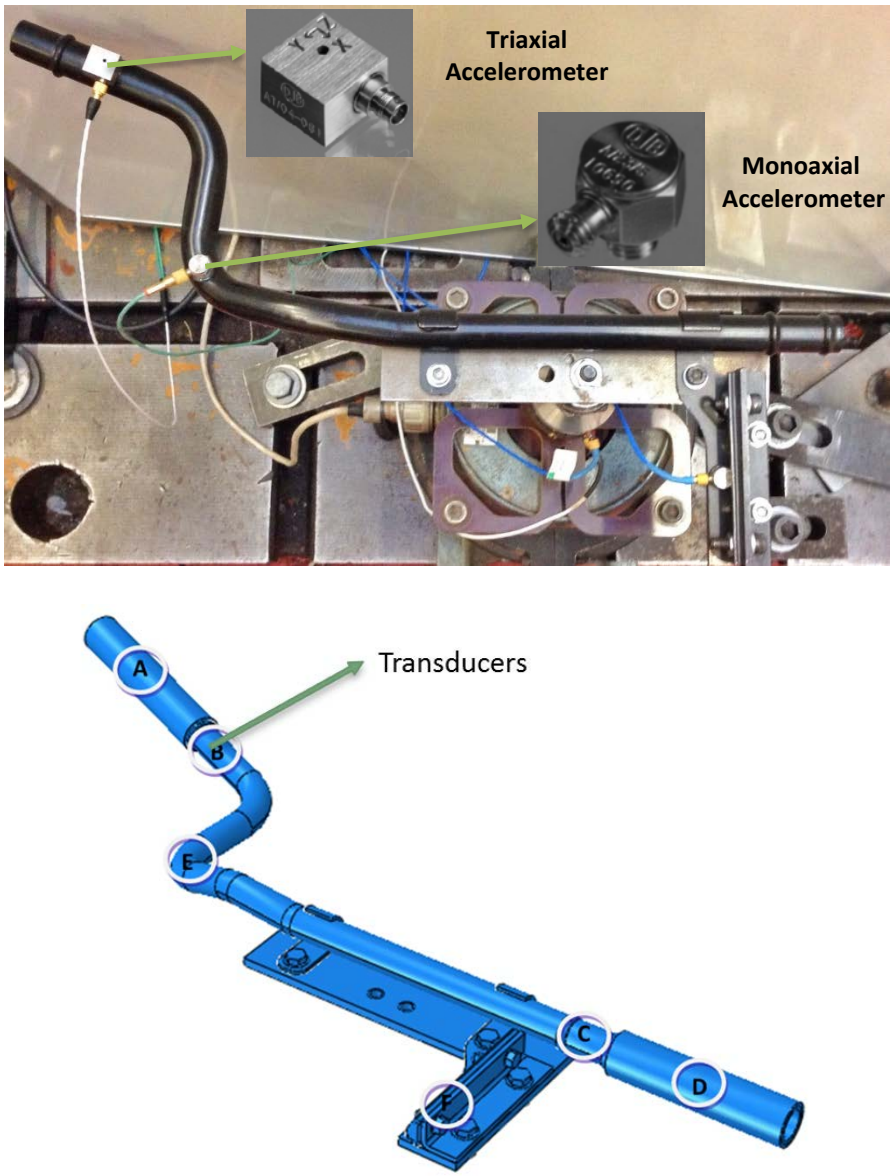


Figure 4.9: Setup of sensors on the coolant rail

The piezoelectric accelerometers are constructed of piezoelectric material such as quartz or alternatives such as ceramics in which analogue electrical charge in induced proportional to the input stress when these materials are compressed in response to acceleration/deceleration (Dytran Instrument, 2014).

The electric charge released by the piezoelectric element is measured in the unit of ppico Coulomb. In order to convert the charge output into a useable proportional voltage signal, a charge amplifier is necessary with charge output vibration sensors. A BERAN 700 series signal conditioning unit was used in this research for this purpose as shown in Figure 4.10. Before doing any test, the transducers must be calibrated.



Figure 4.10: BERAN 700 series Amplifier

Both load cell and accelerometer of Impedance Head, Model 2110E must be calibrated individually. In the first step of the calibration process, the shaker delivers a vibration signal at 40Hz with 2N force (F) output in solid mass of known weight 1 kg and 2 kg, (m_1, m_2) to calculate the effective mass of the shaker by using the equation below. The output acceleration (a_1 , a_2)is readable on the oscilloscope.

$$m_{effective\ mass} = \frac{a_2 m_2 - a_1 m_1}{a_1 - a_2} \qquad \text{Equation 4.1}$$

By reading out the acceleration and using the above equation, the effective mass of the shaker can be calculated, which was 0.76 kg. With the DJB accelerometer, a solid mass of known

weight and effective mass of shaker, the resultant frequency response function is a straight line according to the following equation.

$$A(\omega) = \frac{a}{F} = \frac{1}{m}$$ Equation 4.2

By substitution of effective mass, mass of weight and acceleration in above equation, the sensitivity of the force transducer can be calculated, which is 2.4 pC/N. The sensitivity of the accelerometer of Impedance Head is calculated by comparing with the amplitude from the DJB accelerometers installed in the same place as the impedance head. The resultant sensitivity is 187pC/g.

4.2.4 Data acquisition and analysis

The test control and data acquisition software for the vibration testing of the coolant rail were developed in the LabVIEW software. Figure 4.11 demonstrates how the natural frequencies were extracted from vibration test.

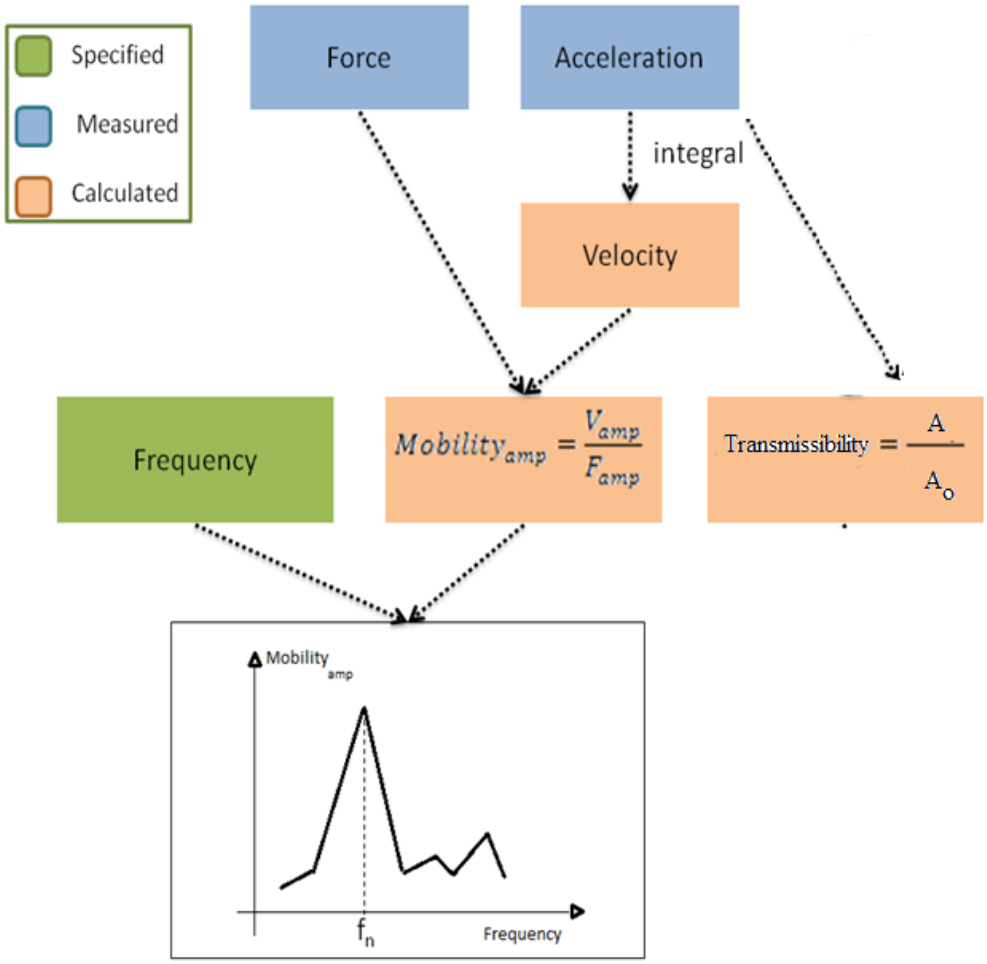


Figure 4.11: The schematic of data acquisition approach

The system works on the principle of measuring the mobility response of the coolant rail when excited over a range of frequencies (40 Hz -800 Hz). At each test frequency the shaker was run at an initial voltage command amplitude. The load amplitude was then measured and the absolute error value between the measured and desired load amplitude was computed and used to correct the input voltage amplitude. The input voltage was iterated until the error was within the predefined threshold at which point the responses from the transducers were recorded over 20 sine cycles. The same procedure is then repeated for the next frequency up to 800 Hz.

4.2.4.1 Vibration parameters

Vibration modes of the EGR coolant rail are characterised through extracting a relation between the input excitation point where it is connected to the shaker and the points of interest where the vibration modes are more apparent as shown in Figure 4.12. In this research, the vibration modes are measured based on the mechanical mobility and transmissibility terms which are defined in the following. Traditionally, the mechanical mobility method is widely used in structural dynamic tests for obtaining the dynamic performance parameters of various vehicle components because of its flexibility of application as well as its capability to represent the dynamic characteristics of a complex component.

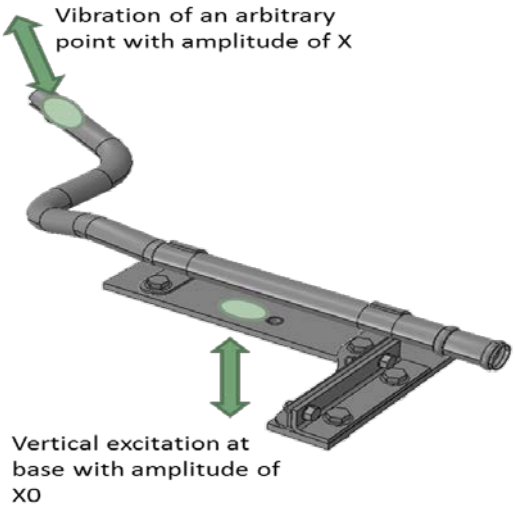


Figure 4.12: An example of points of interest in EGR coolant rail

The general expression for the mobility function can be expressed as an alternative form of frequency response function (Ewins, 2000)

$$M_{jk}(\omega) = \frac{V_j}{F_k} = i\omega \sum_{r=1}^{n} \frac{\left({}_r\Phi_j\right)\left({}_r\Phi_k\right)}{\lambda_r^2 - \omega^2} \qquad \text{Equation 4.3}$$

Where:

- M_{jk} : mobility function between point *j* and *k*
- V_j : velocity at point *j*
- λ_r^2 : eigenvalue of the r^{th} mode
- F_k : driving input force at point *k*
- ${}_r\Phi_j$: j^{th} element of the r^{th} eigenvector $\{\Phi\}_r$ (i.e. the relative displacement at that point during vibration in the r^{th} mode)
- *n*: number of degrees of freedom (modes)

Equation 4.3 indicates a direct connection between the modal properties of a system and its response characteristics.

Transmissibility can be used to identify the modal parameters namely natural frequency, mode shape, and damping factor. This parameter explains the influence of input displacement amplitude at the exciting point to the resulting displacement amplitude at the point of interest.

$$Transmissibility = \frac{A}{A_0} \qquad \text{Equation 4.4}$$

Transmissibility measures the amplitude of the vibrational response (A) per amplitude of the vibrational input (A_0). Therefore the higher the transmissibility, the higher the vibration amplitude generated for a given input excitation. Each peak of the transmissibility response corresponds to a resonant frequency. Plotting the transmissibility modulus versus frequency is one of the technique of presenting the data. At resonance, while the excitation frequency

is equal to the natural frequency $\omega=\omega_n$, the transmissibility modulus become maximum and is limited only by the amount of damping in the system.

4.2.4.2 The LABVIEW program

The test was set up by entering parameters such as start frequency, stop frequency, frequency increment, number of samples and threshold force (Figure 4.13). From the measured data, Mobility response is plotted against excitation frequency. The while loop defining the program is terminated when the frequency reaches a maximum defined by the user. The detailed procedure of vibration testing is presented in Figure 4.14. Figure 4.15 shows the block diagram of the program for vibration testing in LabVIEW software.

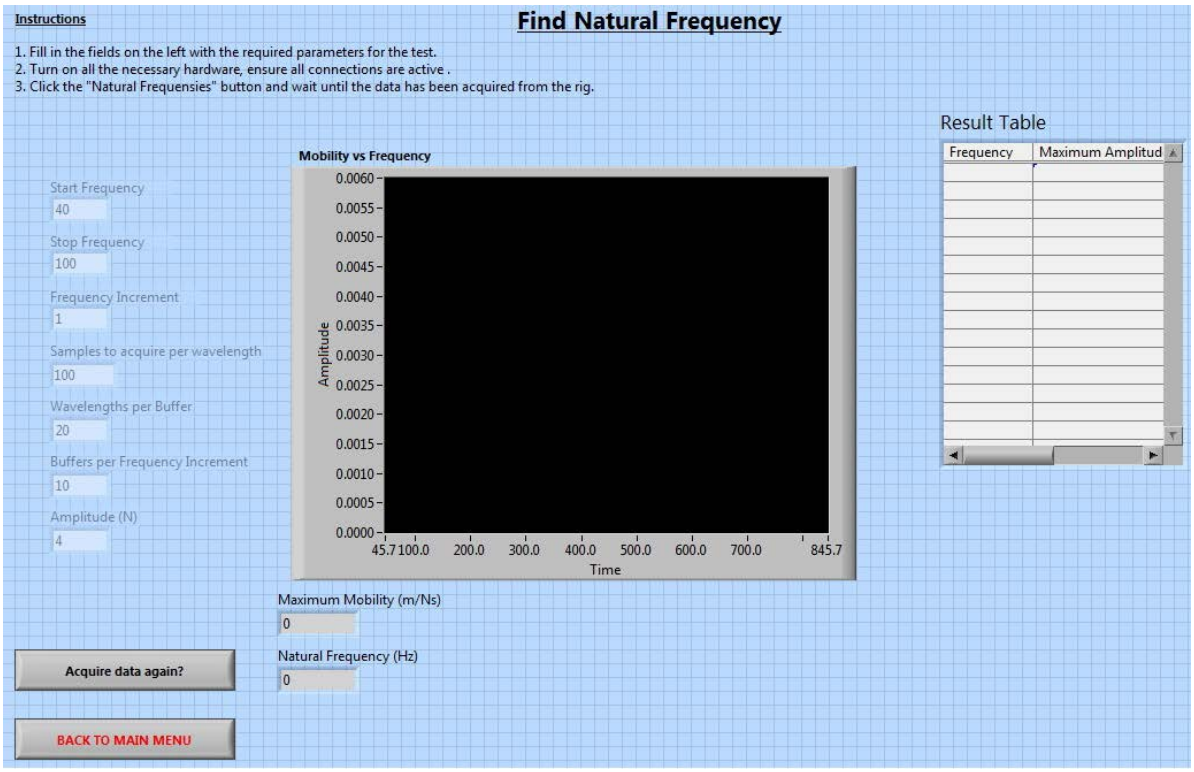


Figure 4.13: Block diagram of vibration test control/measurement

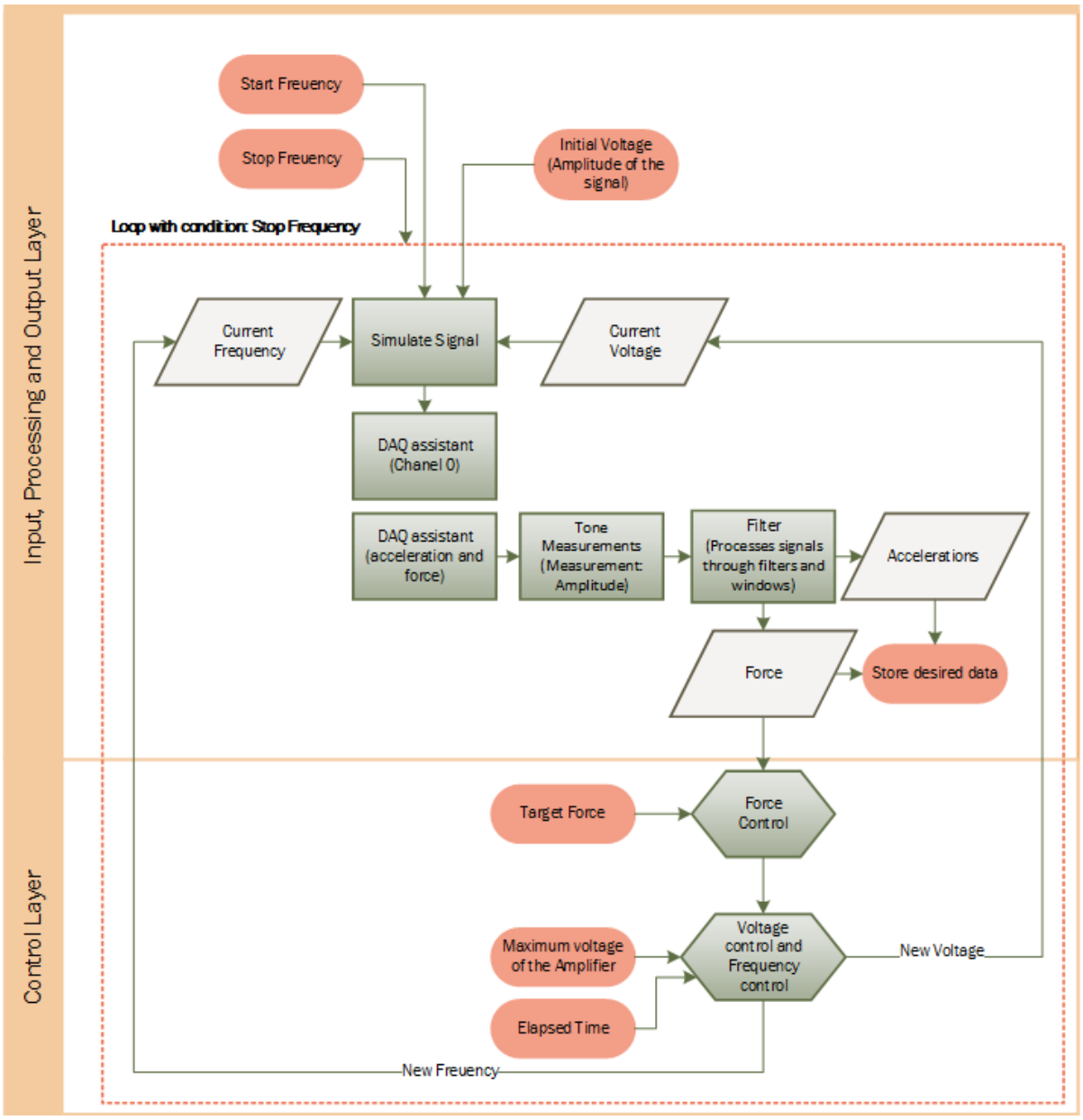


Figure 4.14: Flowchart of the data flow and procedure

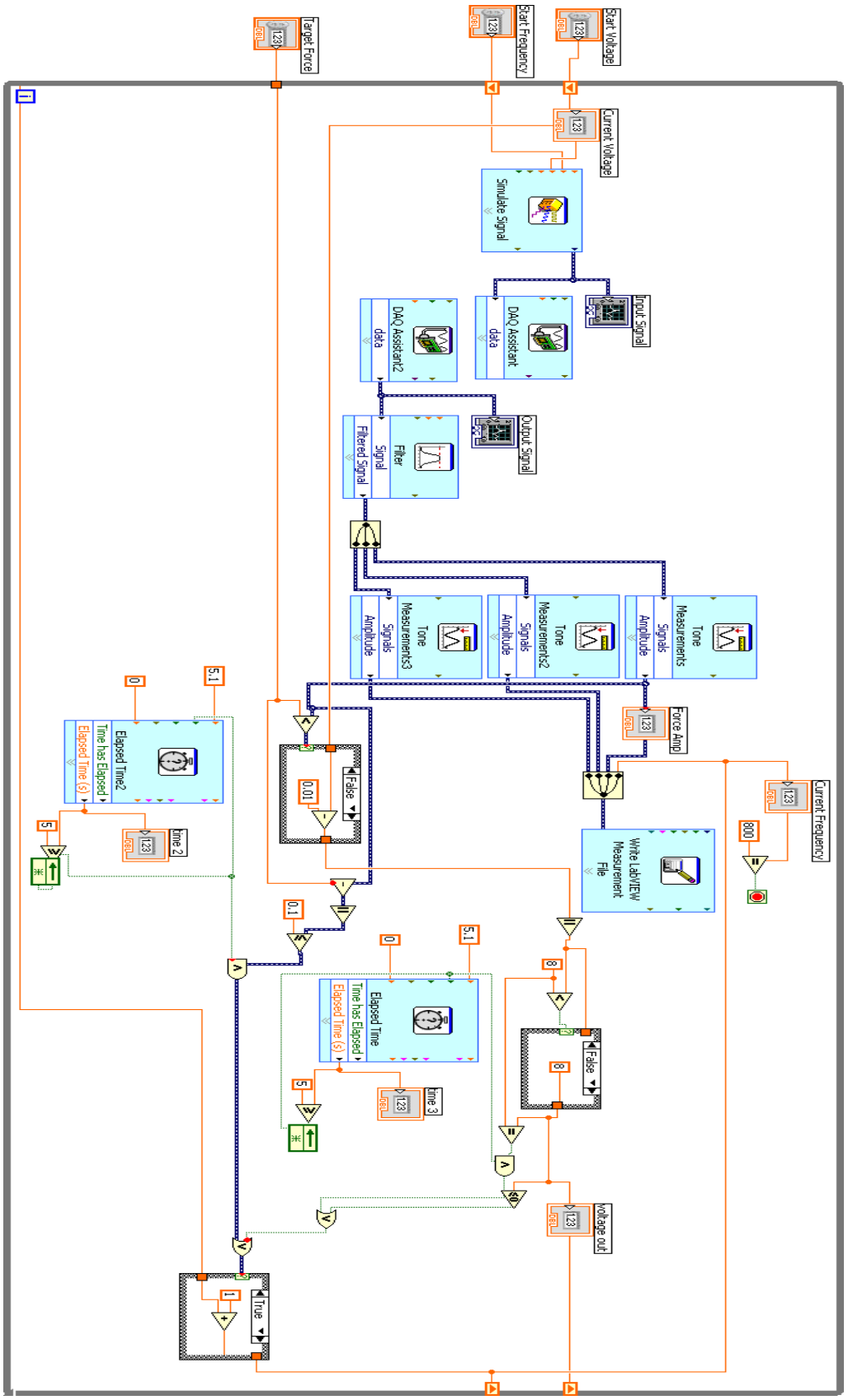


Figure 4.15: Vibration test program

4.3. Free vibration test

In order to eliminate rig and constraint effects, the natural frequency analysis without any boundary conditions (free-free analysis) has been done in this step. An instrumented hammer was used for hitting the coolant rail. The dominant frequencies in the response of the structure depend on the applied force and what kind of hammer that is used.

The impact vibration testing by hammer as a usual and preliminary vibration characterization test come with advantages and drawbacks. To start with advantages, the hammer test setup and analysis of output data is fairly simple. The instrumented hammer with load cell can be connected to the most common data acquisition devices and provide the frequency domain analysis using post-processing software promptly. It is also offered in a portable version where the data is recorded in universal flash memory and transferred to computers for further post-processing. Hence, its accessibility and simplicity of hammer usage in addition to its portability and lower initial and maintenance cost in comparison with shaker setup introduces a powerful probe tool for quick verification and preliminary observation of vibration in structures. Nevertheless, the hammer test is deprived of fidelity control in the impact frequency and amplitudes as it is an open loop test. This implies that the hammer testing would be useful only if test is desired to be carried out in linear range where the structural and geometry nonlinearities are neglected. As another shortcoming to this method, the range of frequency can be very limited and strongly depends on the hammer tip hardness and its shape. Also, the hammer test inconsistency is always a question due to human engagement in conducting the test. The angle of impact should be preferably as perpendicular as possible to the surface and the same spot should be impacted to check the repeatability of vibration testing. Moreover, the hammer test does not guarantee to excite all the modes of

interest and requires high experience and consistency in load impact for appearance of the modes of interest.

A vibration test rig for free-free analysis has been designed and built as shown in Figure 4.16. This vibration testing method makes use of the fact that the structure responses with its eigenvalues when a structure is excited using of a pulse. It was connected to the computer in a similar manner to that illustrated in Figure 4.17 through the FFT-analyser (Ole Dossing, 1988).

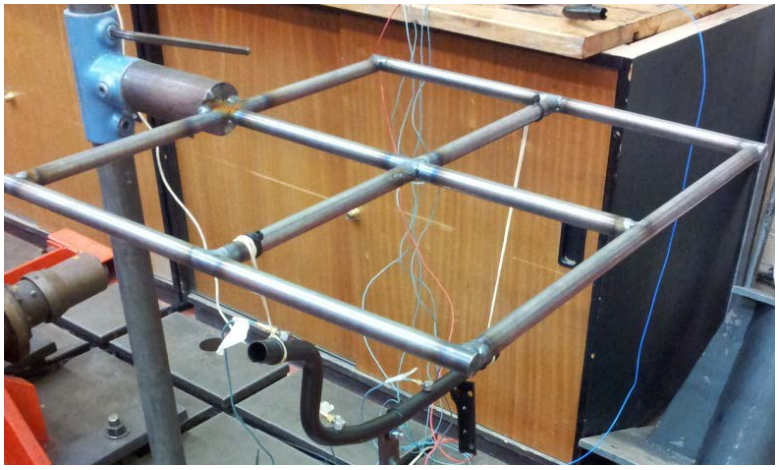


Figure 4.16: free- free vibration test set up

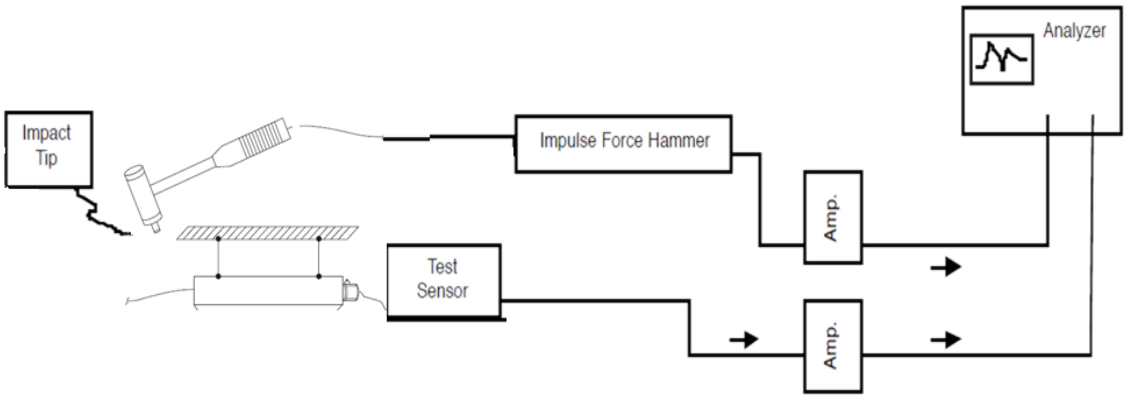


Figure 4.17: schematic setup for free- free vibration system

In order to estimate the natural modes of a free system, the tube is suspended from soft elastic cords. Then the low frequency rigid body modes generated by the effect of elastic cords is quite away from the natural modes of the tube. Then an instrumented hammer can be employed to hit the rail in order to provide impact excitation and the acceleration is recorded using TestPoint software for frequency response (FR) analysis and mode extraction.

The test results in the conducted experiments didn't cover the whole range of resonant modes of the coolant rail and a few of modes are more difficult to excite and therefore exhibited less response in terms of acceleration to the excitation in specific directions. In addition, a few modes need rotational excitation or even a more complex type of excitation in order to activate some complex mode shapes that are a combination of rotational and directional modes. In the hammer test for extraction of free modes, the hammer was applied in different directions and location with various impact forces. As a result, a substantial number of tests were carried out to make sure that all the modes were identified. The directions are chosen somehow to cover the excitation in most important and dominant directions where the first modes are most likely to occur.

4.4. Damping factor

The modal frequencies are distinguished simply by detecting the maximum magnitude on the Frequency Response Function (FRF), but the modal damping is not easy to identify and will regularly be the parameters with uncertainty in measurement.

The height of the resonance peak is determined as a function of damping, which can be assessed using the half power method. The half power method can be applied by means of the peak amplitude technique. The half power method identifies the half power frequency

bandwidth from two half power points (-3dB) on the resonance frequency of the mode as shown in Figure 4.18.

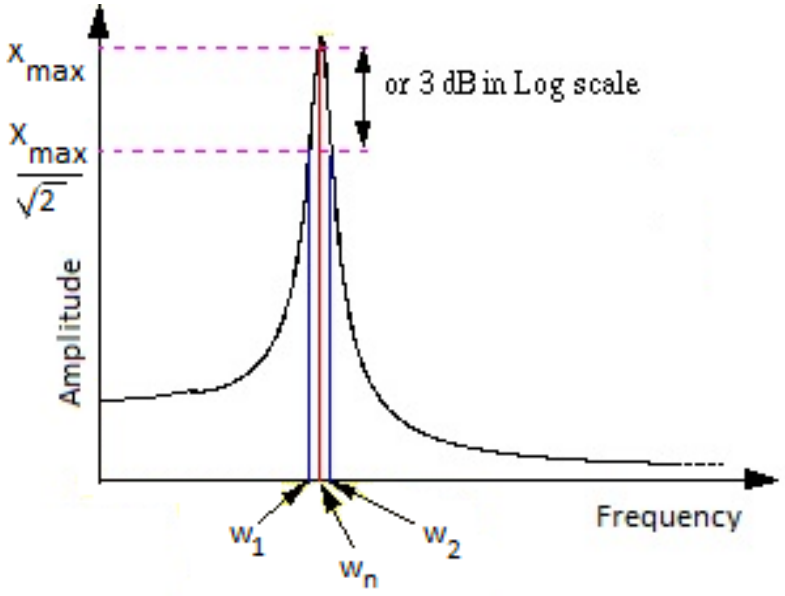


Figure 4.18: Half power bandwidth method

The damping factor can be determined from the following equation (Friswell, M. I. and Mottershead, J.E., n.d.).

$$\zeta = \frac{1}{2}\frac{w_2 - w_1}{w_n} \qquad \text{Equation 4.5}$$

The formula demonstrates that the more the damping, the higher the frequency range between these two points. Half-power bandwidth is described as the ratio of the frequency range between the two half power points to the natural frequency at this mode.

The corresponding values of damping in each particular natural frequency were extracted by using the half power bandwidth method.

4.5. Summary

In this chapter, the vibration rig, measurement and data acquisition devices were introduced. The process of forced vibration testing and rig developments was explained for three

conditions: coolant rail without rubber hose, coolant rail with rubber hose but no fluid, and finally the coolant rail and rubber hose attached to it and filled with water. At the next step, the free-free vibration was initially carried out on the coolant rail and its attached brackets in order to determine the natural frequency in free boundary condition. The methods to calculate the mobility, transmissibility and damping were also described in this chapter to use for post-processing and analysis of vibration. These methods are used in the next chapter for the comparison of natural frequencies and modes in abovementioned cooling rail setups.

Chapter 5: EGR Coolant Rail Finite Element Modelling

5.1. Introduction

As explained in Chapter 2, the FE approach is used for idealisation and discretisation of a complex geometry to perform a wide range of mechanical analysis. The FE discretisation are developed and implemented in different approaches where a performance index is targeted for investigation. This can change the way that a problem is idealised and discretised for certain analyses and applications. These approaches are including, but not limited to, the mesh type i.e. the way that each individual element is formulated, mesh size and the question that how refined an FE model should be, simplification of complex structure and decide how much geometrical data should be involved to represent a model.

In this research, the FE simulations have been organised in the following categories:

I. Model #1: Coolant rail without rubber hoses: a finite element model which is capable of accurately representing the vibration testing of a Diesel Engine EGR Coolant Rail without rubber hoses attached.
II. Model #2: Coolant rail with rubber hoses: an extended finite element model to include rubber hoses which are attached and grounded.
III. Model #3: Coolant rail with equivalent spring and damper: a simplified extended FE model of the coolant rail, including a representation of the rubber hoses in terms of stiffness and damping.
IV. Model #4: Coolant rail with water flowing inside it.

In this chapter, the finite element modelling for simulation of EGR coolant rail behaviour is created, then its validity is studied compared to the vibration test data. Firstly, a standard methodology for modelling, simulation, and analysis is described. The applicable method is identified based on various features including the reinforcement modelling in the rubber

hoses, contact modelling, analysis type, boundary condition setup and different types of meshing techniques and mesh density. Following section two, the simulation of damping is explained in section three. Having implemented the FE models, a number of simulations are performed in section four and the FE results are verified through comparison with corresponding vibration test procedures explained in chapter 4. In addition to validation of the FE models of coolant rail with and without rubber hoses, eventually a simplified extended FE model of the coolant rail, including a representation of the rubber hoses is developed and validated against test results and extended FE model.

In this chapter, Finite element models #1, #2 and #3 are explained and model #4, coolant rail with water flowing inside it, is discussed in the next chapter. The simulation approach in this research has been organised through the process shown in the chart below, as demonstrated in Figure 5.1.

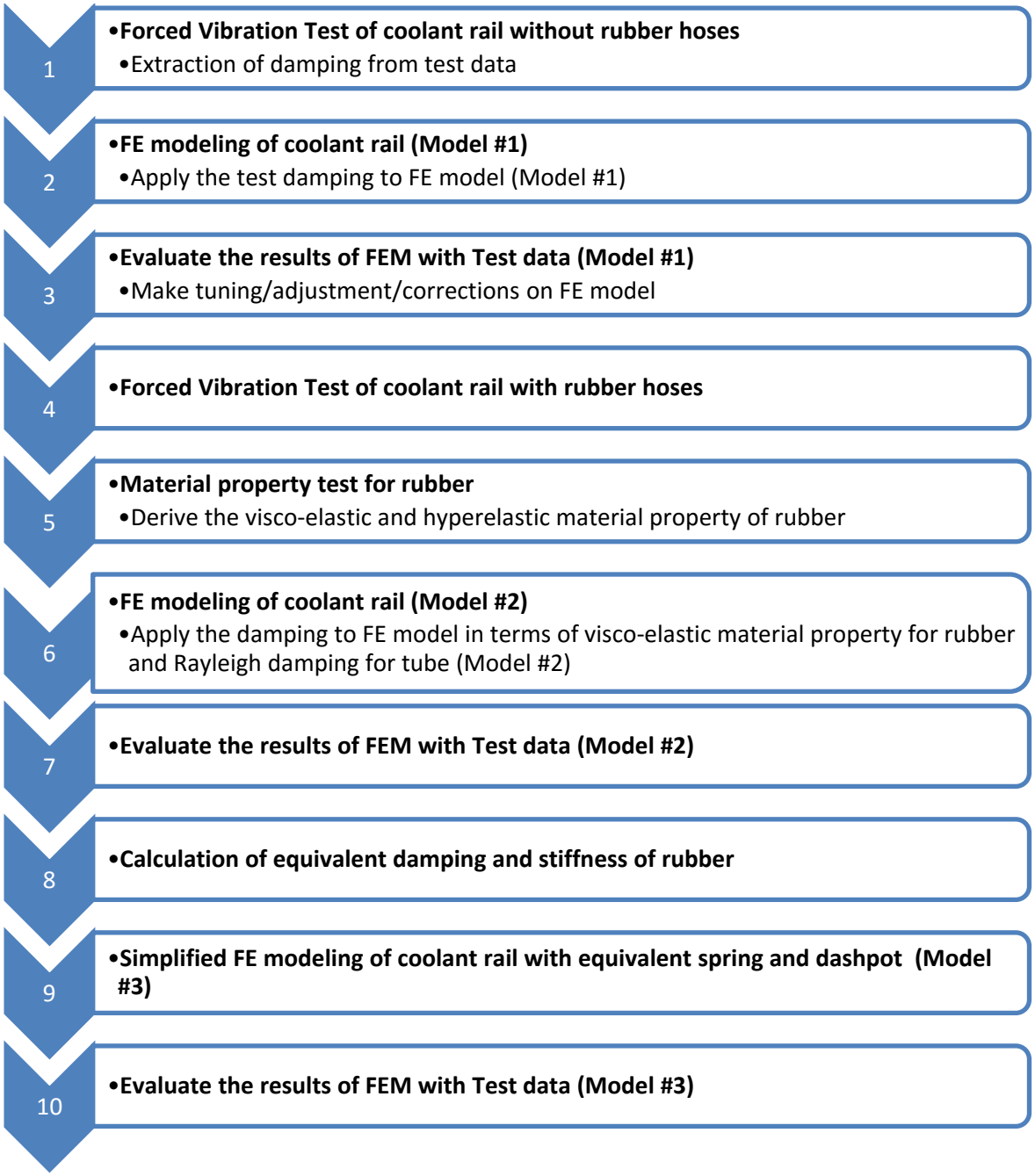


Figure 5.1: Procedures for FE simulation of EGR coolant rail

5.2. Methodology development for FE modelling

5.2.1 Coolant rail geometry

The detailed geometry of the EGR coolant rail tube was provide by JLR through a CAD model in IGES format which is an acceptable extension to import into Abaqus CAE environment. For

checking FE model validity against test outputs, the FE model was built to correspond as closely as possible to the test condition. The rig was modelled in as much detail as possible including plates, bolts, and nut in Abaqus™ CAE sketch tools. The generated models is shown in Figure 5.2 for the models without rubber hose (a) and with rubber hose (b).

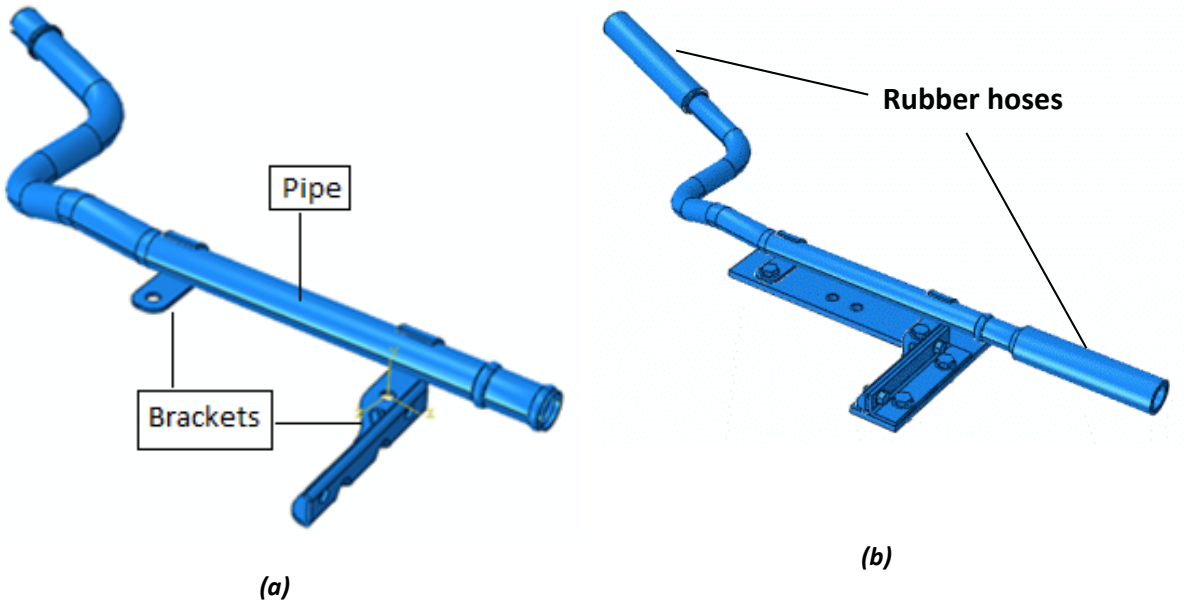


Figure 5.2. (a) Coolant rail without rubber hoses, model #1, (b) coolant rail with rubber hoses model #2

5.2.2 Rubber Hose Reinforcement modelling

Taking advantage of the use of commercial finite element software—ABAQUS™, the reinforcement cord in the rubber hose can be represented by rebar elements and the rubber can be represented by solid elements. In developing the FE models of coolant rail with rubber hoses, a method on the basis of rebar elements concept was used to model the rubber hoses. Rebar elements are employed to describe layers of uniaxial reinforcement in surface elements, shell and membrane (suchlike layers are treated as a smeared layer with a constant thickness equal to the area of each reinforcing bar divided by the reinforcing bar spacing). In this modelling approach, rebar elements are assumed as an embedded surface with little thickness in comparison with its topping thickness in order to enhance the strength of the

entire layer. The host region makes a stable shape for the entire body where the embedded region is typically created of very thin layers (Behroozi, et al., 2012) (Simulia, 2013). In rubber hoses modelling, reinforcements are actually cords embedded in rubber which are woven in some directions.

Figure 5.3 shows a rubber hose specimen that was used for material testing and simulation. As it can be seen, the yellow lines represent cords embedded into the rubber region.

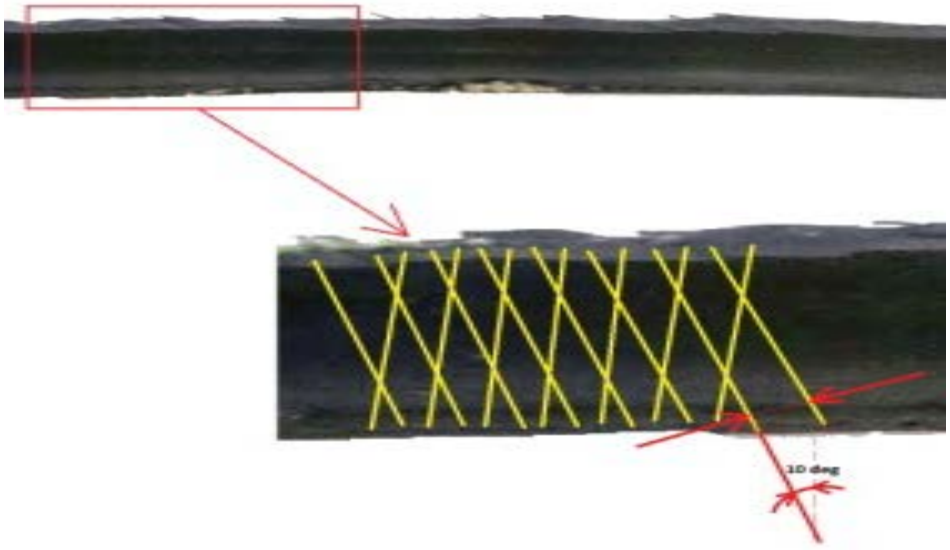


Figure 5.3: Rubber hose specimen

The following data (Table 5.1) are essential inputs for modelling rubber hoses behaviour by means of the rebar method:

Table 5.1: Reinforcement cord data

Cords Spacing: space between centre of two consecutive cords:	(2mm)
Cords cross section area	(0.125 mm^2)
Cord material property	(Cotton fibre- Poisson's Ratio: 0.3, Young's Modulus: 6650 Mpa, Density: 541 kg/m^3)
Cords orientation inside the rubber hose	(10 , -10 deg)
Number of cord layers woven on each other	(2 layers)

5.2.3 Vibration Analysis type

In order to simulate the EGR coolant rail vibration behaviour, several analyses exist which are explained in the following sections, and suitable vibration analysis was chosen to acceptably achieve the required efficiency and precision in EGR coolant rail mechanical behaviour.

First, normal modes analysis was performed in the frequency range of 0 to 1600 Hz. Then a forced response analysis was performed in the frequency range 50 to 800 Hz.

5.2.3.1 Eigenvalue extraction

One of the important aspects of vibration analysis is extracting the eigenvalues of the system to achieve its natural frequencies of vibration. The mathematical eigenvalue problem is a classical field of study, and plentiful work has been done to provide eigenvalue extraction techniques such as Wilkinson's book (Wilkinson, 1965). The eigenvalue problems arising out of finite element models are specific cases: they include large but typically narrowly banded matrices, and only a small number of eigenpairs are generally needed. The matrices are symmetric for many significant cases. The eigenvalue problem for natural modes of vibration of a finite element model is based on equation 5.1.

$$(\mu^2[M] + \mu[C] + [K])\{\phi\} = 0 \qquad \text{Equation 5.1}$$

Where $[M]$ is the mass matrix, $[C]$ is the damping matrix, $[K]$ is the stiffness matrix; μ is the eigenvalue, which is an imaginary eigenvalue for symmetric eigenproblems, $\mu = i\omega$ where ω is the circular frequency, and ϕ is the eigenvector—the mode shape of vibration. This equation is available immediately from a linear perturbation of the equilibrium equation of the system.

The Lanczos theory of Eigen-solver was applied to extract natural frequencies in the first step because of its performance and providing a high level of details as an appropriate approach to carry out the frequency analysis with all boundary conditions.

The implementation of the Lanczos Eigen solver as a great tool for extraction of the eigenvalue and the corresponding eigenvector of a symmetric generalized eigenproblem was discussed by a number of authors; (Ericsson & Ruhe, 1980) (Parlett, 1980) (Simon, 1984) (Parlett & Nour-Omid, 1989). The Lanczos process consists of several Lanczos runs, in each of which a set of iterations steps is completed (Simulia, 2013). For each Lanczos run the subsequent spectral transformation is exerted

$$[M]([K] - \sigma[M])^{-1}[M]\{\phi\} = \theta[M]\{\phi\} \qquad \text{Equation 5.2}$$

where $\{\phi\}$ is the eigenvector, θ is the eigenvalue and σ is the shift. This transformation causes rapid convergence to the looked-for eigenvalues. The eigenvectors of the symmetrized problem (Equation 5.1) and the transformed problem (Equation 5.2) are similar, though the eigenvalues of the original problem and the transformed problem are related in the following way:

$$\omega^2 = \frac{1}{\theta} + \sigma \qquad \text{Equation 5.3}$$

A frequency range of 0 to 1600 Hz was assumed to extract the natural frequencies and mode shapes.

5.2.3.2 Steady state dynamics-Modal

Steady-state linear dynamic analysis predicts the linear response of a structure exposed to continuous harmonic excitation. Usually such analysis is carried out as a frequency sweep by applying the loading at a series of various frequencies and recording the response. In many cases steady-state linear dynamic analysis employs the set of extracted eigenmodes in a prior eigenfrequency step to compute the steady-state solution as a function of the frequency of the applied excitation. Abaqus™/Standard also has a "direct" steady-state linear dynamic analysis method, wherein the equations of steady harmonic motion of the system without using the eigenmodes are solved directly, and a "subspace" steady-state linear dynamic analysis technique, wherein the equations are projected onto a subspace of carefully chosen eigenmodes of the undamped system (Simulia, 2013). These options are intended for systems in which the behaviour is dependent on frequency, for when the model includes damping, or for systems in which the governing equations are not symmetric. These methods are presented in the following section.

Steady state dynamics-Modal

Eigen value analysis and mode-based steady state dynamic analysis procedure were employed to obtain coolant rail response (without rubber hoses, model #1) to harmonic excitation. First, normal modes analysis was performed in the frequency range 0 to 1600 Hz. Then a mode-based steady state dynamic response analysis was performed in the frequency range 50 to 800 Hz.

Linear dynamic analysis using modal superposition is computationally reasonable and can obtain beneficial insight into the dynamic behaviour of a system. The basic theory of modal superposition is that the response of the structure is stated in terms of a relatively small number of eigenmodes of the system. The orthogonality of the eigenmodes uncouples this system. Moreover, only eigenmodes which are close to the frequencies of interest are typically required.

The projection of the equations of motion of the system onto αth mode gives

$$\ddot{q} + c_\alpha \dot{q} + \omega_\alpha^2 q_\alpha = \frac{1}{m_\alpha}(f_{1\alpha} + if_{2\alpha})exp(i\Omega t) \qquad \text{Equation 5.4}$$

where q_α is the amplitude of mode α, c_α is the damping associated with this mode which will be explained in the section 5.3, ω_α^2 is the undamped frequency of the mode, m_α is the general mass associated with the mode, and $(f_{1\alpha} + if_{2\alpha})\exp(i\Omega t)$ is the forcing associated with this mode.

Steady state dynamics-subspace and direct

Abaqus™/Standard has "subspace" procedure that uses some of the eigenmodes of the system on which the equilibrium equations are projected. The system's eigenmodes are used as a set of global basis vectors for computing the dynamic response, even though the system exhibits nonlinear or frequency-dependent effects during the dynamic response. This method is cost-effective compared to fully nonlinear dynamic response analysis developed in terms of all the system's degrees of freedom.

The discretized form of the linearized dynamic virtual work equation for a structural system can be expressed as (Simulia, 2013)

$$\left\{M^{NM}\ddot{u}^M + C^{NM}\dot{u}^M + (K^{NM} + iK_s{}^{NM})u^M - P^N\right\} = 0 \qquad \text{Equation 5.5}$$

where the C^{NM} is the viscous damping matrix, M^{NM} is the mass matrix, K^{NM} is the stiffness matrix, ${K_s}^{NM}$ is the imaginary stiffness proportional damping matrix representing a structural damping matrix, $\dot{u}$ and $\ddot{u}$ are the velocity and the acceleration, P^N is the external load vector and M and N are degrees of freedom.

The eigenfrequency step prior to the subspace-based steady-state dynamic analysis has extracted n eigenmodes of the undamped system using

$$(-\omega^2 M^{MN} + K^{MN})\phi^N = 0 \qquad \text{Equation 5.6}$$

where ω is the eigenfrequency in radians/time and ϕ^N is the eigenvector. The procedure assumes that the complex displacement changes for the damped system can be written in the form

$$u^M = \phi_\beta^M a_\beta\,, \quad \beta = 1, \dots, n \qquad \text{Equation 5.7}$$

where α_β are the complex modal amplitudes. Using Equation 5.7 in Equation 5.5 and premultiplying with ϕ_α, the equation of motion projected onto the subspace is provided:

$$\phi_\alpha^N M^{NM} \phi_\beta^M \ddot{a}_\beta + \phi_\alpha^N C^{NM}(\Omega)\phi_\beta^M \dot{a}_\beta + \left(\phi_\alpha^N K^{NM}(\Omega)\phi_\beta^M + i\phi_\alpha^N K {K_s}^{NM}(\Omega)\phi_\beta^M\right)a_\beta = \phi_\alpha^N P^N(\Omega),\ \alpha, \beta = 1, \dots, n \qquad \text{Equation 5.8}$$

A similar option is provided for direct harmonic response analysis without using the eigenmodes as a basis. The direct method is significantly more expensive computationally than the modal method. It is needed if the system is non-symmetric or if the system's behaviour includes frequency-dependent parameters. The formulation is based on the discretized form of the dynamic virtual work equation as

$$\left\{M^{NM}\ddot{u}^M + (C_{(m)}^{NM} + C_{(k)}^{NM})\dot{u}^M + \left(K^{NM} + i{C_s}^{NM}\right)u^M - P^N\right\} = 0 \qquad \text{Equation 5.9}$$

The “subspace” technique is normally less expensive than the direct method. Subspace-based steady-state harmonic response analysis procedure was used for vibration analysis of coolant

rail with rubber since this method allows frequency-dependent effect to be modelled and is greatly cheaper than the direct analysis technique. Structural and viscous damping can be included in the procedure using the Rayleigh and structural damping coefficients specified under the material definition. The procedure can also be used for viscoelastic material modelling. Discrete damping such as mass, dashpots, spring, and connector elements can be included. The main benefit of this technique is that it allows frequency dependent behaviour to be considered at a relatively small cost increase over the purely linear analysis via the "modal" procedure.

5.2.3.3 Base motions in modal-based procedures

The support motion is simulated by "base motion" since vibration comes through the structure constraint. The suppressed degrees of freedom are grouped into one base.

The rig plate motions are *relative* to the base motion u_b. The total response u_t of the dynamic system will now consist of the relative response $\{u\}$ and the applied base motion excitation $\{u_b\}$ as presented in the equation 5.10.

$$\{u_t\} = \{u\} + \{u_b\} \qquad \text{Equation 5.10}$$

with similar expressions for velocities and accelerations. Substituting $\{u_t\}$ in the linearized equation of motion gives

$$[M]\{\ddot{u}\} + [C]\{\dot{u}\} + [K]\{u\} = -[M]\{\ddot{u}_b\} \qquad \text{Equation 5.11}$$

The base acceleration is converted into applied inertia loads $-[M]\{\ddot{u}_b\}$. Here it has been assumed that there is no damping on rigid body modes. The base motion vector can be stated in terms of the rigid body mode vectors $\{T\}_j$ and time dependent base motion values Z_j :

$$\{u_b\} = \sum_{j=1}^{6}\{T\}_j Z_j \qquad \text{Equation 5.12}$$

Projecting the equation of motion into the eigenspace we have

$$\ddot{q}_m + \frac{c_m}{m_m}\dot{q}_m + \frac{k_m}{m_m}q_m = -\sum_{j=1}^{6}(T_m)_j \ddot{z}_j \qquad \text{Equation 5.13}$$

where q_m is the relative generalized coordinate for the mode m; k_m, c_m and m_m are modal stiffness, modal damping, and modal mass, respectively; and j is degree of freedom.

5.2.4 Contact modelling

The bracket and tube nodes were merged together providing a Surface-to-Surface contact with specified tolerance. The tube and bracket were joined together during manufacture of the coolant rail using resistance welding hence it was reasonable to assume that the whole inner area of bracket and outer surface of tube were welded together. Therefore assumption of merging all the contact nodes is acceptable.

The interaction is built to deal with the contact problem between bolt and rig plate as well as the rig plate and shaker rod. In order to prevent penetration of elements of one surface by another one, the contact mechanism can be described between two opposite surfaces of a contact pair. In this research, a surface-to-surface contact type was selected to model the behaviour of solids in their interaction. In this technique, the contact condition is enforced between a group of adjoining nodes in slave and master surfaces to provide an improved enveloping and more precise contact interaction.

5.2.5 Meshing techniques

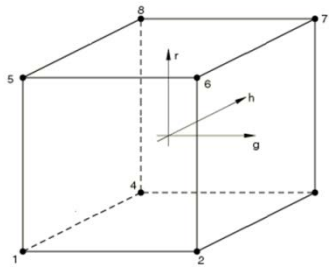
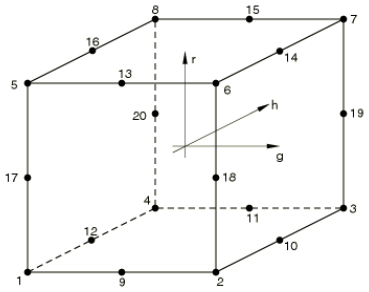
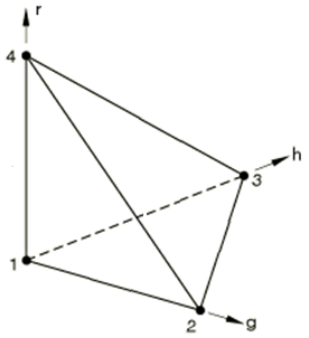
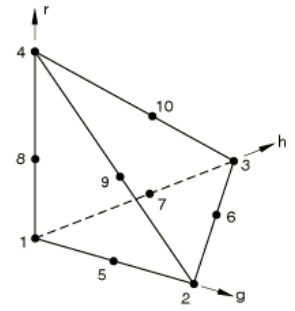
Frequency analysis of EGR coolant rail can be done by using different element types and sizes. The correct choice of element for an individual simulation is essential if accurate results are to be obtained at a reasonable cost. In order to find the appropriate mesh density and element type, four types of elements – linear and quadratic tetrahedral, and hexahedral

elements – were used with different mesh densities to predict frequency. Then these simulation results were compared to free-free vibration test data and finite element meshes were selected for further analysis.

Hexahedrons and tetrahedrons are usual three dimensional finite elements which were indicated in linear (first-order) or quadratic (second-order) construction. Moreover, the elements can be selected from full integration, reduced integration, and incompatible mode formulations. Furthermore to the displacement degrees of freedom, incompatible deformation modes are added internally to the incompatible elements. The main effect of these degrees of freedom is to remove the so-called parasitic shear stresses which are detected in regular displacement element if they are loaded in bending.

Different types of element in ABAQUS™ are presented in Table 5.2.

Table 5.2: FE Elements for vibration analysis

Element Types	Geometric order		Full integration	reduced integration	incompatible mode
Hexahedral	Linear		C3D8	C3D8R	C3D8I
	Quadratic		C3D20	C3D20R	
Tetrahedral	Linear		C3D4		
	Quadratic		C3D10		

The mesh quality is determined on the base of the convergence rate, solution accuracy and CPU time needed. To determine the solution accuracy, the Impact Hammer test was carried out for free-free vibration of coolant rail to compare the test results with FE models. Figure 5.4 shows the frequency response of the free-free vibration test of coolant rail.

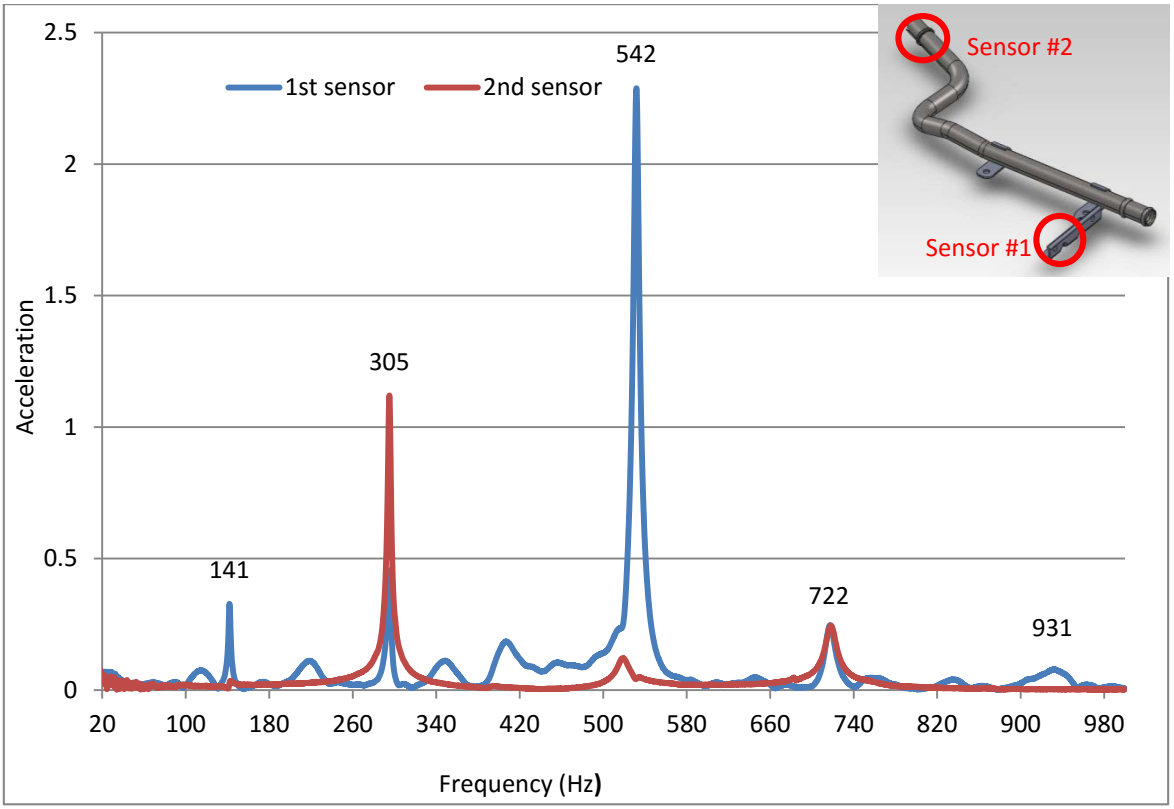


Figure 5.4: Frequency response of free test vibration

Figure 5.5 shows a typical FE model of EGR coolant rail.

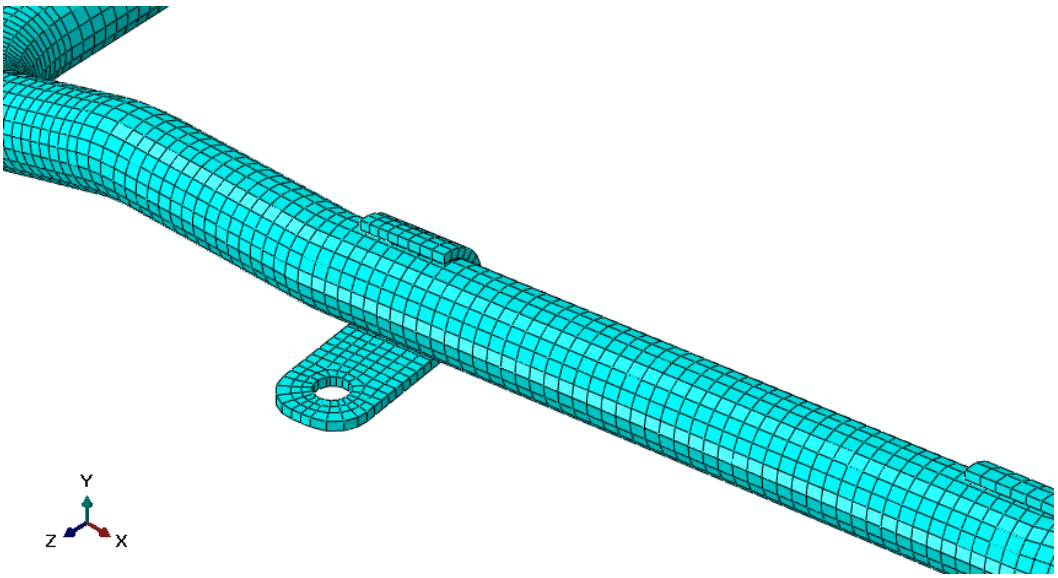


Figure 5.5 FE model of EGR coolant rail

Primary set of results which are shown are for models based on Table 5.2, created with various mesh density. These results were compared to the experimental data mentioned.

5.2.5.1 Linear Hexahedral Elements Results (C3D8, C3D8R, C3D8I)

Figure 5.6 illustrates that increasing the linear hexahedral full integration element mesh density causes the calculated frequencies to decrease. The linear hexahedral full integration (C3D8) element response was extremely relied on mesh density. As additional C3D8 elements are added predicted response improves.

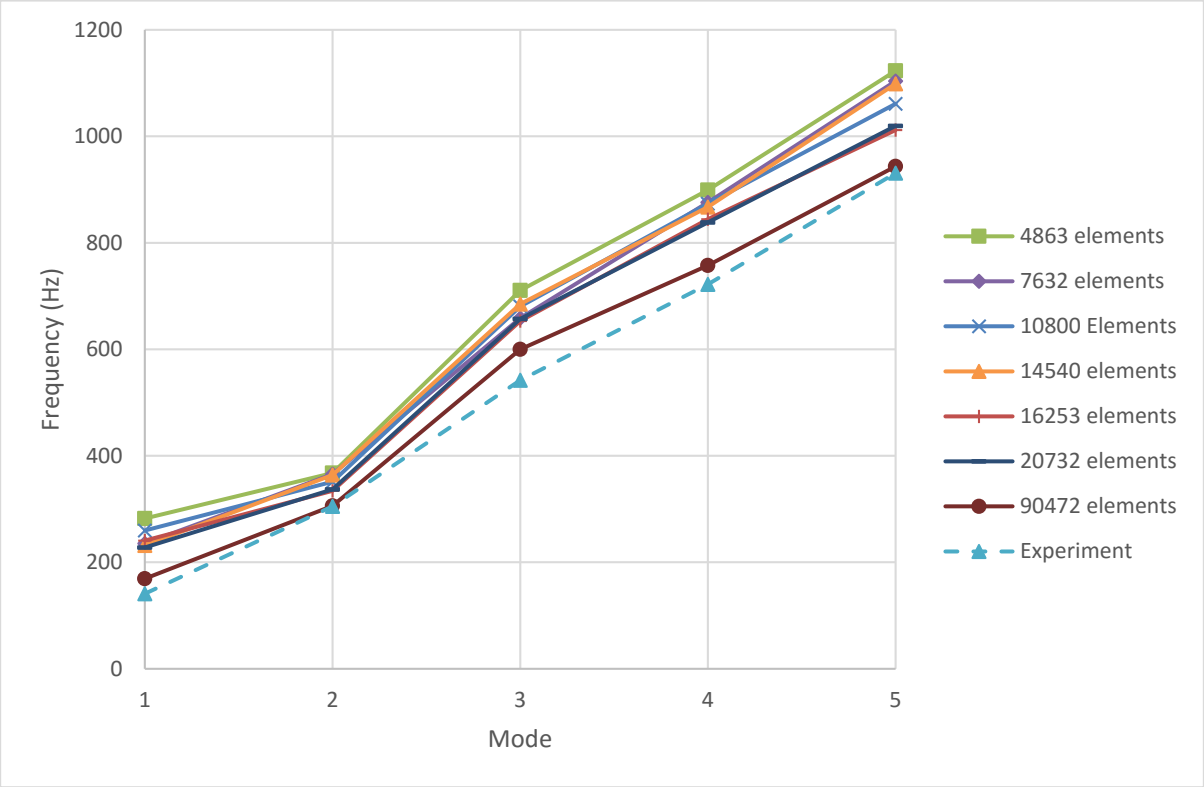


Figure 5.6: Effect of mesh density with C3D8 elements

Figure 5.7 indicates that the frequency values achieved with the linear hexahedral reduced integration (C3D8R) were lower than test results and produced spurious singular modes.

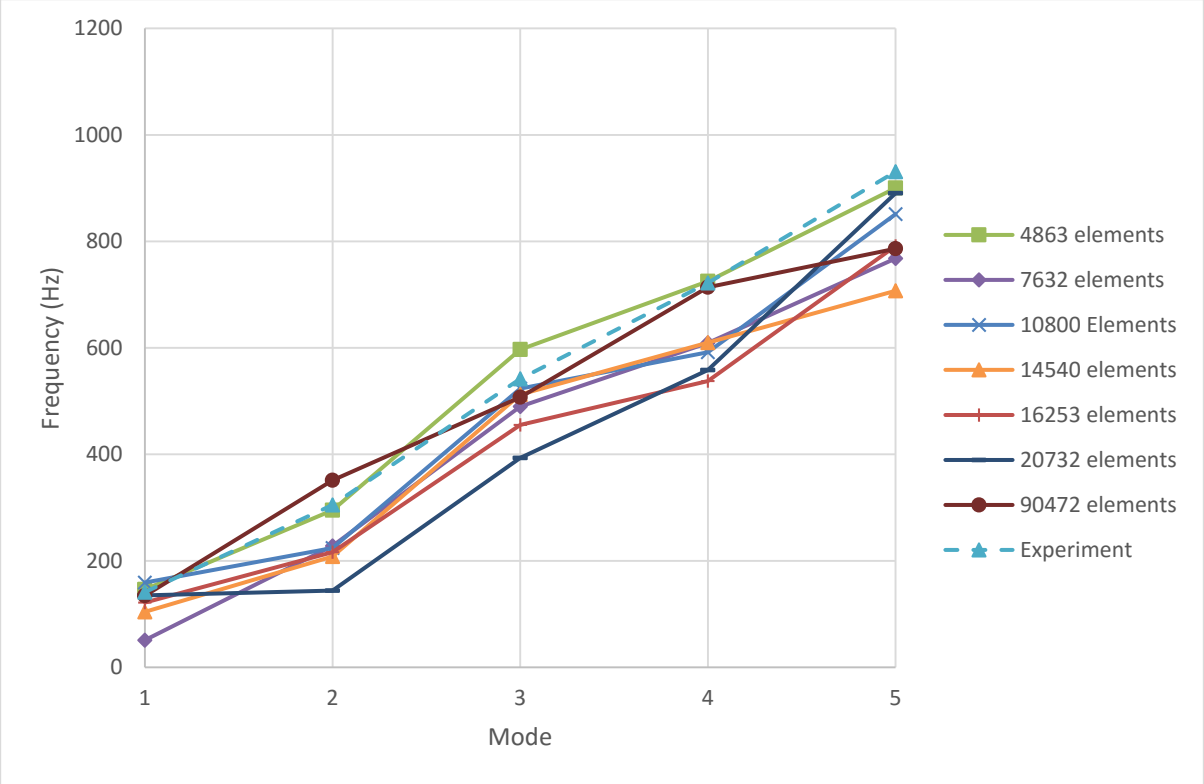


Figure 5.7: Influence of mesh density with C3D8R elements

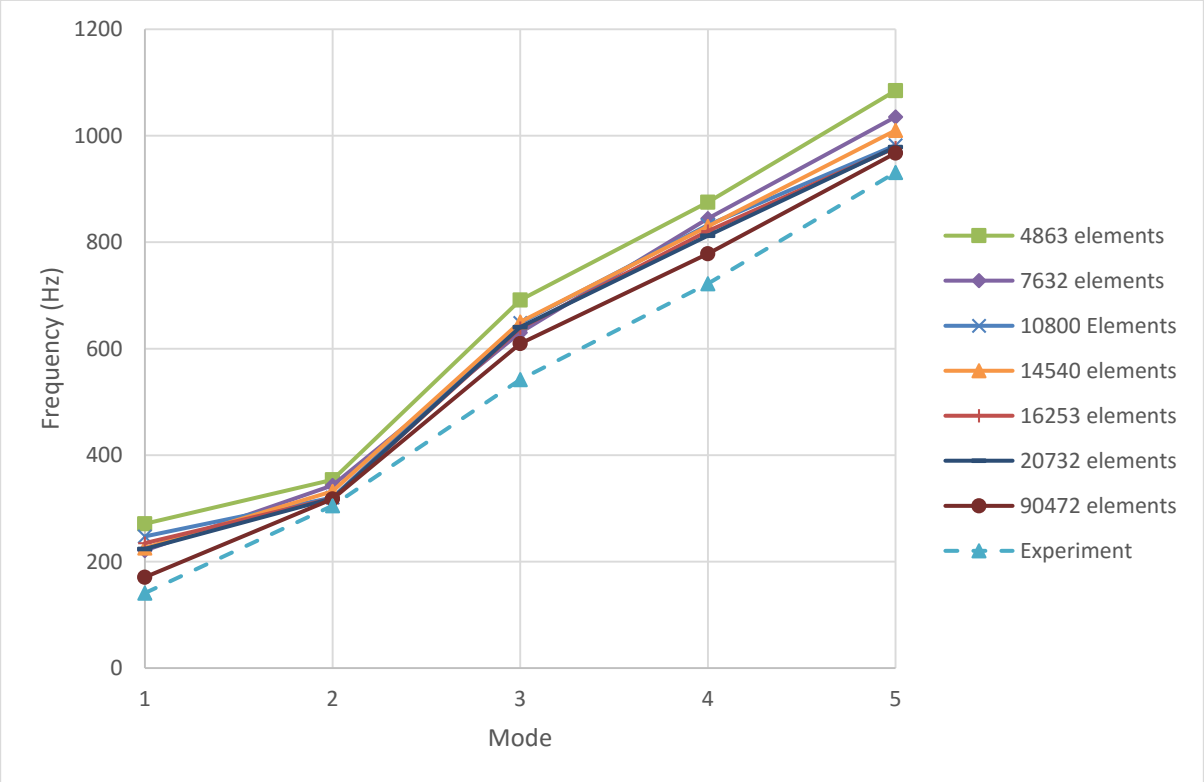


Figure 5.8: Influence of mesh density with C3D8I elements

Figure 5.8 shows that linear hexahedral incompatible mode (C3D8I) elements are sensitive to mesh density for the considered element size range, and there is poor agreement between the FE results and test data.

All of the linear hexahedral elements available in ABAQUS™ were inaccurate for modal analysis, as the number of elements increased the result improved but their accuracy was still low.

5.2.5.2 Quadratic Hexahedral Elements Results (C3D20, C3D20R)

Figure 5.9 shows that the quadratic hexahedral full integration (C3D20) elements predict frequency well with meshes far coarser than that for the linear elements.

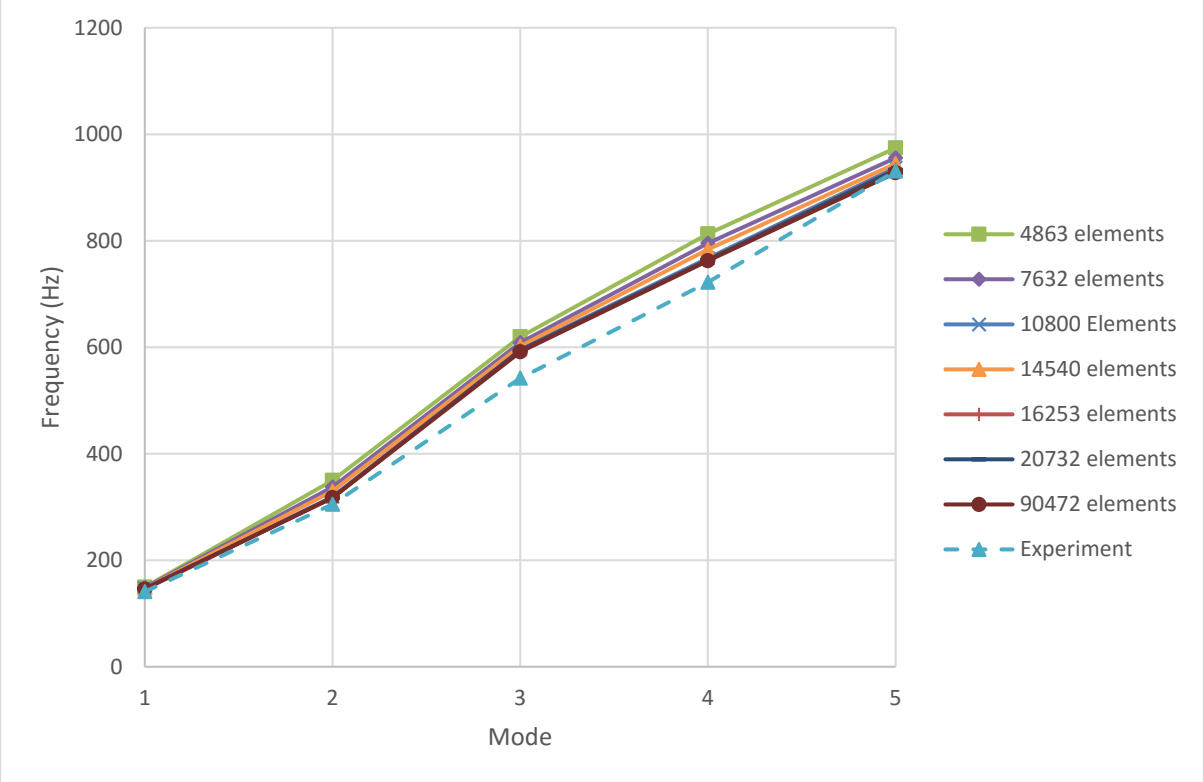


Figure 5.9: Effect of Increased C3D20 Mesh Density

Figure 5.10 indicates that the quadratic hexahedral reduced integration (C3D20R) elements obtain results comparable to the quadratic hexahedral full integration (C3D20) elements.

They seem to be more precise than the C3D20 element especially at the lower mesh density, The C3D20R elements show good frequency results even with less number of elements. Figure 5.10 shows that C3D20R element was insensitive to mesh density and increasing C3D20R elements has negligible effect on calculated results.

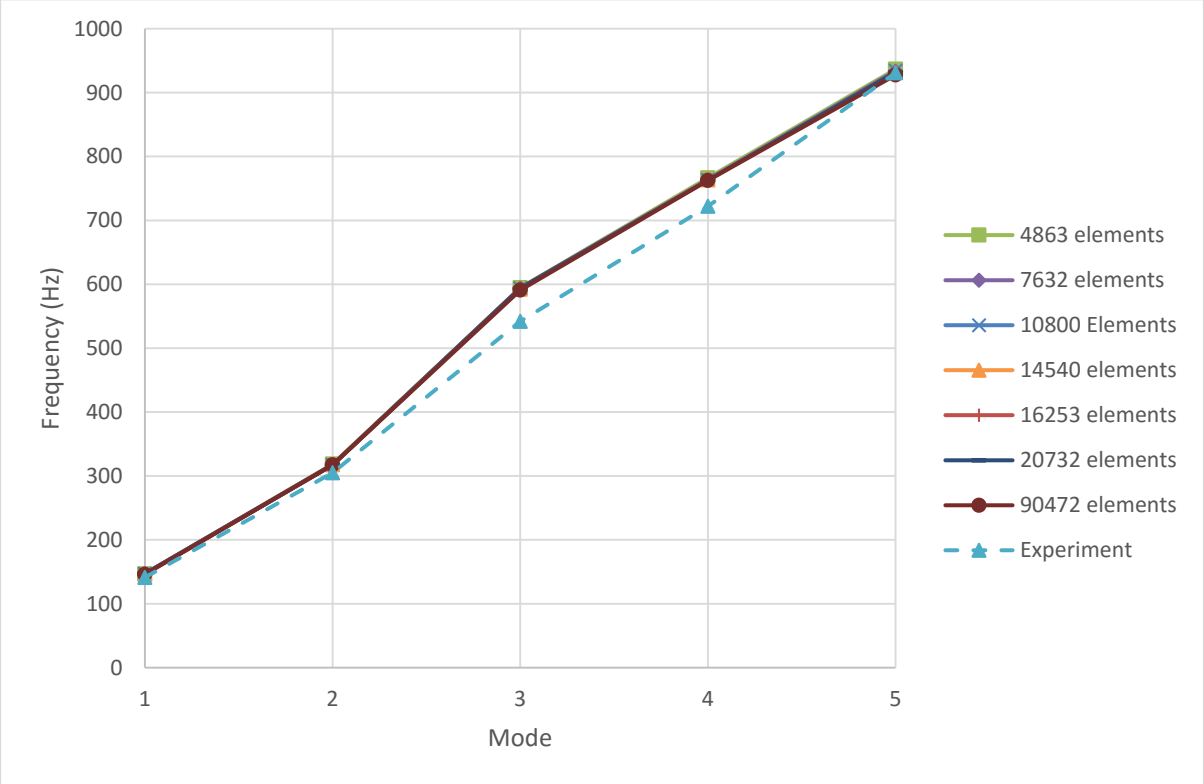


Figure 5.10: Effect of Increased C3D20R Mesh Density

One major variable controlling the analysis time efficiency is the mesh density. The larger the element size, the less number of elements and less time required to analyse it. However, a higher number of elements does not necessarily guarantee better accuracy, and there is a convergence point at which changes in the results due to choosing finer mesh are negligible. Of the quadratic hexahedron elements in ABAQUS™ both the full integration C3D20 and reduced integration C3D20R elements obtain precise frequency values with course meshes. Of the two, the C3D20R is to some extent more accurate.

In addition to comparing the result of natural frequency at different mesh density, An investigation of maximum Von Mises stress has been performed at different mesh levels for C3D20R, and a convergence point is obtained in which all mode shapes produce accurate and consistent result as shown in Figure 5.11. The stress data has been normalized in the [0, 1] range for better visualization. The plot in Figure 5.11 identifies that the maximum stress results in all modes converge at number of elements 16000 with less than 10% of total variation range (0.1 on vertical axis of Figure 5.11).

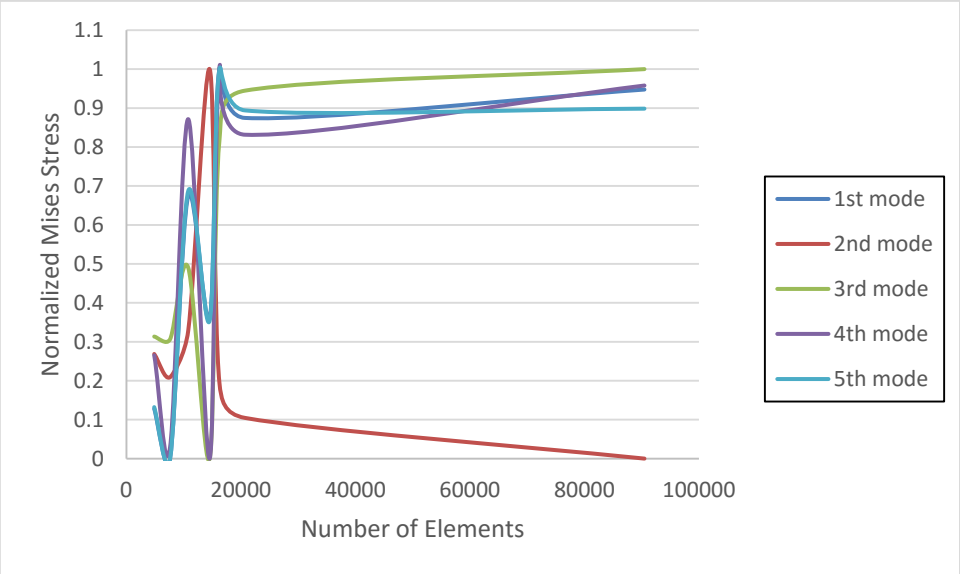
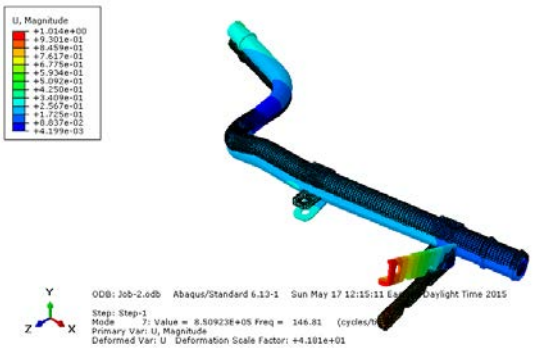
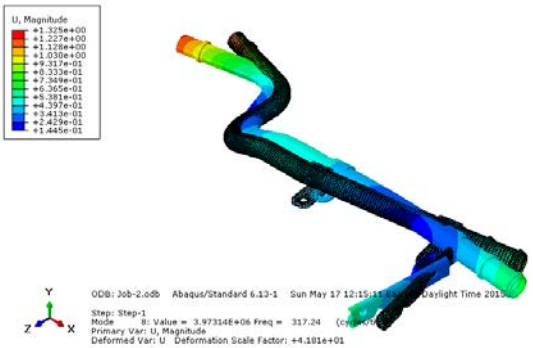
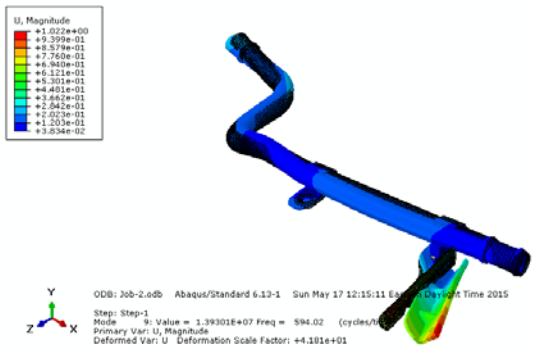


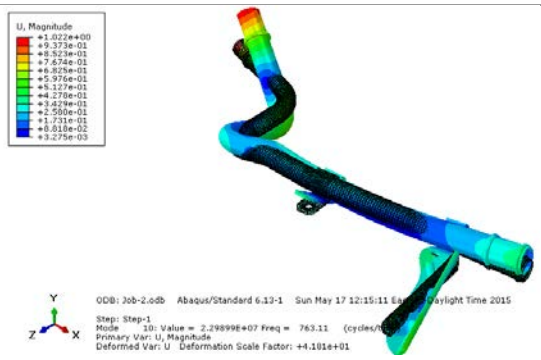
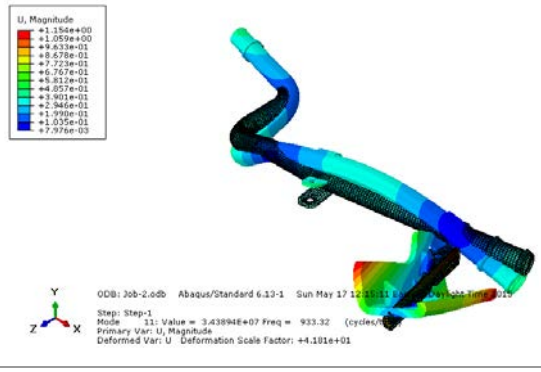
Figure 5.11: Mesh convergence for C3D20

Table 5.3 summarizes the frequency values from the quadratic hexahedral reduced integration elements (C3D20R) and compares them to the experimental data. 16000 elements were used to create the mesh. C3D20R results were quite close to the experimental data (deviation is under 5% for most modes). Only at the third mode which belongs to the big bracket, is the deviation higher than 5% (9%). This is as a result of not considering the stiffening of the big bracket due to the effect of the mass of accelerometers installed in the big bracket in FE model. By adding the mass of the accelerometers to the FE model and re-

calculating the modes, the frequency of the 3rd mode decreased to 560 Hz giving a deviation of 3.5%.

Table 5.3: The comparison between C3D20R model and experimental result

Mode	*FE model C3D20R 16000 Elements*	*Experiment*	*Error*	*Mode shape*
1st Mode	*146.81*	*141*	*-5 Hz / 4.11%*	
2nd Mode	*317.24*	*305*	*12 Hz / 4%*	
3rd Mode	*594.02*	*542*	*-52 Hz / 9.5%*	

4th Mode	***763.11***	***722***	***41 Hz / 5%***	
5th Mode	***933.32***	***931***	***-2Hz / 0.24%***	

5.2.5.3 Tetrahedral Elements Results (C3D4, C3D10)

Figures 5.12 shows that the linear tetrahedral (C3D4) develop extremely stiff results. Even by increasing the number of elements to over 140,000 elements, the solution remained still imprecise. More increases in mesh density might end up converging to an accurate solution, but it would be extremely inefficient in terms of computational cost. Figures 5.12 and 5.13 illustrate that the quadratic tetrahedral elements results ,C3D10, are extremely close to that of the C3D20R element, however require more elements (41000) to converge to a solution with longer solution time (111 sec) in comparison to C3D20R (72 sec).

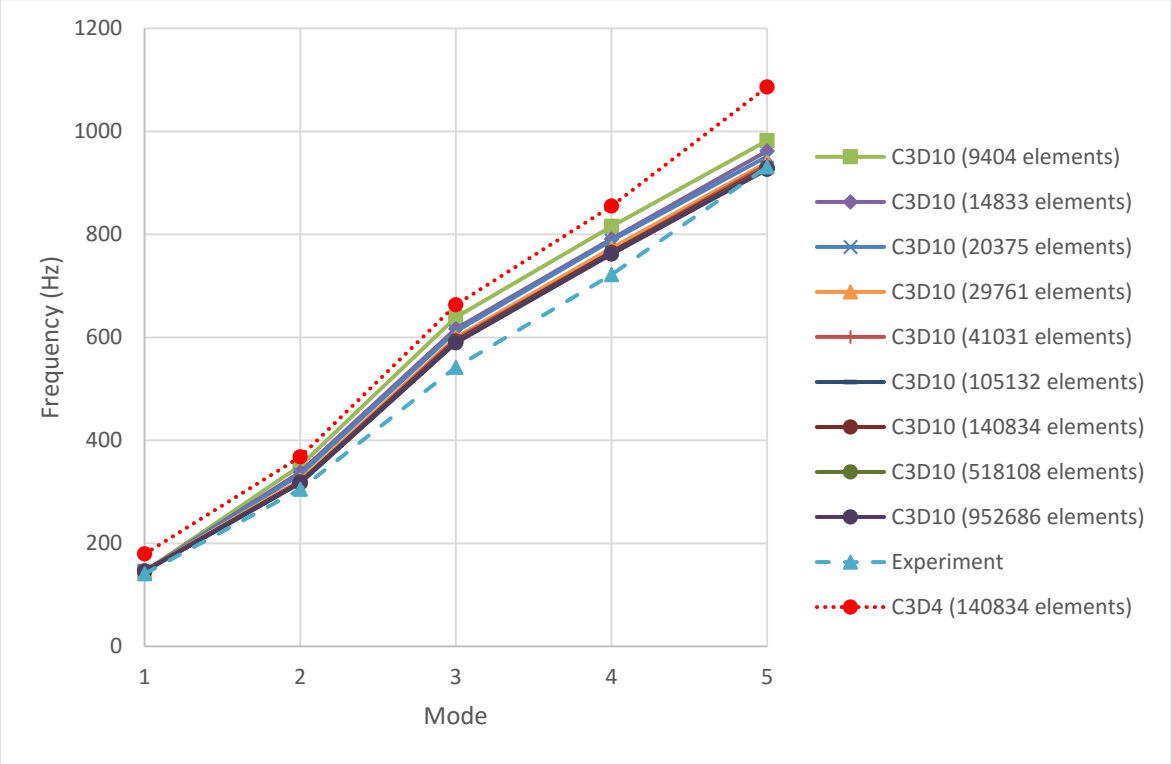


Figure 5.12: Effect of mesh density on C3D10 and compare to C3D4

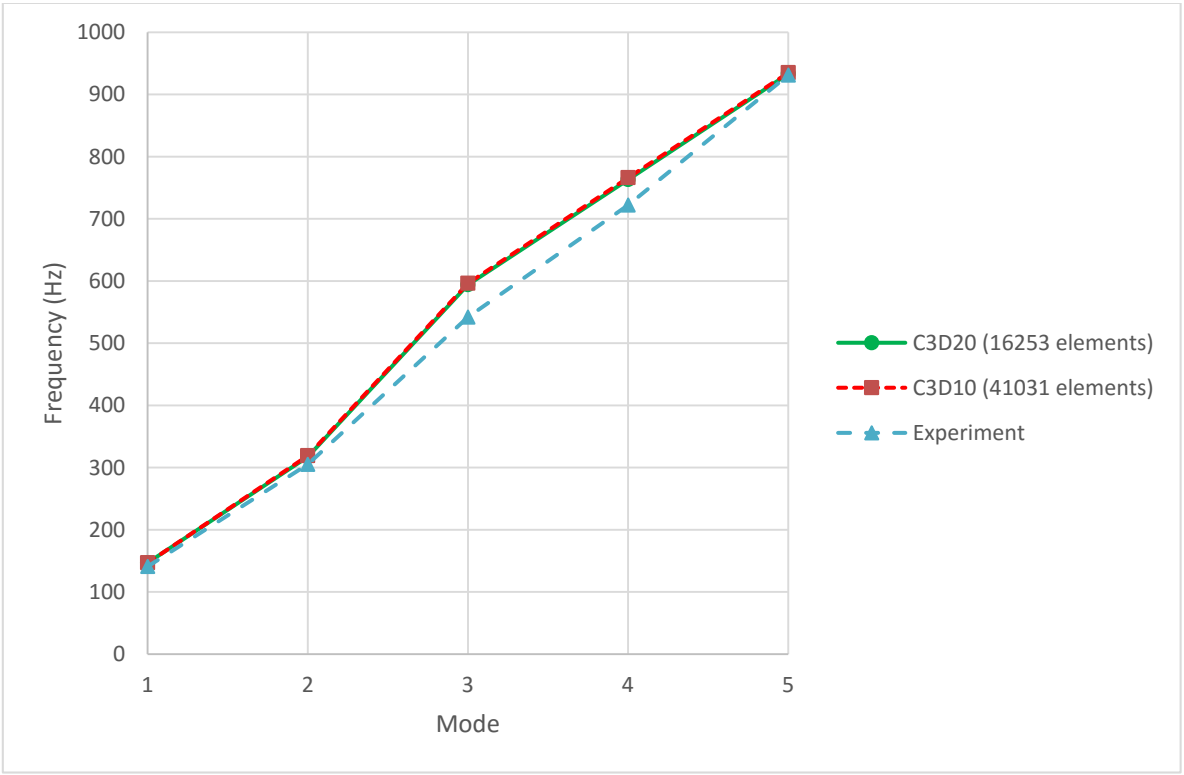


Figure 5.13: Comparison between hexagonal and tetragonal models

The quadratic hexahedral reduced integration element (C3D20R) was presented to be the best economical and accurate element for frequency analysis in ABAQUS™ which is used in next analysis. The ABAQUS™ quadratic hexahedral full integration element (C3D20) provided the same consistent and accurate results with somewhat longer solution time.

5.2.6 Boundary condition setup

The fully constrained boundary condition was applied at the bolted joints between bracket and plate as illustrated in Figure 5.14.



Figure 5.14: Boundary condition

5.3. Damping Simulation

5.3.1 Tube Damping:

Several representations of damping are provided in FE modelling according to the type of analysis. Damping of the EGR coolant rail was applied as a material damping and modal damping in Abaqus™/Standard in this research.

The modal damping method was employed in Mode-based Steady-State Dynamics analysis for the vibration analysis of EGR coolant rail without rubber, model #1. This method represents a simple model for damping in various frequencies in ‘’Step’’ definition level in Abaqus™. However, this method is not active during the Steady-State Dynamics - Subspace simulation. Therefore the damping coefficients are only available in Material definition level

for consideration of tube damping characteristics using Rayleigh damping method. Material damping was applied in the FE model of coolant rail with rubber hoses, model #2, as Rayleigh damping for tube.

In this simulation, the Rayleigh damping coefficients α and β were also computed based on the damping values derived from the vibration test of coolant rail without rubber. These coefficients were utilised as material properties, known as the mass proportional damping (α) and stiffness proportional damping (β). In this method, it is supposed that the material damping is proportional to structure mass and stiffness, and will form the following equation (Liu & Gorman, 1995):

$$\zeta_i = \frac{\alpha}{\omega_i} + \beta\omega_i \qquad \text{Equation 5.14}$$

where ω_i is natural frequency and ζ_i is damping ratio in the corresponding natural frequency. The damping ratio for each mode from the frequency response function obtained in the experiment was extracted by means of the Half-power bandwidth method explained in section 4.4. Having a number of damping ratios for the corresponding modal frequencies, a curve fitting method was employed based on the least square error (LSE) method to determine the coefficients of Equation 5.14. Consequently the following values of α and β were obtained:

$$\alpha = 3.7, \beta = 0.0001$$

Also the value of damping constant vs frequency was plotted in Figure 5.15.

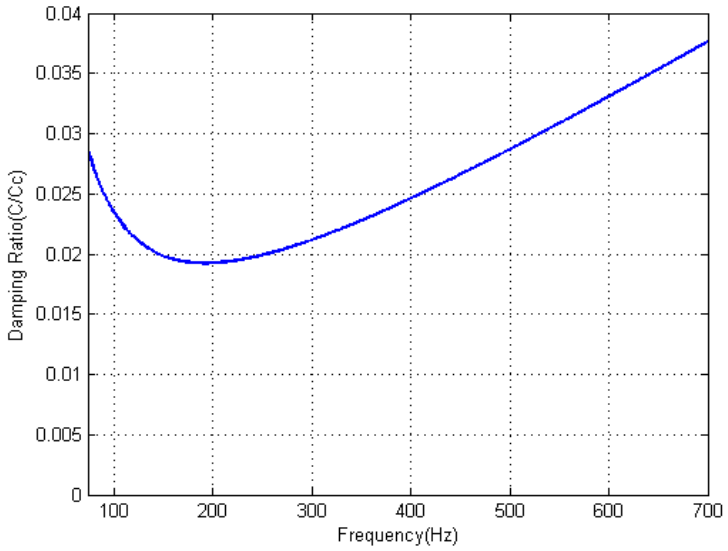


Figure 5.15: Damping Ratio

5.3.2 Viscoelastic damping of rubber:

Material damping has been applied in the model as viscoelastic damping for rubber.The frequency domain viscoelastic material model is used for modelling rubber damping which defines frequency-dependent material behaviour in steady-state harmonic oscillations for rubber material in which dissipative losses caused by “viscous” (internal damping) effects, has been modelled in the frequency domain explained in chapter 3. The Subspace-based steady-state dynamic analysis procedure was used for viscoelastic material modelling.

5.4. Simulation results and validation

It was necessary to validate the finite element models created based on the material properties and geometry information. The validated FE model can be used as a virtual simulation platform to provide reliable predicted data instead of experiment. Therefore, the validation of FE results against available test data will be discussed in this section.

5.4.1 Job solving strategy

For solving Abaqus™ jobs, the High Performance Computation (HPC) facility in University of Birmingham was utilized. ''BlueBEAR'' is a cluster of processors with 848 processing cores, 2.2 GHz speed per core with 256GB RAM available per job submission (University of Birmingham, 2013) which is based on IBM's iDataPlex servers and consists of modern and high end computational capacity with unlimited physical memory allocation on-demand (maxed out only when threshold is reached). Input deck files (INP) are submitted to the Abaqus™/Solver with different settings which differ based on the type of requested analysis. The HPC is capable of running parallel jobs in cases where 2 or more simulations are not coupled or running in sequence, but interacting in a parallel configuration or where single simulation can be broken into 2 or more runs. HPC allocates INP in a parallel fashion when more processors are required.

In this research, three types of jobs are generated to run on the HPC machine: First, a time-domain analysis in explicit/implicit mode without CFD co-simulation running in parallel (no water in EGR coolant rail) where the steps are solved in sequence. Only one processor is enough to handle this analysis and more allocations are wasted. Second, the time-domain analysis that shows up in simulation of the EGR coolant rail with water inside the hose and tube where a Fluid-Structural Interaction (FSI) analysis is conducted. In this case, the simulation can be performed in two separate processors where a processor handles the Finite Element (FE) solution, and within the other one, a Computation Fluid Dynamics (CFD) analysis is performed and data is exchanged between two processors at each time step. This allocation improves the runtime by running twice as fast. Third, the frequency-domain modal analysis can be broken into 5 frequency ranges where those ranges are independent of each other

and one would not influence the results of others due to the mathematics behind it. Then, 5 Abaqus™/solver tokens are called and jobs are submitted to 5 separate processors where the analysis is performed. This will reduce the time of analysis by running 5 times faster.

5.4.2 Forced vibration analysis: Model#1

The forced vibration analysis was carried out and the results are shown in Table 5.4. The simulation outputs were analysed in the first seven modes and corresponding results are reported for the rail without rubber hoses in Table 5.4 and Figure 5.16. For the purposes of modelling accuracy, the bolts and nuts were also taken into account in order to assess their effect on the modal behaviour. However, the comparison does not show a great impact on the model apart from the first and fourth modes. The test data shows reasonable agreement with FE results with difference of under 5% for all the modes. The mobility response is presented using logarithmic scale because of the wide dynamic range of the response. The mobility of the rail in Model #1 for the transducers B and C were calculated and plotted in Figure 5.17, 5.18 respectively. The first eight mode shapes are shown in Figure 5.19 as well.

Table 5.4: Comparison between forced vibration simulation and test results of model #1

Modes	FE Model (Hz)		Test Result (Hz)	Deviation	
	Model without nut and bolt (1)	Model with nut and bolt (2)		(1)	(2)
1st Mode	69	73.7	74	6.8%	0.4%
2nd Mode	177	178	178	0.6%	0.0%
3rd Mode	284	283.5	288	1.4%	1.6%
4th Mode	489	503.9	531	12.2%	5%
5th Mode	701	693.7	720	2.6%	3.7%
6th Mode	838	833.8	838	0.0%	0.5%
7th Mode	873	860.1	872	0.1%	1.4%

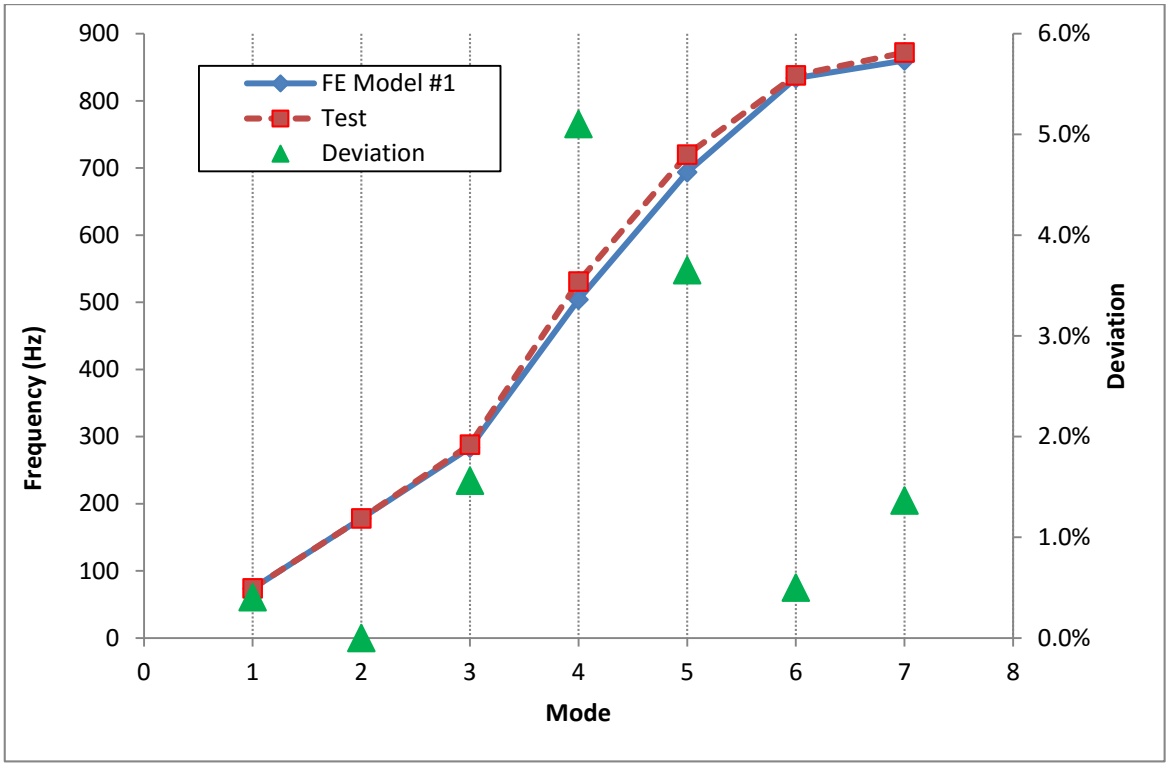


Figure 5.16: Comparison between forced vibration simulation and test results of model #1

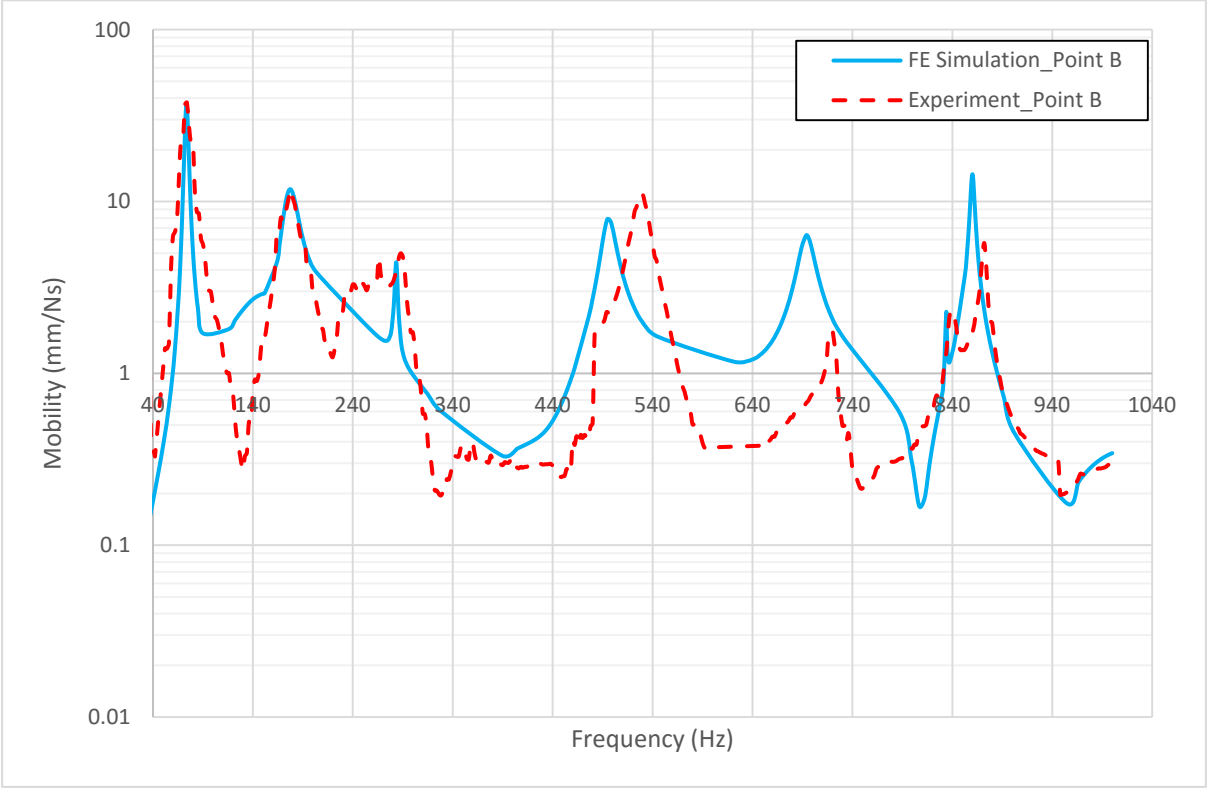


Figure 5.17: Comparison between forced vibration analysis and test results of model #1 (Transducer #B)

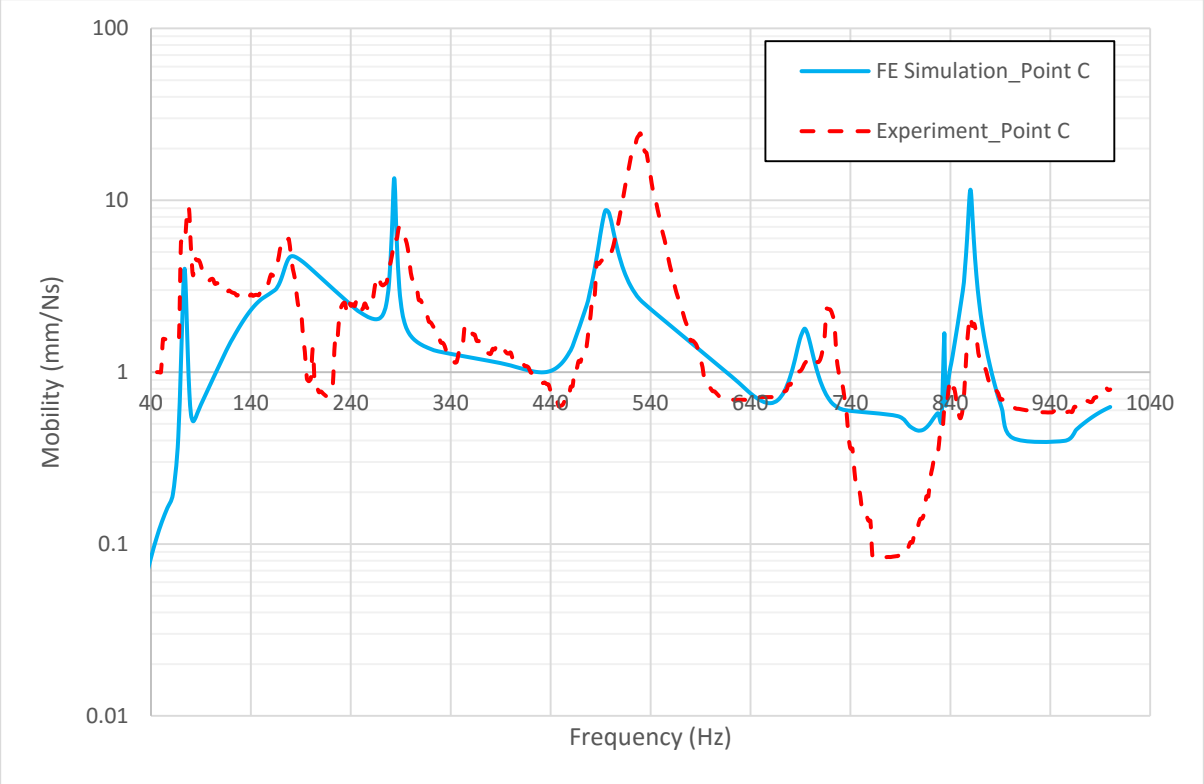
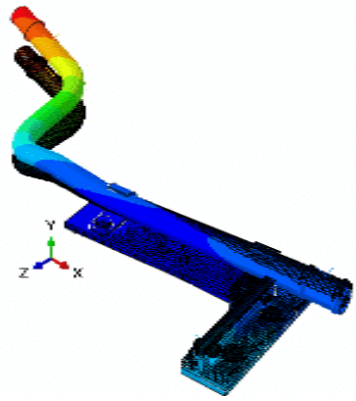
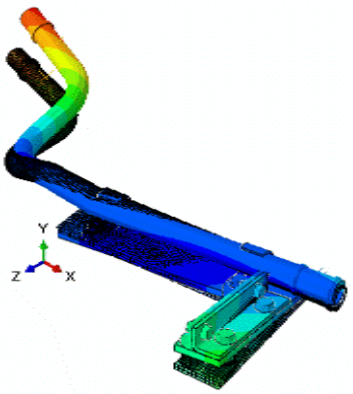


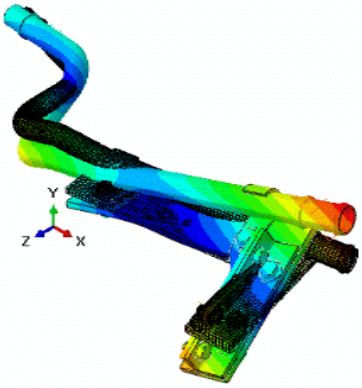
Figure 5.18: Comparison between forced vibration analysis and test results of model #1 (Transducer #C)



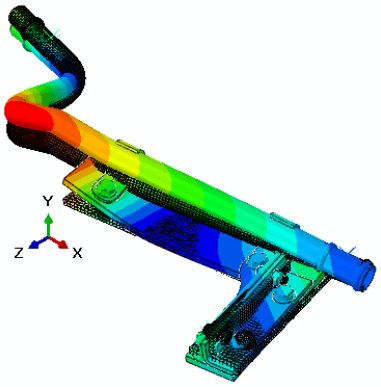
(Mode 1)



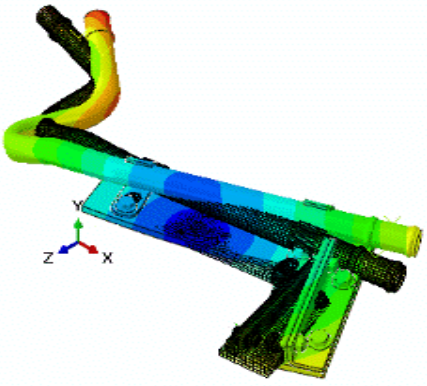
(Mode 2)



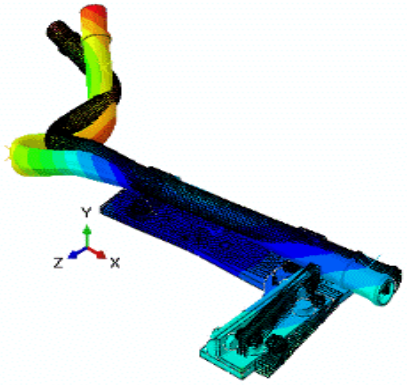
(Mode 3)



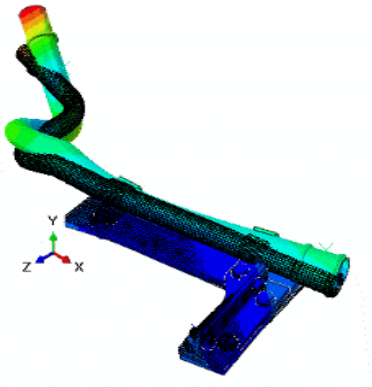
(Mode 4)



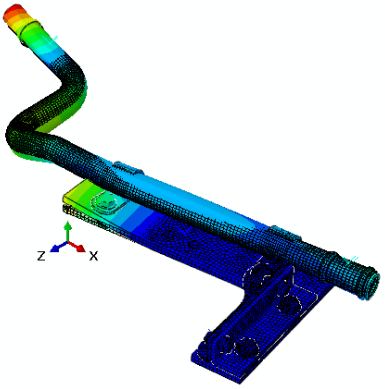
(Mode 5)



(Mode 6)



(Mode 7)



(Mode 8)

Figure 5.19: Mode shapes of forced vibration analysis of model #1

5.4.3 Forced vibration analysis: Model#2

The results of the forced vibration analysis are shown in Figure 5.20 for Model #2 when the rubber hoses were attached to the ends of the rail. The deviation of test data from FE results was less than 9% for most of the modes as shown in Table 5.5. The mobility of the coolant rail in Model #2 for the transducers A and B were calculated and plotted in Figure 5.21 and 5.22. Mode shapes of forced vibration analysis of EGR coolant rail with rubber hoses are presented in Figure 5.23.

Table 5.5: Comparison between forced vibration simulation and test results of model #2

Modes	FE Model (Hz)	Test Result (Hz)	Deviation
1st Mode	81.2	85	4.5%
2nd Mode	150.1	160	6.2%
3rd Mode	187.8	201	6.6%
4th Mode	216.6	222	2.4%
5th Mode	252.6	241	4.8%
6th Mode	268.5	280	4.1%
7th Mode	312.4	340	8.1%
8th Mode	421.3	430	2.0%
9th Mode	454.2	486	6.5%
10th Mode	502.6	510	1.5%
11th Mode	582	568	2.5%
12th Mode	614.9	600	2.5%
13th Mode	684	672	1.8%

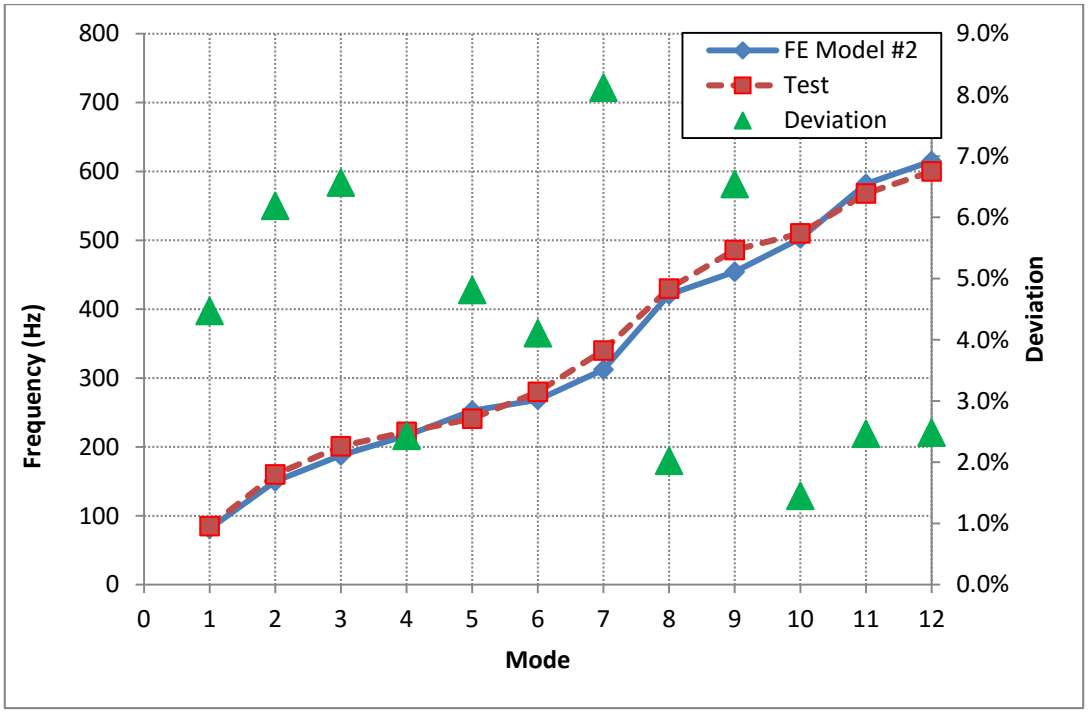


Figure 5.20: comparison between forced vibration simulation and test results of model #2

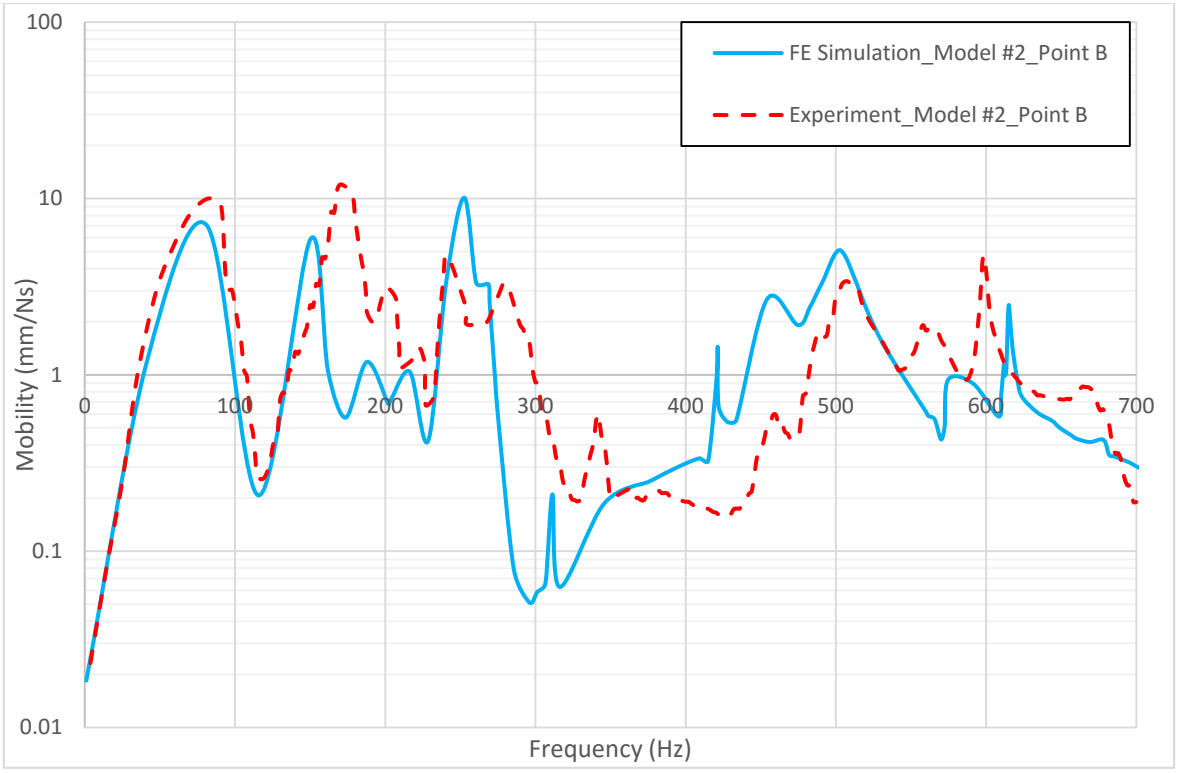


Figure 5.21: Comparison between forced vibration analysis and test results of model #2 (Transducer B)

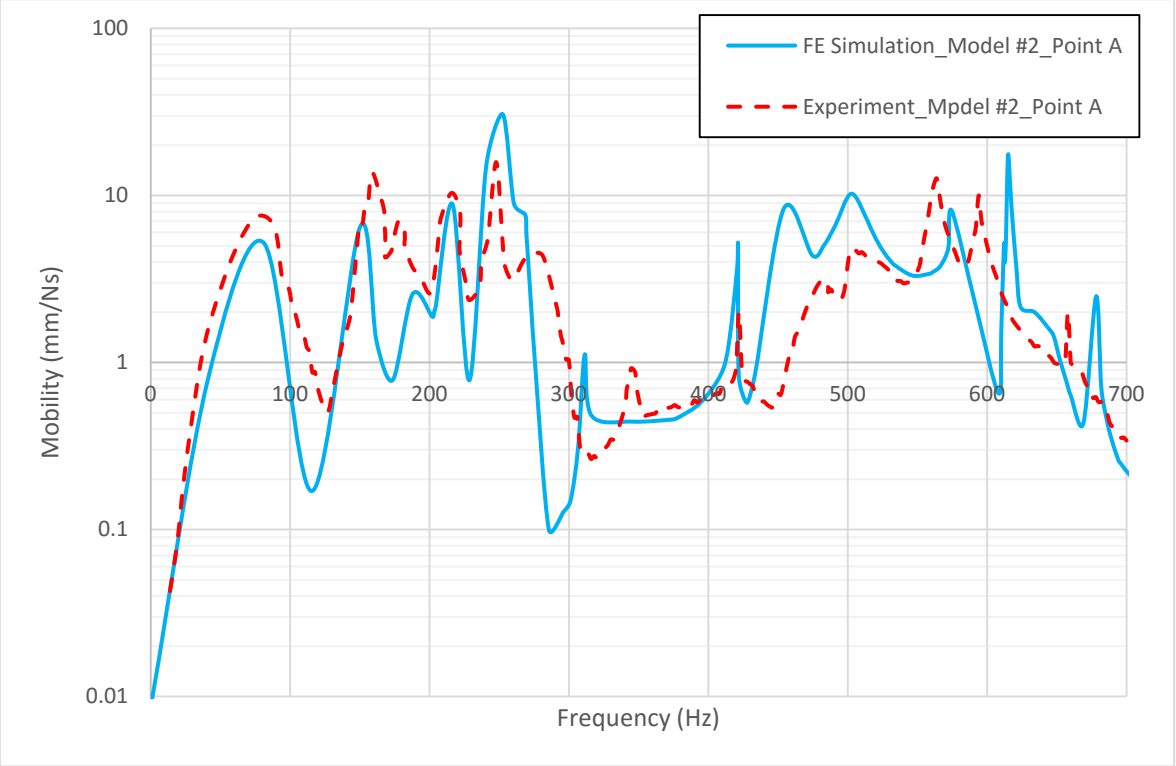
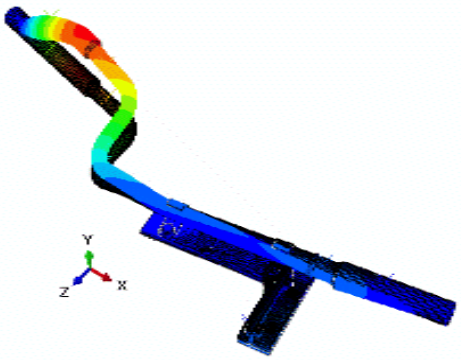


Figure 5.22: Comparison between forced vibration analysis and test results of model #2 (Transducer A)

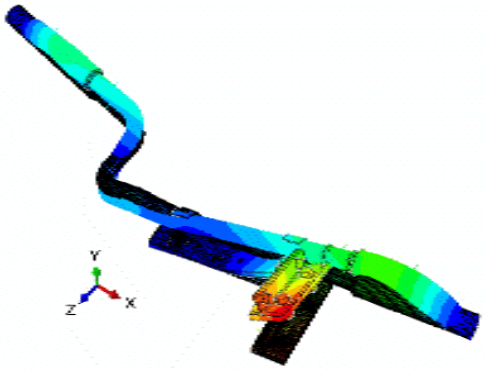
Additional modes and deviation of mobility in test in comparison with simulation can be interpreted using the following reasons:

- ✓ The shaker mount didn't give complete translation, and caused a certain amount of rotation.
- ✓ Since the shaker was physically mounted to the structure via the load cell, it was possible of altering the dynamic of the structure.
- ✓ The technique of supporting the shaker was another issue that can influence on the force imparted to the test rig.
- ✓ Very little force is needed to get a response at a resonance point with a small effective mass. So in the district of the resonance, it causes a sudden drop in the force amplitude which can result in the force measurement to be susceptible to noise.
- ✓ The attachment points had some degree of flexibility owing to the bolted connections.

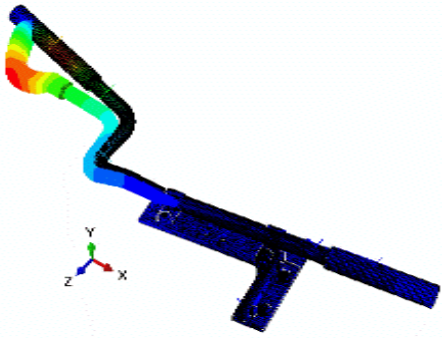
✓ There was not enough resolution in damping values to reasonably cover the frequency range under study (It is commonly called the damping resolution over the range of forced vibration analysis).



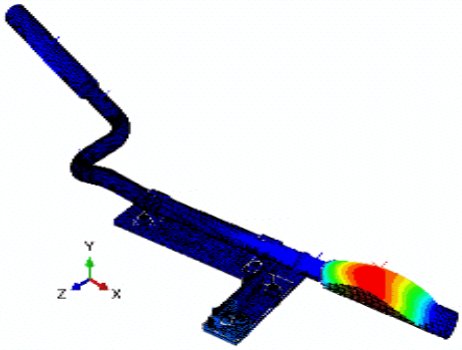
(Mode 1)



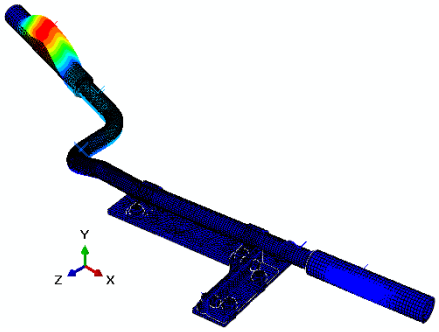
(Mode 2)



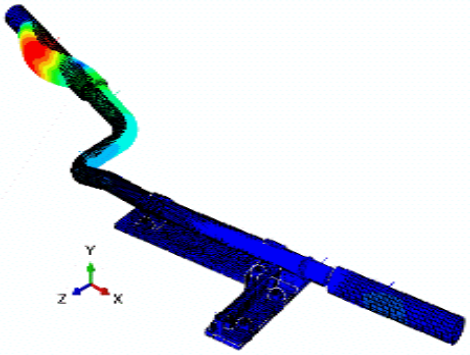
(Mode 3)



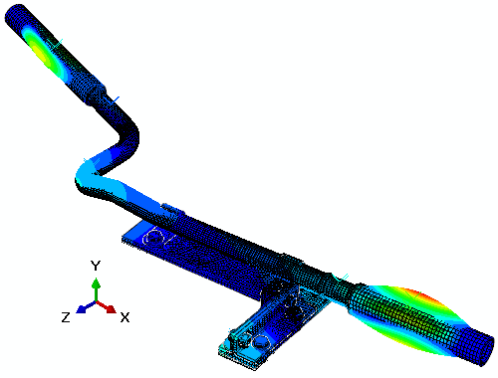
(Mode 4)



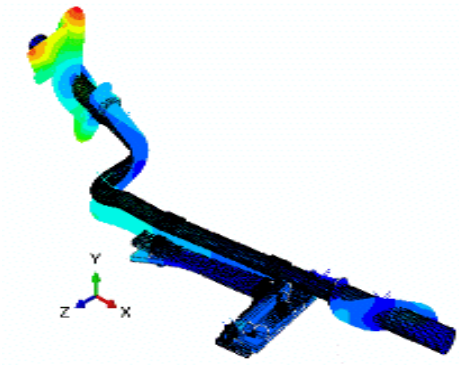
(Mode 5)



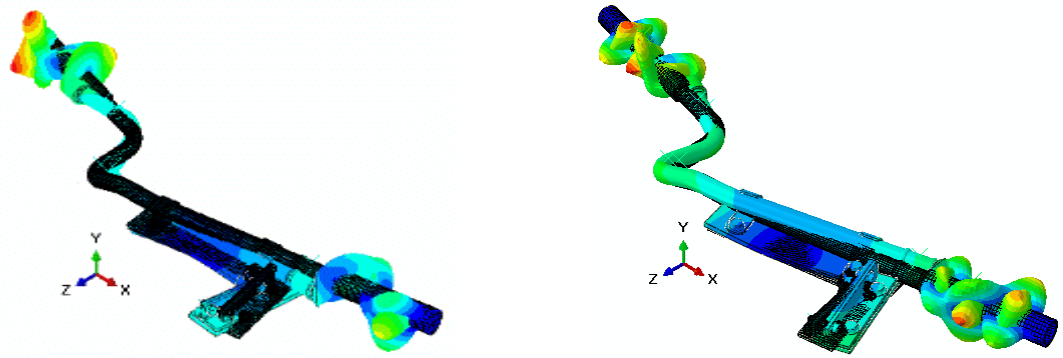
(Mode 6)



(Mode 7)



(Mode 8)



(Mode 9) (Mode 10)

Figure 5.23: Mode shapes of forced vibration analysis of model #2

The simplest design rule to prevent fatigue failure is

$$\sigma_{max} < S_e$$

Where σ_{max} is maximum stress and S_e is endurance limit, stress level below which failure will never occur. In most of the natural modes of EGR coolant rail, the maximum stress is less than endurance limit of EGR coolant rail except the 2nd and 9th modes which are over 210MPPa and related to the big bracket and tube as shown in Figure 5.24.

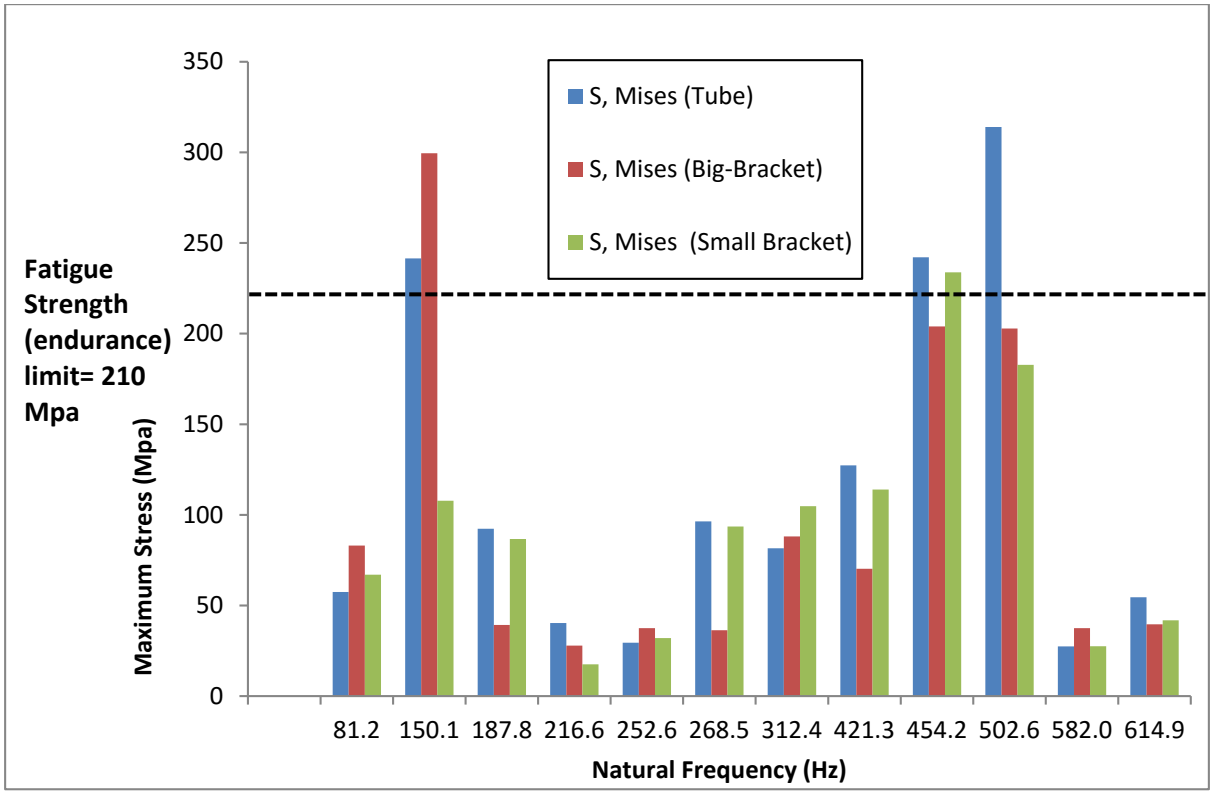


Figure 5.24: Maximum Von Mises stress of forced vibration analysis of model #2

5.4.4 Representation of rubber hoses (Model #3)

In Model #3, the rubber hoses were removed and equivalent spring-dashpot elements were added to both ends radially perpendicular to the axial direction of tube. As a first estimation, the spring stiffness and damping coefficients were calculated based on two methods. A schematic of this element attached to the rail is shown in Figure 5.25.

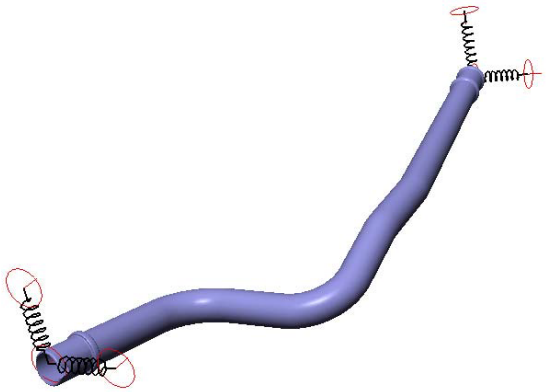


Figure 5.25: Schematic of SPRING-DASHPOT element

For calculation of k, the added element stiffness, the rubber hose at each end of the tube was modelled in Abaqus™ as a cantilever using its hyper-elastic properties. The load/deflection graph in bending condition was extracted for small deflection, and the average stiffness was calculated based on the applied load and deflected shape. The rubber boundaries were kept identical in comparison with the boundaries of model #2.

The dashpot characteristics were calculated by a transient dynamic analysis with time-dependent material response. The goal was to simulate an equivalent damping from viscoelastic properties. In this method, a cantilever model of a rubber sample was rigidly constrained at one end and excited at different frequencies. Then the dissipated energy was calculated in one of the stable cycles per frequency and divided by the total strain energy for loss factor calculation. Then the damping ratio of the rubber is half of loss factor value according to equation 5.15 (De Silva, 2000)

$$\eta = \frac{D}{2\pi} = \frac{\Delta U}{2\pi U_{max}} \qquad \text{Equation 5.15}$$

where ΔU is the energy loss per cycle and U_{max} is the total stored reversible energy of the system.

The values of damping at different frequencies were obtained using equation 5.15. Since the range of values was small, an average value was used in the simulation as the equivalent damping.

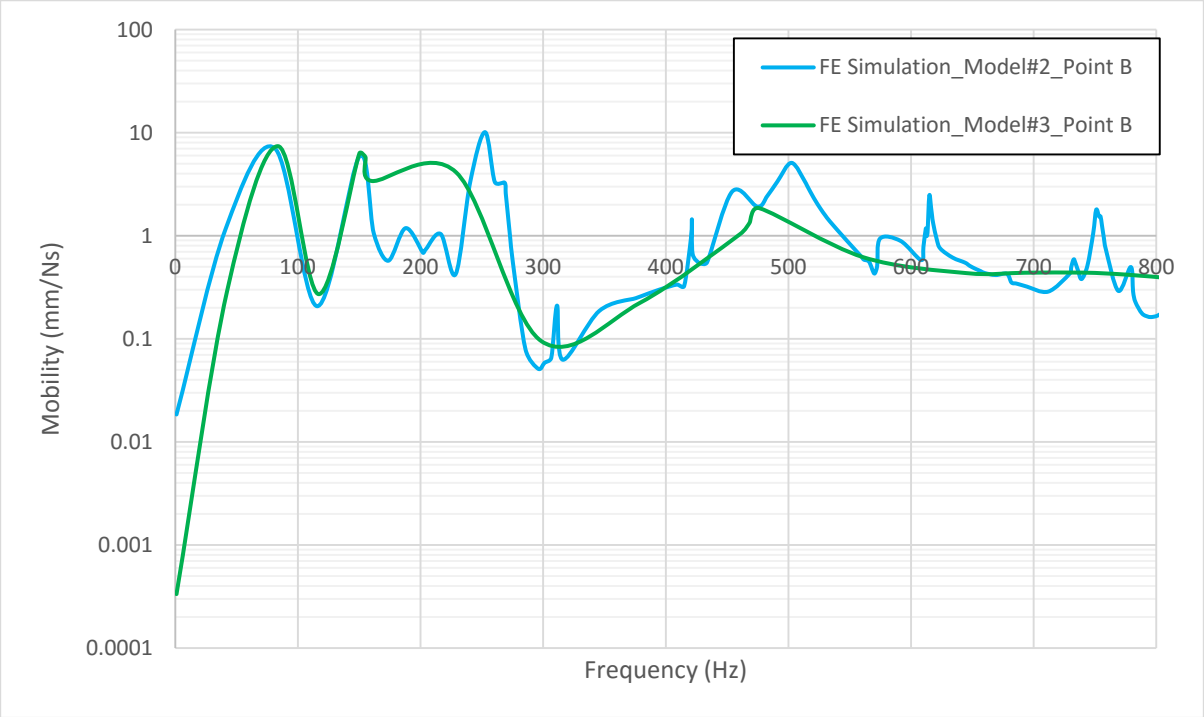


Figure 5.26: Comparison between simulation and test results for coolant rail with rubber (Transducer A)

The result of calculated mobility in this step is compared with results obtained from Model #2 in Figure 5.26. Close agreement for mobility in Model #2 and Model #3 with test results can be observed particularly at low frequency in Figure 5.26. As a result, replacing hoses with the spring-dashpot elements at the ends of rail can save a considerable amount of calculation cost by reduction in number of nodes/elements and avoiding the time-consuming viscoelastic simulation. The above-mentioned methods can be applied to hoses with different sizes providing the viscoelastic properties are available.

5.5. Summary

In this chapter, the FE method was described to recognize the useful parameters and a wide range of vibration FE simulations was performed. Coolant rail geometry was explained to get a better conception of the reinforced layer modelling of rubber hoses in Finite Element and the rebar element method was used as a method for modelling of the uniaxial reinforcement in rubber hoses.

Moreover, a comparison research was performed on the various mesh types and mesh density of the FE simulation of coolant rail with hammer test results to realise which approach is more appropriate for the vibration analysis of coolant rail. The quadratic hexahedral reduced integration (C3D20R) was discovered to be the most cost-effective and accurate element for vibration analysis. The quadratic hexahedral full integration (C3D20) created the same consistent and precise values with a slightly longer solution time. The linear hexahedral incompatible mode elements (C3D8I) are sensitive to mesh density and there isn't good agreement between the FE results and test data. The linear hexahedral reduced integration element (C3D8R) was imprecise with few number of element, however the results improved by increasing the mesh density. However its accuracy was still poorer than the above element. The response of the linear hexahedral full integration element (C3D8) was highly reliant on mesh density.

Taking advantage of the use of commercial finite element software, the rubber hoses were modelled by representing the reinforcement cord and rubber by rebar elements and solid elements respectively. The simulation of the dynamic response of the coolant rail was carried out by modal and Subspace based Steady-State Dynamic Analysis in Abaqus™, and the FE result compared reasonably well with the result obtained from the physical rig tests. Accuracy

of simulated dynamic responses was not unduly affected in low frequency by replacement of the rubber hoses with appropriate spring-dashpot elements which can offer substantial savings in computational costs.

Some of the modes revealed by FE simulation could not be excited in the physical tests due to their complex nature involving a combination of translational and rotational motion. This is thought to be responsible for some of the discrepancies in mobility response in physical tests in comparison with those obtained from FE simulation.

Finite element simulation can be used to predict the response of the EGR coolant rail in a physical test. With a view to optimising its design, FE simulation can be used to predict changes to its modal parameters if physical modifications (mass, damping, stiffness, and substructures) are added. The vibration response of the structure to different excitation forces applied in any of the defined degrees of freedom can therefore be predicted using FE simulation.

Chapter 6: Fluid Structural Interaction

Vibration Analysis of the EGR Coolant Rail

6.1. Introduction

In this chapter, the influence of the fluid dynamics on the vibration of a mechanical structure is presented. A Finite Element (FE) analysis was conducted to simulate the vibration behaviour of an EGR coolant rail consisting of a metal tube and rubber tubes at both ends of the metal tube with water flowing inside it. The excitation was applied in the form of sine sweeps with progressive frequency in the range of 40 Hz to 800 Hz, which represents the frequency domain of the engine and road excitation. A precise dynamic implicit approach was used to implement a displacement-controlled analysis, applied from the engine mounted support. The metal tube was characterised by its elasticity (Young's modulus) while the rubber material property was modelled using visco-hyperelastic constitutive equations. In order to check the validity of the simulation results, a test rig was designed and developed to replicate the rail operating condition on the engine and a shaker was used to produce the unidirectional excitation from where the rail is mounted, while the tube was filled with water. The correlation study suggests a close agreement between the test and simulation results in terms of the prediction of the natural frequencies. This analysis enables design engineers to extract the natural modes and frequencies of vibrating parts with flowing fluid in order to investigate the failure modes and redesign brackets, supports, and fittings for desired strength.

6.2. Methodology Definition

Due to geometrical complexities in most real-world applications, the analytical approaches are not satisfactorily helpful and, in most cases, are not adequate to describe the vibration problem of fluid-structure interaction. Therefore, the well-known finite element (FE) approach is proposed for analysis of such problems, in which a discretised model of the actual

structure into elements and nodes is developed and the analytical equations are applied to each element-node locally to form a set of either linear or nonlinear equations.

In this research, the vibration of solid-fluid structures in the time domain is investigated using a coupled implicit approach. A time-domain analysis is selected initially because such analysis is capable of directly replicating the real-world testing and boundary conditions. Secondly, the appropriate approach for analysis of fluid-structure interaction in the frequency domain is not commercially available. As a closing point, the inherent material nonlinearities and transient behaviours of both solid and fluid can be modelled in time-domain analysis with the least limitation in comparison to modal analysis in the frequency domain. However, an appropriate virtual testing procedure should be designed in the time domain analysis to ensure the majority of the mode shapes are captured. On the other hand, the time-domain data require to be post-processed to extract the mode shapes and resonant frequencies. This type of analysis is also computationally expensive especially if it is used in conjunction with an implicit approach where the internal forces are amended based on Newton-Raphson iterative approach (Huang, 2007). Rate-dependent material damping is employed and fluid-solid equations are coupled so that the overall structure behaviour is dependent on both solid and fluid behaviour.

6.3. Theory and Terminology

6.3.1 Frequency Analysis approaches

There are a number of different approaches to performing a vibration analysis that can be listed as the following: linear perturbation, steady state, and transient. In linear perturbation approach, the natural frequencies are extracted by converting the equations of motion into the eigenvalue problem (Fu & He, 2001). In steady state approach, the inhomogeneous term

in solution of the equations of motion is taken and frequency response function is calculated based on input/output comparison (Simulia, 2013). The homogeneous and inhomogeneous responses are summed up in the transient solution. In this method, the frequency response components, phase lag and amplitude, are indirectly calculated using phase lag and amplitude detection function (Qian, et al., 2013) (Tekeli & Hazar, 2009). The computational cost in this method is very high due to consideration of the whole dynamic terms and data post-processing steps. However, the transient approach is capable of simulating the rate-dependent material behaviour and transient fluid dynamics while other methods do not support such simulations.

The dynamic transient technique can be compromised if the equilibrium condition in each time increment is not controlled. On the base of this fact, there are two techniques to propose a solution for a transient dynamic analysis: the implicit and explicit methods. In implicit method, the dynamic equilibrium situation is assessed by comparing the result of external load and the internal force. Afterward, the complete dynamic equilibrium is enforced within the structure by changing the internal forces in elements through the iterative Newton-Raphson method. To put it differently, the implicit method solves the equation in time $t+\Delta t$ on the base of itself and the solution at time t, and as a consequence, the solution is totally stable and gives for larger time increments. When the equilibrium condition is satisfied, the new stiffness matrix is made on the base of the enhanced externally applied load, and the solution is continued until the load has its eventual magnitude (Sun, et al., 2000). But In explicit approach, the above mentioned procedure is not considered and the dynamic equilibrium is not checked, therefore, the equilibrium is not essentially satisfied dissimilar the implicit approach. Final value in explicit method can deviate extremely from the exact

solution. The time increment size have to be sufficiently small to make sure that the solution does not want to drift from the correct solution (Jinting & Xiuli, 2002) (Xiaozhi, et al., 2002) (Xueliang, et al., 2006). In this research, the implicit approach is selected, knowing that the solution time may take longer using this approach.

6.3.2 Co-simulation

Co-simulation is commonly known as a method to link between physics and corresponding analysis which should be solved concurrently (Blades, et al., 2011). In this approach, the data flow of different analysis environments are linked at every time step, i.e. an analysis output of the simulation environment “A” is fed into the environment “B” and the inverse data flow which contains the output data of environment “B” at the same time step is fed back to “A”. This method is typically used when coupling of two or more physics is not properly achievable due to complex geometry or inconsistent solution methods. The two-state problem of fluid-solid interaction which is presented in this research is an example where the co-simulation method can be employed. The solid structure deformation under the applied load is computed using the FE analysis, and as a result, the boundary condition of flowing fluid is changed. This FE analysis output including the speed and deformed geometry is used to update the boundary condition of the CFD problem.

6.4. FE Simulation

The approach to simulate the behaviour of fluid-filled coolant rail is discussed in this section. The goal is to replicate the condition under which the test was conducted. An overview of the process is demonstrated in a flowchart, as it can be seen in Figure 6.1.

A fluid-solid interaction is modelled in Abaqus™ in order to mimic the dynamic behaviour of the flowing fluid inside the solid structure. The inner surface of the metal and rubber tube is

used to form the wall for the fluid in a separate model which is solved by CFD approach in Abaqus tools. The fluid wall is built from the solid by making a shell from the solid volume to ensure the exact geometry is used for the interaction.

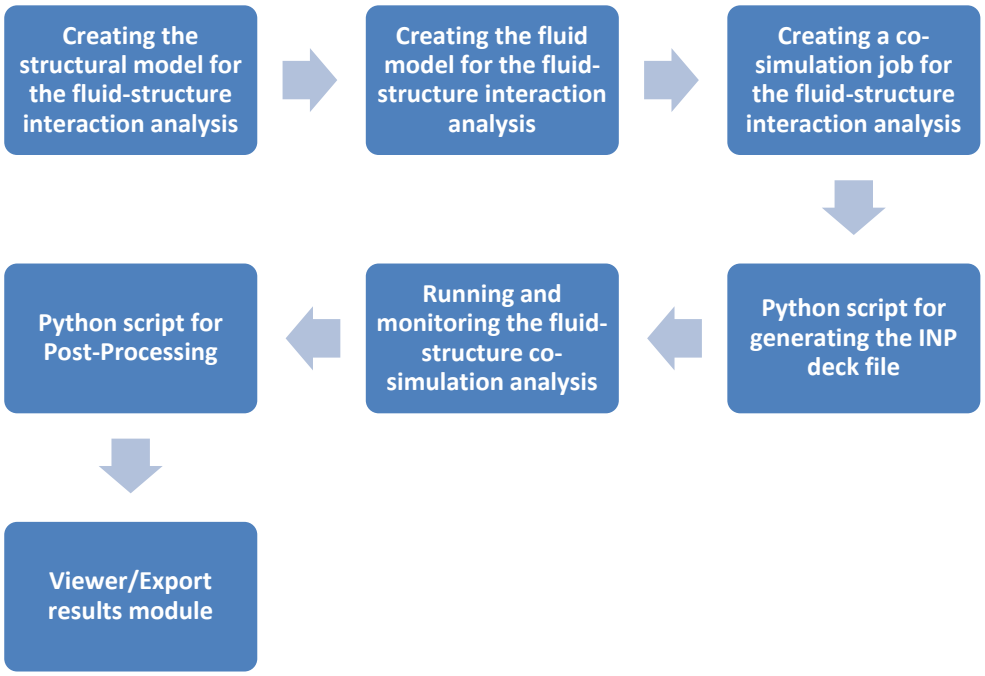


Figure 6.1: FSI vibration analysis process

The INP files were automatically generated by a pre-written python script for frequency ranges from 40 Hz to 800 Hz at every 2 Hz. Then, each INP file was automatically submitted to the Abaqus™ solver based on the co-simulation approach, for which the whole process was managed by the same script as presented in Appendix A.

In order to maintain the fidelity of time domain data, the step time is linked to the frequency content of the procedure. Therefore, a python script was written to ensure 20 time points are calculated per cycle of the sinusoidal excitation, which is enough to construct a sinusoidal shape. In solid material, the implicit analysis was conducted based on a quasi-static approach. The fluid analysis is considered to be incompressible fluid flow and the time integration approach is set to the trapezoid type.

After the output files were generated for the frequency range 40 to 800 Hz, a Matlab m-file script was developed to extract the data file including the recovered forces from the boundary condition and displacements at predefined nodes as indicated in Appendix A. The displacements were taken at six different points by averaging over several nodes of the finite element model. The displacement and recovered force were also extracted from the shaker-to-plate interface for calculation of the transmissibility and mobility.

6.5. Results and discussion

The water was static in the experiment, so the flow was simulated with very low velocity near zero for comparison. The simulation results and its comparison with experiment at point B are presented as an example for the vibrational behaviour in the coolant rail. Figure 6.2 illustrates the comparison between the co-simulation FE model and experiment in terms of the mobility magnitudes for point B. Lower frequency modes exhibit good agreement between simulation results and experimental results in terms of both frequency and amplitude since these modes have high vibrational energy content, hence signal noise and disturbances have limited effects on the results. In the higher frequency ranges, the resonant frequencies at which modes occur are less accurately predicted. This is also true for the amplitude. These discrepancies between simulation and experiment can be attributed to a number of reasons, namely: physical mounting of shaker to the structure via the load cell creates the probability of changing the dynamics of the structure; in the vicinity of a resonance with a small effective mass, very little force is needed to get a response, affecting the force quantity to be susceptible to noise; rotation in the structure reduces accuracy of measured acceleration by uniaxial transducer. Location of the measure points has been presented in Figure 4.9.

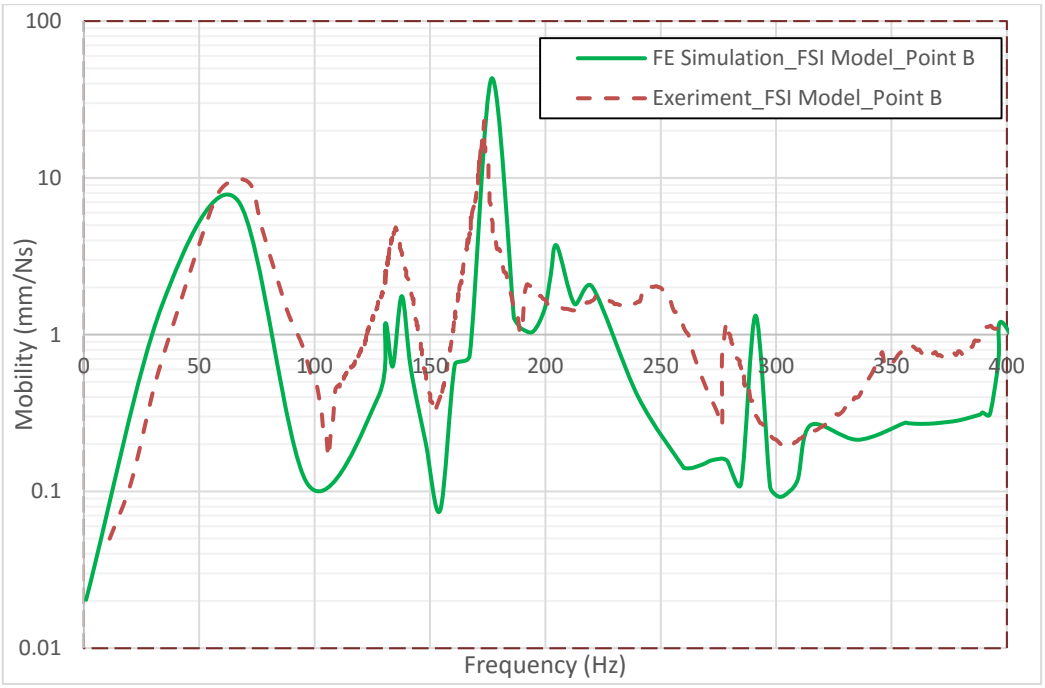


Figure 6.2: Comparison between coolant rail FSI vibration analysis and test result at V~0

Table 6.1: Comparison between forced vibration analysis and test results

Modes	FE FSI model resonant frequencies (Hz)	Test Result with water resonant frequencies (Hz)	Deviation
1nd Mode	67	72	6.9%
2nd Mode	138	136	1.5%
3rd Mode	177	172	2.9%
4th Mode	204	192	6.3%
5th Mode	221	226	2.2%
6th Mode	275	250	10.0%
7th Mode	291	274	6.2%
8th Mode	357	360	0.8%
9th Mode	397	396	0.3%
10th Mode	469	453	3.5%
11th Mode	524	537	2.4%
12th Mode	598	575	4.0%
13th Mode	674	700	3.7%

The corresponding modes from the co-simulation and experiment were extracted from the Figure 6.2 and shown for evaluation of the prediction of resonant frequencies in Table 6.1 and

Figure 6.3. The measured and predicted resonant frequencies are shown to follow the same tend and the percentage difference for each mode is shown. The difference between predicted and measured resonant frequency in all modes is less than 10% for point B as shown in Figure 6.3 as well as at the other measured positions. The first three dominant modes with highest mobility amplitude are also shown in Figure 6.4. This Figure demonstrates where, in the coolant rail, the most severe deformation occurs, which can be used as a guide for design changes.

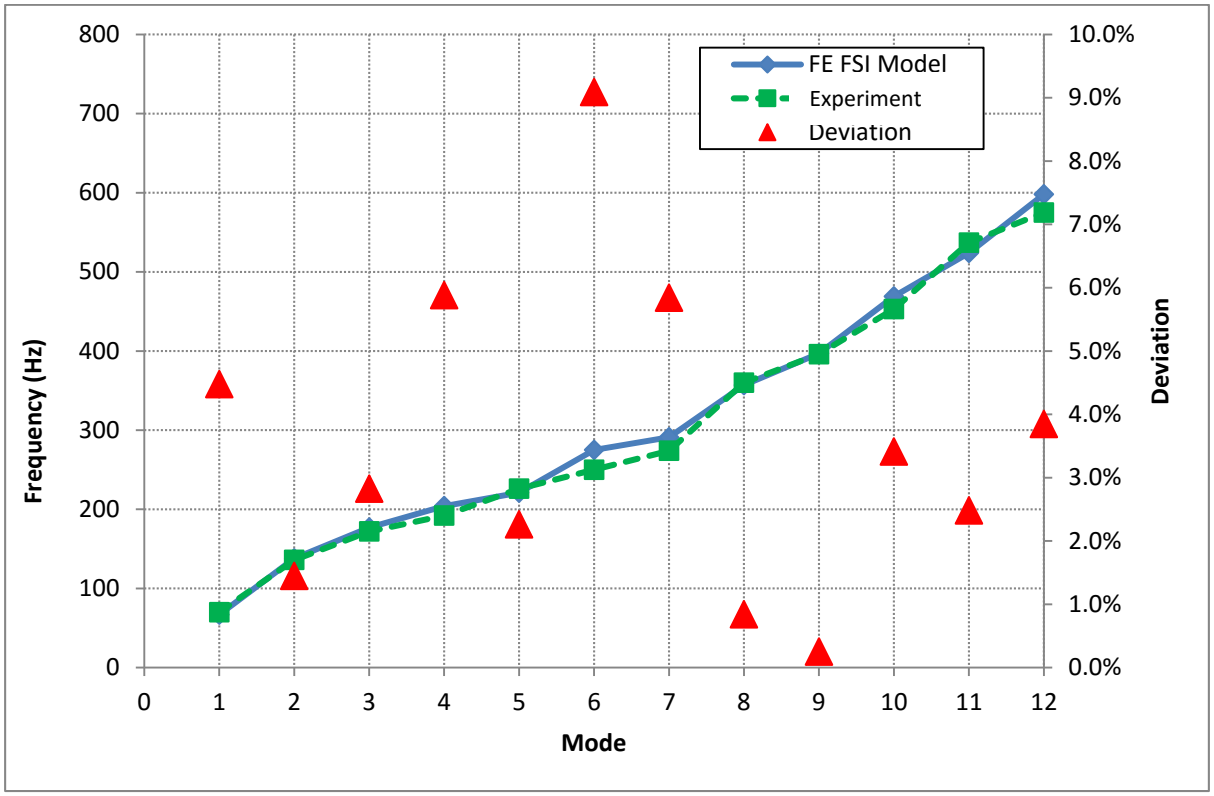
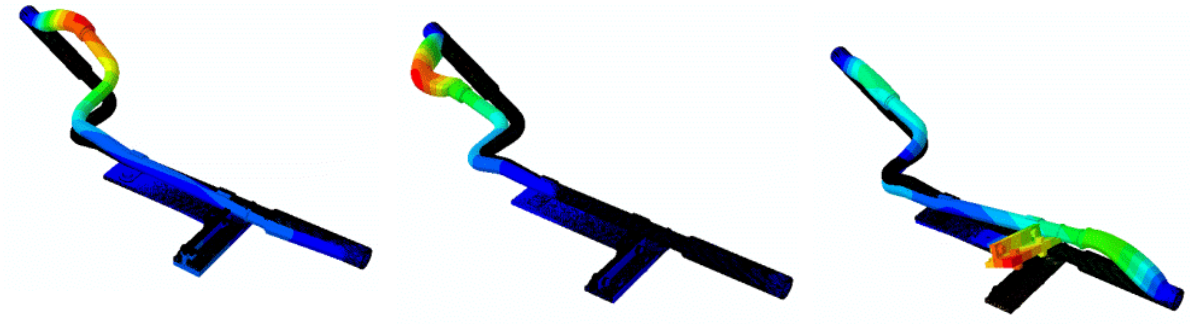


Figure 6.3: Comparison between forced vibration simulation and test results



(Mode 1) (Mode 2) (Mode 3)

Figure 6.4. Mode shapes of forced vibration analysis of FSI model

Furthermore, the influence of water in tube vibration in response to the shaker excitation was investigated in comparison to the tube when it is not filled with water, as shown in Figure 6.5 for a number of points. The resonant frequencies which are the frequencies at peak transmissibility in this Figure are lowered due to added water mass along the rail, which reduces both amplitude and resonant frequencies according to the linear first order representation of vibration model between the input and the point of interest. In the experiment with water, a number of modes either moved to a lower frequency as shown in Figure 6.6, which makes sense with a higher mass or were entirely damped out.

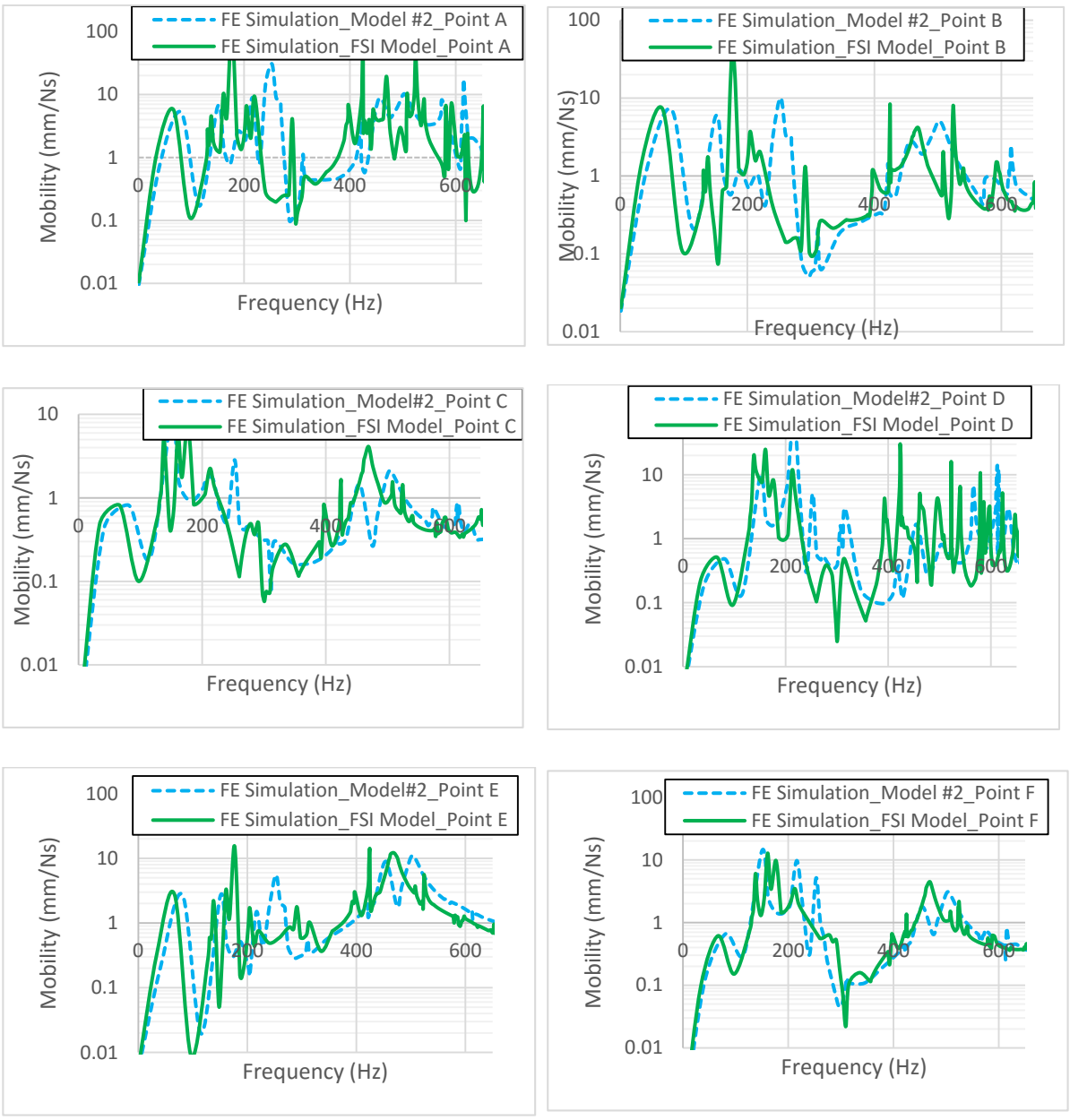


Figure 6.5: A comparison between forced vibration analysis in model with water and without water

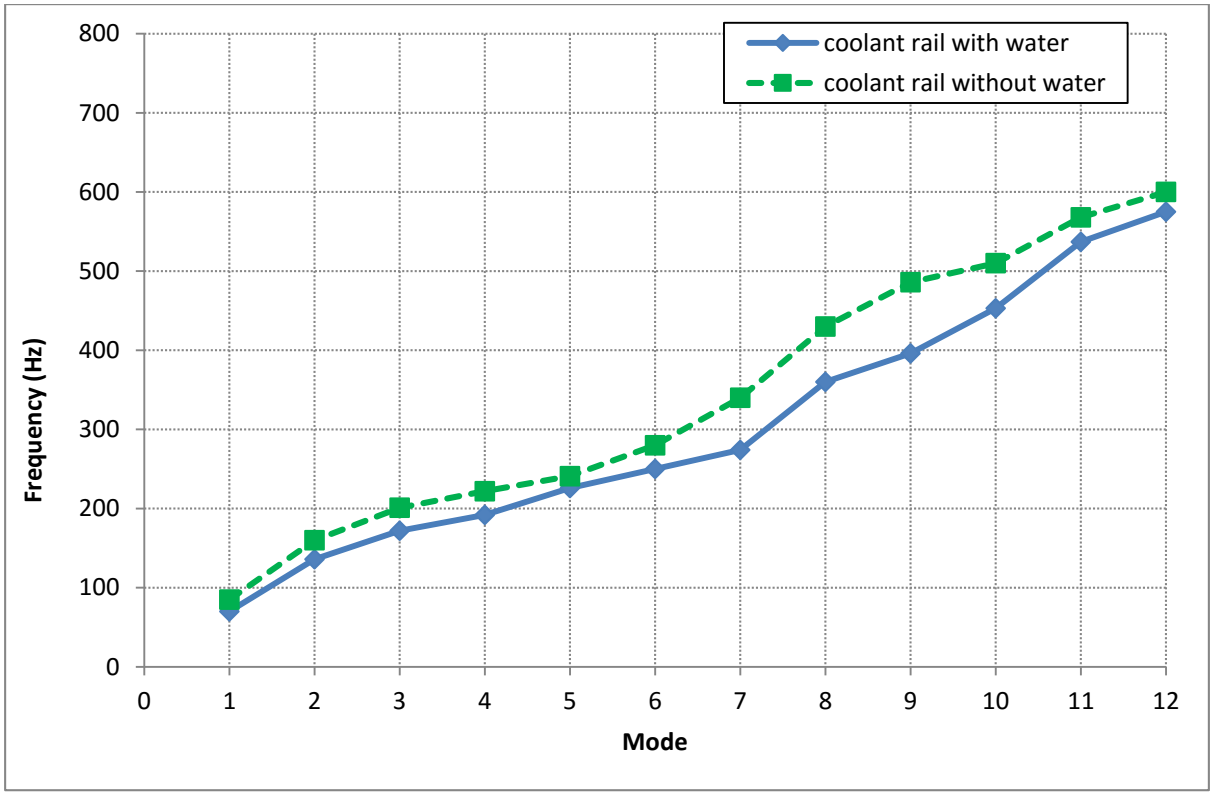


Figure 6.6: A comparison between resonant frequencies in model with water and without water

In order to see the effect of the flow velocity on the pipe vibration, the FSI analysis was carried out in the frequency range 40 to 80 Hz where the first model occurs. Since each run takes a long time to complete, an unequal step for changing the velocity is chosen so that a wider range of speed is covered. As it can be seen in Figure 6.7, the fluid inlet velocities 0, 5, 20, and 50 mm/s were selected in that the range is wide enough to capture a clear exposure on the decay trend in first harmonic in the simulated frequency range. The Figure 6.7 shows that the first harmonic which appears to be 67 Hz at zero flow velocity drops and ends up to 59 Hz at the velocity of 50 mm/s.

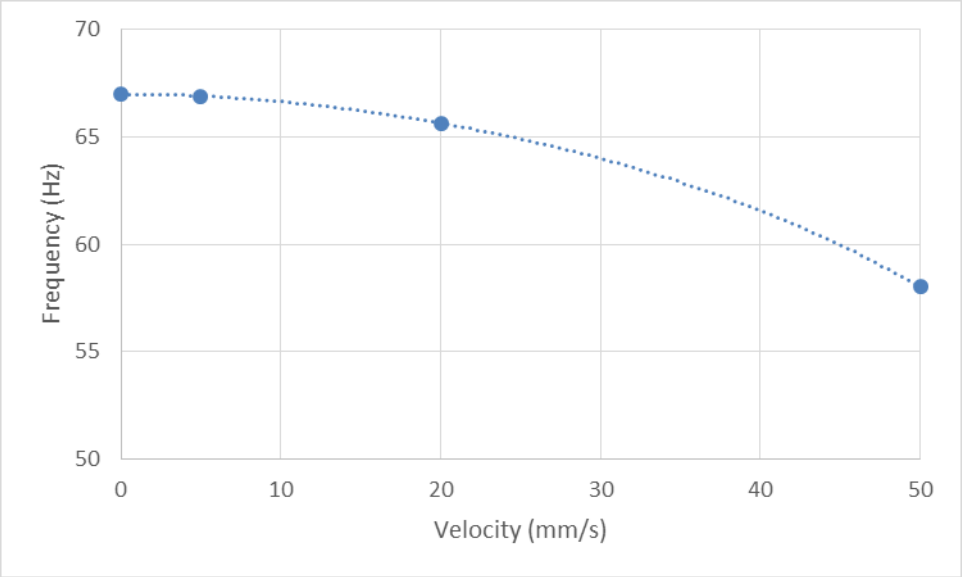


Figure 6.7: Effect of velocity of fluid flow on the first natural frequency of the coolant rail

6.6. Summary

The vibration of EGR coolant rail with water flowing inside it, was investigated in this chapter. An implicit multi-physics co-simulation approach was employed in conjunction with the solid-fluid interface to analyse the vibration behaviour of the coolant rail which was filled with water. The test was conducted using a shaker attached to the coolant rail to generate vibration inputs in the frequency range 40 to 800 Hz. The same frequency range was used to vibrate the rail in Abaqus™ simulation environment and the resonant frequencies and modes were extracted. In general, it was found that the water moves the modes to lower frequencies as shown in the response plot due to the added mass of the water into the structure. In addition, the comparison of resonant modes from test and simulation indicated a prediction error of less than 10% for most of the resonant modes. In conclusion, the co-simulation approach suggests a good correlation with the experiment results and can be used as a part of design synthesis process.

Chapter 7: Conclusion and Future Work

7.1. Conclusion

In this section, thesis approach, accomplishments and contribution of this research are discussed.

Thesis approach:

- Developed a finite element model which is capable of accurately representing the vibration testing of a Diesel Engine EGR Coolant Rail without rubber hoses attached.
- Measured the vibration response of the EGR Coolant rail on a vibration rig with a view to correlating the results of the finite element model.
- Material modelling and testing for characterization of the Rubber Hoses overall behaviour
- Extended the finite element model to include rubber hoses which are attached and grounded.
- Validated the extended finite element model with vibration response obtained from a vibration test on the EGR coolant rail with rubber hoses attached.
- Developed techniques for estimating the elastic stiffness and damping introduced by the addition of the rubber hoses.
- Used Finite Element Approach as a numerical-physical model for analysis of the EGR Coolant Rail behaviour which is field with water (multi-physics co-simulation)

The highlights of **achievements** are listed below and discussed in more details in the following.

- Benchmarked available material models comprehensively

- Proposed procedures for material testing and parameterisation of material properties.
- Obtained rubber hoses material properties with university of Birmingham test facilities
- Designed and developed free and forced vibration test rig.
- Developed the testing interface in LabVIEW software by National Instruments™ for customized input functions and data acquisition system. Conducted vibration test of coolant rail with and without rubber hoses.
- Developed coolant rail models with reinforced layer modelling of rubber hoses in Finite Element.
- Optimised the diesel engine EGR coolant rail FE models based on the mesh size, type and solver configuration. Subsequently investigated the effect of mesh element type of Finite Element Model on coolant rail vibration analysis. Compared different types of mesh used for vibration investigation in terms of accuracy and computation time/cost.
- Verified the FE model accuracy in prediction of coolant rail vibration behaviour against vibration experiments
- Implemented multi-physics co-simulation in conjunction with the fluid solid interactions to analyse the vibration behaviour of the coolant rail which was filled with water

Generally three type of nonlinearities are identified on the problem of this research: the material nonlinearity in mechanical behaviour of the rubber hose, the geometrical nonlinearity in the contact problem, and the nonlinear interaction in physics between the

solid structure and fluid. The main achievement of this research is bringing the effect of these three major nonlinearity parameters in the vibration analysis and solved it using dynamic implicit approach.

Moreover, a comparison study was performed on the various mesh types and density of the finite element simulation of coolant rail with hammer test results to realise which approach is more appropriate for the vibration analysis of coolant rail. The C3D20R element type was found to be the most cost-effective and precise element for frequency analysis. The C3D20 element provided the same consistent and accurate results with a slightly longer solution time. The linear hexahedral incompatible mode elements C3D8I are sensitive to mesh density and does not provide good agreement between the FE results and test data. The linear hexahedral reduced integration element C3D8R was imprecise with low mesh density but increasing the mesh density caused improving the results. However its accuracy was still poorer than for the above element. The accuracy of the C3D8 element was highly reliant on mesh density.

Taking advantage of the use of commercial finite element software, the rubber hoses were modelled by representing the reinforcement cord and rubber by rebar elements and solid elements respectively. The simulation of the dynamic response of the coolant rail was carried out by modal and Subspace based Steady-State Dynamic Analysis in Abaqus™, and the FE results compared reasonably well with the results obtained from the physical rig tests. Accuracy of simulated dynamic responses was not unduly affected at low frequency less than 200Hz by replacement of the rubber hoses with appropriate spring-dashpot elements which can offer substantial savings in computational costs.

Some of the modes revealed by FE simulation could not be excited in the physical tests due to their complex nature involving a combination of translational and rotational motion. This is thought to be responsible for some of the discrepancies in mobility response in physical tests in comparison with those obtained from FE simulation.

Finite element simulation can be used to predict the response of the EGR coolant rail in a physical test. With a view to optimising its design, FE simulation can be used to predict changes to its modal parameters if physical modifications (mass, damping, stiffness, and substructures) are added. The vibration response of the structure to various excitation forces applied in any of the defined degrees of freedom may therefore be predicted using FE simulation.

An implicit multi-physics co-simulation approach was employed in conjunction with the solid-fluid interface to analyse the vibration behaviour of the coolant rail which was filled with water in chapter 6. The test was conducted using a shaker attached to the coolant rail to generate vibration inputs in the frequency range 40 to 800 Hz. The same frequency range was used to vibrate the rail in Abaqus™ simulation environment and the resonant frequencies and modes were extracted. In general, it was found that the water moves the resonant modes to lower frequencies as shown in the response plot due to the added mass of the water into the structure. In addition, the comparison of resonant modes from test and simulation indicated a prediction error of less than 10% for most of the resonant frequencies. In conclusion, the co-simulation approach suggests a good correlation with the experiment results and can be used as a part of design synthesis process.

Contribution

- Designed and Developed vibration test rig.
- Tackled nonlinearities and convergence issues encountered in solution of FE EGR coolant rail model with rubber hoses and fluid.
- Found a fast and accurate material model for rubber
- Investigated the optimized diesel engine EGR coolant rail FE models, solver configuration and mesh quality
- Investigated various methods of vibration analysis
- Developed a two-phase CFD-FEA vibration analysis using the co-simulation approach.

7.2. Future work

A number of simulations and tests would be considered as future works. These modifications can increase the simulation output accuracy in comparison with test data and ease the approach of extracting appropriate spring/dashpot characteristics in the model. These modifications can be described as below:

In this thesis, the cord fabric material was not tested to obtain its material property due to difficulties in extracting it healthily. Rather, typical properties were taken from a text book. The cord can be however extracted using appropriate instruments and the material properties of it can be obtained from the same test facility in which the rubber is tested. In addition, a design synthesis by different type of cord material, spacing and orientation could be performed to investigate the impact of cord geometry and material on mode shapes and resonant frequencies.

In this thesis, the impact of static coolant fluid in the vibration of coolant rail system was only investigated due to insufficiency of test rig and equipment available for vibration testing. The effect of cooling fluid velocity in the tube on the vibration response can be considered using identical FSI approach which was used in chapter 6 to potentially increase the accuracy in prediction of resonant frequency and damping. A similar study can be arranged to investigate the influence of coolant fluid pressure, viscosity and temperature. In latter case, the temperature has a considerable influence on hyperelastisity and viscoelasticity of rubber hose which directly impact the mechanical behaviour and mode shape formation. This becomes even more highlighted owing to the fact that the fluid and engine temperature can rapidly change in different operating and weather conditions.

The rubber hose in chapter 4 was simply modelled using a dashpot and spring which means the frequency dependency is assumed to be negligible. However, assuming an average value for damping ratio would lead to potential inaccuracy in the frequency response analysis. Using frequency dependent characteristics for equivalent rubber spring stiffness and dashpot can be considered rather than the average constant value used in this thesis.

References

1. Abu-Abdeen, M., 2010. Single and double-step stress relaxation and constitutive modeling of viscoelastic behavior of swelled and un-swelled natural rubber loaded with carbon black. *Material and Design,* Volume 31, pp. 2078-2084.

2. Agilent Technologies, 2000. The Fundamental of Modal Testing. [Online] Available at: http://literature.agilent.com/litweb/pdf/5954-7957E.pdf

3. Allahverdizadeh, A. et al., 2013. Structural modeling, vibration analysis and optimal viscoelastic layer characterization of adaptive sandwich beams with electrorheological fluid core. Mechanics Research *Communications,* Volume 51, pp. 15-22.

4. Arruda, E. M. & Boyce, M. C., 1993. A three-dimensional model for the large stretch behavior of rubber elastic materials. *Journal of the Mechanics and Physics of Solids,* 41(2), pp. 389-412.

5. Austrell, P. & Olsson, A., 2012. Considering amplitude dependence during cyclic loading of elastomers using an equivalent viscoelastic approach. Polymer Testing, 31(7), pp. 909-915.

6. Auweraer, H. V. d. & Janssens, K., 2007. Virtual Prototyping for Sound Quality Design of Automobile, Leuven, Belgium : LMS International.

7. Ballarini, R., 2006. The Da Vinci-Euler-Bernoulli Beam Theory, s.l.: Mechanical Engineering Magazine Online..

8. Baqersad, J. et al., 2012. Dynamic Stress–Strain on Turbine Blade Using Digital Image Correlation Techniques Part 1: Static Load and Calibration. Conference Proceedings of the Society for Experimental Mechanics Series, Volume 2, pp. 215-220.

9. Baqersad, J., Carr, J., Niezrecki, C. & Avitabile, P., 2012. Dynamic Stress–Strain on Turbine Blades Using Digital Image Correlation Techniques Part 2: Dynamic Measurements. Conference Proceedings of the Society for Experimental Mechanics Series, Volume 2, pp. 221-226.

10. Baqersad, J., Lundstrom, T., Niezrecki, C. & Avitabile, P., 2012. Using High-Speed Stereophotogrammetry Techniques to Extract Shape Information from Wind Turbine/Rotor Operating Data. Conference Proceedings of the Society for Experimental Mechanics Series, Volume 6, pp. 269-275.

11. Bechira, H., Chevalierb, L., Chaouchec, M. & Boufalaa, K., 2006. Hyperelastic constitutive model for rubber-like materials based on the first Seth strain measures invariant. European Journal of Mechanics - A/Solids, 25(1), p. 110–124.

12. Behroozi, M., Olatunbosun, O. & Ding, W., 2012. Finite element analysis of aircraft tyre – Effect of model complexity on tyre performance characteristics. Materials & Design, Volume 35, pp. 810-819.

13. Behroozi, M., Olatunbosun, O. & Ding, W., 2012. Finite element analysis of aircraft tyre – Effect of model complexity on tyre performance characteristics. Materials & Design, 35(810-819).

14. Berger, H., Erne, O. & Klein, M., 2012. The Use of Stereo-Photogrammetry to Precisely Determine 3D-Positions, Motions and Deformations on Sports Equipment. Conference Proceedings of the Society for Experimental Mechanics Series, Volume 6, pp. 481-486.

15. Bergstrom, J. S. & Boyce, M. C., 2001. Deformation of Elastomeric Networks: Relation between Molecular Level Deformation and Classical Statistical Mechanics Models of Rubber Elasticity. Macromolecules, 34(3), pp. 614-626.

16. Bhadeshia, H. & Honeycombe, S. R., 2006. Steels. Third ed. s.l.:Butterworth Heinemann.

17. Blades, E. et al., 2011. Multiphysics Simulation Capability using the SIMULIA Co-Simulation Engine. Honolulu, Hawaii, 20th AIAA Computational Fluid Dynamics Conference .

18. Bolarinwa, E., 2004. Finite Element modelling of the pneumatic tyres, Birmingham: University of Birmingham.

19. Bolarinwa, E. & Olatunbosun, O., 2004. Finite Element Simulation of the Tyre Burst Test. Proceedings of the Institution of Mechanical Engineers Part D: Journal of Automobile Engineering, 218(11), pp. 1251-1258.

20. Bolarinwa, E., Olatunbosun, O. & and Burnett, M., 2004. A Study of Cornering Behaviour using a Finite Element Model. Beijing, China, s.n.

21. Boyce, M. C. & Arruda, E. M., 2000. Constitutive Models of Rubber Elasticity: A Review. Rubber Chemistry and Technology, 73(3), pp. 504-523.

22. Bruke, A. M., 1998. Finite Element Simulation and Experimental Analysis of Stationary and Rotating Tyre Behaviour, Ph.D. Thesis, s.l.: The University of Birmingham.

23. Carrera, E., Zappino, E. & Filippi, M., 2013. Free Vibration Analysis of Thin-Walled Cylinders Reinforced With Longitudinal and Transversal Stiffeners. Journal of Vibration and Acoustics, 35(1).

24. Carroll, M., 2011. A Strain Energy Function for Vulcanized Rubbers. Journal of Elasticity, 103(2), pp. 173-187.

25. Chang, T., Saleeb, A. & Li, G., 1991. Large strain analysis of rubber-like materials based on a perturbed Lagrangian variational principle. Computational Mechanics, 8(4), pp. 221-233.

26. Chen, W. & Saleeb, A. F., 1982. Constitutive Equations for Engineering Materials, Vol. 1, Elasticity and Modeling. 1st ed. New York: Wiley.

27. Chen, Z.-y.et al., 2011. Finite Element Analysis of Light Vehicle Cab's Hydraulic Mount Based on Fluid-Structure Interaction Method. Detroit, USA, SAE International.

28. De Silva, C., 2000. Vibration: fundamentals and practice. s.l.:CRC Press LLC, v.

29. DJB Instruments, L., 2008. http://www.djbinstruments.com. [Online] Available at: http://www.djbinstruments.com/images/datasheets/monocharge/A23.pdf

30. DJB Instruments, L., 2008. http://www.djbinstruments.com. [Online] Available at: http://www.djbinstruments.com/images/AT04_revised.pdf

31. Dostal, H., 1939. The Statistical Theory of the Elasticity of Rubber. Rubber Chemistry and Technology, 12(1), pp. 56-63.

32. Dunlop, 2013. Tyre reprository. [Online] Available at: http://www.dunlopaircrafttyres.com/

33. Dunn, J. W., 1972. Experimental and Theoretical Mechanical Mobility Characterising Functions of Rolling And Non-Rolling Tyres. s.l., Science and Motor Vehicle Symposium, University of Belgrade, pp. 171-185.

34. Dunn, J. W., 1972. The Mechanical Mobility of Rolling Tyres, Ph.D. Thesis, s.l.: The University of Birmingham.

35. Dunn, J. W. a. O. ,. O. A., 1988. A new Electro-Hydraulic Triaxial Tyre Test Facility for Low-Frequency Rolling Tyre Dynamics. International Journal of Vehicle Design, 9(2), pp. 242-251.

36. Dunn, J. W. & Olatunbosun, O. A., 1989. Linear and Non-Linear Modelling of Vehicle Rolling Tyre Low Frequency Dynamic Behaviour, The Dynamics of Vehicles on Roads and Tracks. Kingston, Ontario, Proceedings 11th IAVSD Symposium, pp. 179-189.

37. Duvigneau, F., Nitzschke, S., Strackeljan, J. & Gabbert, U., 2015. VIRTUAL ENGINEERING APPROACH FOR THE ANALYSIS OF THE ACOUSTIC BEHAVIOR OF AN ENGINE. Florence , Italy, the 22nd international congress on sound and vibration .

38. Dytran Instrument, 2014. Dytran Instrument. [Online] Available at: http://www.vibrationdata.com/tutorials/Dytran.pdf [Accessed 10 11 2014].

39. Ericsson, T. & Ruhe, A., 1980. The Spectral Transformation Lanczos Method for the Numerical Solution of Large Sparse Generalized Symmetric Eigenvalue Problems. Mathematics of Computation, Volume 35, pp. 1251-1268.

40. Ewins, D., 2000. Modal Testing: Theory, Practice and Application. 2nd ed. s.l.:Baldock: Research Studies Press.

41. FAA, 1997. Advisory Circular, s.l.: Federal Aviation Administration.

42. Ferry, J. D., 1980. Viscoelastic Properties of Polymers. 3rd ed. s.l.:Wiley.

43. Flory, P. J., 1967. Principles of Polymer Chemistry. 1st ed. Lincoln: Cornell University Press.

44. Flory, P. J., 1977. Theory of elasticity of polymer networks. The effect of local constraints on junctions. The Journal of Chemical Physics, 66(12), pp. 5720-5729.

45. Flory, P. J. & Erman, B., 1982. Theory of elasticity of polymer networks. Macromolecules, 15(3), pp. 800-806.

46. Friswell, M. I. and Mottershead, J.E., n.d. Finite Element Model Updating In Structural Dynamics. s.l., Kluwer Academic Publishers Group, Dordrecht.

47. Fu, Z.-F. & He, J., 2001. Modal Analysis. first ed. Oxford: Butterworth-Heinemann.

48. Gagliano, C., Tondra, M., Fouts, B. & and Geluk, T., 2009. Development of an Experimentally Derived Tire and Road Surface Model for Vehicle Interior Noise Prediction. s.l., SAE World Congress & Exhibition.

49. Gent, A., 1996. A new constitutive relation for rubber. Rubber Chemistry and Technology, 69(1), pp. 59-61.

50. Gent, A., 2001. Engineering with Rubber 2E: How to Design Rubber Components. 2nd ed. New York: Hanser Publications.

51. Gent, A. & Thomas, A., 1958. Forms for the stored (strain) energy function for vulcanized rubber. Journal of Polymer Science, Volume 28, pp. 625-628.

52. Ghoreishy, H., 2012. Determination of the parameters of the Prony series in hyper-viscoelastic material models using the finite element method. Materials & Design, Volume 35, pp. 791-797.

53. Göktepe, S. & Miehe, C., 2005. A Micro-Macro Approach to Rubber-Like Materials. Part III: The Micro-Sphere Model of Anisotropic Mullins-Type Damage. Journal of the Mechanics and Physics of Solids, 53(10), pp. 2259-2283.

54. Guo, Z. & Sluys, L. J., 2006. Application of a new constitutive model for the description of rubber-like materials under monotonic loading. International Journal of Solids and Structures, 43(9), pp. 2799-2819.

55. Haupt, P., 2000. Continuum mechanics and theory of materials. 1st ed. Berlin: Springer-Verlag.

56. Hirate, N., Komada, M., Yoshioka, T. & Thomann, S., 2009. V6-SUV Engine Sound Development. s.l., SAE Technical Paper.

57. Holzapfel, G. A., 2000. Nonlinear Solid Mechanics: A continuum approach for engineering. 1st ed. s.l.:John Wiley &Sons Ltd.

58. Hong, S., 2008. CAE Virtual Durability Tests of Automotive Products in the Frequency Domain. AE Int. J. Passeng. Cars - Mech. Syst, 1(1), pp. 165-174.

59. Hooke, R., 1676. Description of Helioscopes. s.l.:s.n.

60. Huang, S., 2007. DYNAMIC ANALYSIS OF ASSEMBLED STRUCTURES WITH NONLINEARITY, PhD Thesis. london: Department of Mechanical Engineering Imperial College London.

61. Hughes, T. J. R., 2000. Finite Element Method: Linear Static and Dynamic Finite Element Analysis. 2nd ed. New Jersey : Dover.

62. Isihara, A., Hashitsume, N. & Tatibana, M., 1951. Statistical Theory of Rubber-Like Elasticity. IV. (Two-Dimensional Stretching). Journal of Chemical Physics, Volume 19, pp. 1508-1512.

63. Jaguar Company, 2012. Jaguar XF Workshop Manual 3.0 TDV6. [Online] Available at: http://www.jagdocs.com/index.php?main_page=product_info&cPath=68_104&products_id=881

64. James, H. & Guth, E., 1943. Theory of the elastic properties of rubber. The Journal of Chemical Physics, 11(10), pp. 455-481.

65. Jiang, X. C. & Mao, K. M., 2014. Strain Gauges Applied to the Lightweight Structures Modal Testing. Aplied Mechanics and Materials, Volume 635-637, pp. 208-213.

66. Jinting, W. & Xiuli, D., 2002. An Explicit Difference Method for Dynamic Analysis of a Structure System with Damping. Engineering Mechanics, 1(3), pp. 109-112.

67. Jung, H. S. et al., 2013. Advancement of Noise, Vibration and Harshness (NVH) Performance of Vehicle Rubber Hoses. Asian Journal of Chemistry, 25(9).

68. Kaliske, M. & Rothert, H., 1997. On the finite element implementation of rubber-like materials at finite strains. Engineering Computations, 14(2), pp. 216-232.

69. Kim, M., Jo, J., Sohn, J. & Yoo, W., 2003. Reduction of Road Noise by the Investigation of Contributions of Vehicle Components. s.l., SAE 2003 Noise & Vibration Conference and Exhibition.

70. Kook, H., Lee, D. & IH, K., 2011. VEHICLE INTERIOR NOISE MODEL BASED ON A POWER LAW. International Journal of Automotive Technology, 12(5), pp. 777-785.

71. Kuhn, W. & Grün, F., 2003. Statistical behavior of the single chain molecule and its relation to the statistical behavior of assemblies consisting of many chain molecules. Journal of Polymer Science, 1(3), pp. 183-199.

72. Kumara, A., Jaiswala, H., Pandeya, A. & Patil, P. P., 2014. Free Vibration Analysis of Truck Transmission Housing Based on FEA. s.l., Procedia Materials Science, Elsevier, pp. 1588-1592.

73. Kupchella, R., Kidney, J. & Hutchison, a. W., 2009. Test methods for hyperelastic characterization of rubber. Tire Science and Technology, 37(3), pp. 165-186.

74. Lang, G. F. & Snyder, D., 2001. Multi-actuator vibration control shaker performance. Sound & Vibration, october.

75. Lewandowski, R. & Chorążyczewski, B., 2010. Identification of the parameters of the Kelvin–Voigt and the Maxwell fractional models, used to modeling of viscoelastic dampers. Computers & Structures, 88(1-2), pp. 1-17.

76. Liu, M. & Gorman, D., 1995. Formulation of Rayleigh damping and its extensions. Computers & Structures, 57(2), pp. 277-285.

77. Marlow, R. S., 2003. First-Invariant Hyperelastic Constitutive Model. In: J. Busfield & A. Muhr, eds. Constitutive Models Rubber III. Lisse: Swets & Zeitlinger, pp. 157-160.

78. McConnell, K. G., 1995. Vibration Testing: Theory and Practice. 2nd ed. s.l.:John Wiley & Sons.

79. Measurement Specialties, Inc, 2001. Piezo Film Sensors, Valley Forge, PA : s.n.

80. Meuniera, L. et al., 2008. Mechanical experimental characterisation and numerical modelling of an unfilled silicone rubber. Polymer Testing, 27(6), pp. 765-777.

81. Miehe, C., Göktepe, S. & Lulei, F., 2004. A micro-macro approach to rubber-like materials--Part I: the non-affine micro-sphere model of rubber elasticity. Journal of the Mechanics and Physics of Solids, 52(11), pp. 2617-2660.

82. Miehe, C., Göktepe, S. & Lulei, F., 2004. A micro-macro approach to rubber-like materials—Part I: the non-affine micro-sphere model of rubber elasticity. Journal of the Mechanics and Physics of Solids, 52(11), pp. 2617-2660.

83. Mills, B. a. D. ,. J. W., 1971. The Mechanical Mobility of Rolling Tyres. s.l., Automobile Division Conference of Vibration and Noise in Motor Vehicles, The Institution of Mechanical Engineers,, pp. 90-101.

84. Minck, O., Binder, N., Cherrier, O. & Lamotte, L., 2012. Fan noise analysis using a microphone array. s.l., International Conference on Fan Noise, Technology, and Numerical Methods.

85. Mooney, M., 1940. A theory of large elastic deformation. Journal of Applied Physics, Volume 11, pp. 582-592.

86. Muhr, A. H., 2005. Modelling the stress-strain behaviour of rubber. Rubber Chemistry and Technology, 78(3), pp. 391-425.

87. Nah, C. et al., 2010. Problems in determining the elastic strain energy function for rubber. International Journal of Non-Linear Mechanics, 45(3), pp. 232-235.

88. Nedergaard, N. J., Heinen, F. & Sloth, S., 2014. The effect of light reflections from the snow on kinematic data collected using stereo-photogrammetry with passive markers. Sports Engineering, 17(2), pp. 97-102.

89. Nguyen-Thoi, T., Phung-Van, P., Nguyen-Hoang, S. & Lieu-Xuan, Q., 2014. A coupled alpha-FEM for dynamic analyses of 2D fluid–solid interaction problems. Journal of Computational and Applied Mathematics, Volume 271, p. 130.

90. Oettle, N. et al., 2010. The effects of unsteady on-road flow conditions on cabin noise. s.l., SAE.

91. Ogden, R., 1997. Non-linear Elastic Deformations. 1st ed. Dover, New York: Dover Publications.

92. Ogden, R. W., 1972. Large Deformation Isotropic Elasticity: On the Correlation of Theory and Experiment for Compressible Rubberlike Solids. Proceeding of the Royal Society of Mathematical, Physical, and Engineering Sciences, 326(1567), pp. 565-584.

93. Ogden, R. W. & Roxburgh, D. G., 1999. A pseudo-elastic model for the Mullins effect in filled rubber. Proceeding of the Royal Society of London, 455(1988), pp. 2861-2877.

94. Ogden, R. W., Saccomandi, G. & Sgura, I., 2004. Fitting hyperelastic models to experimental data. Computational Mechanics , 34(6), pp. 484-502.

95. Ogden, R. W., Saccomandi, G. & Sgura, I., 2006. On worm-like chain models within the three-dimensional continuum mechanics framework. Proceeding of the Royal Society of Mathematical, Physical, and Engineering Sciences, 462(2067), pp. 749-768.

96. Olatunbosun, O. A. & Dunn, J. W., 1991. Generalized Representation of Low Frequency Radial Dynamic Parameters of Rolling Tyres. International Journal of Vehicle Design, 12(5/6), pp. 513-524.

97. Olatunbosun, O. & Bolarinwa, E., 2004. FE Simulation of the Effect of Tire Design Parameters on Lateral Forces and Moments. Tire Science and Technology jornal TSTCA, 32(3), pp. 146-163.

98. Ole Dossing, B., 1988. Structural Testing. s.l.:s.n.

99. Ooi, L. & Ripin, Z., 2011. Dynamic stiffness and loss factor measurement of engine rubber mount by impact test. Materials & Design, 32(44), pp. 1880-1887.

100. Park, J., Choi, S. & and Hong, S., 2011. The Prediction of Fuel Sloshing Noise Based on Fluid-Structure Interaction Analysis. SAE Int. J. Passeng. Cars – Mech. Syst., 4(2), pp. 1304-1310.

101. Parlett, B. N., 1980. The Symmetric Eigenvalue Problem. New Jersey: Prentice-Hall, Englewood Cliffs.

102. Parlett, B. N. & Nour-Omid, B., 1989. Toward a Black Box Lanczos Program. Computer Physics Communications, Volume 53, pp. 169-179.

103. Paul, D., 2004. Estimation of Engine NVH Variability. s.l., SAE Technical Paper.

104. Phillips, A., 1971. A Study of Road Noise,, s.l.: The Institution of Mechanical Engineers.

105. Phung-Van, P., Nguyen-Thoi, T., Le-Dinh, T. & Nguyen-Xuan, H., 2013. Static and free vibration analyses and dynamic control of composite plates integrated with piezoelectric sensors and actuators by the cell-based smoothed discrete shear gap method (CS-FEM-DSG3). Smart Materials and Structures, 22(9).

106. Qian, W., Chen, G. & Zhou, Z., 2013. Dynamic transient analysis of squealing vibration of a reciprocating sliding system. Wear, 301(1-2), pp. 47-56.

107. R.R.Bouche, 1965. Ensuring the accuracy of shock and vibration measurment, s.l.: Transducer Engineering Manager Endevco.

108. Ramachandran, T., Padmanaban, K. & Nesamani, P., 2012. Modeling and Analysis of IC Engine Rubber Mount Using Finite Element Method and RSM Procedia Engineering. Procedia Engineering, Volume 38, pp. 1683-1692.

109. Rao , M. N., Schmidt, R. & Schröder, K.-U., 2015. Finite rotation FE-simulation and active vibration control of smart composite laminated structures. Computational Mechanics, 55(4), pp. 719-735.

110. Rivlin, R. S., 1992. The Elasticity of Rubber. Rubber Chemistry and Technology, 65(3), pp. 51-66.

111. Roylance, D., 2001. Engineering Materials. Department of Materials science and Engineering, Massachusetts Institute of Technology Cambridge.

112. Sacks, M. & Brackett, S., 1989. Subjective Evaluation of Simulated Engine Induction Noise. s.l., SAE Transactions, pp. 1170-1178.

113. Safizadeh, ,. M. & Latifi, S., 2014. Using multi-sensor data fusion for vibration fault diagnosis of rolling element bearings by accelerometer and load cell. Information Fusion , Volume 18, pp. 1-8.

114. Sasso, M., Palmieri, G., Chiappini, D. & Amodio, D., 2008. Characterization of hyperelastic rubber-like materials by biaxial and uniaxial stretching tests based on optical methods. Polymer Testing, 27(8), pp. 995-1004.

115. Simon, H. D., 1984. The Lanczos Algorithm with Partial Reorthogonalization. Mathematics of Computation, Volume 42, pp. 115-142.

116. Simulia, 2013. Abaqus Analysis User's Manual, s.l.: Dassault Systèmes.

117. Singh, M., Verma, N. & Moreschi, L., 2003. Seismic Analysis and Design with Maxwell Dampers. J. Eng. Mech., 129(3), pp. 273-282.

118. Stout, J., 2001. Engine Excitation Decomposition Methods and V Engine Results. s.l., SAE Technical Paper.

119. Sun, J., K.H.Lee & H.P.Lee, 2000. Comparison of implicit and explicit finite element methods for dynamic problems. Journal of Materials Processing Technology, 105(1-2), pp. 110-118.

120. Sun, Z., Steyer, G. & Ranek, . M., 2002. FEA Studies on Axle System Dynamics. s.l., SAE.

121. Swanson, S., 1985. A constitutive model for high elongation elastic materials. Journal of Engineering Materials and Technology - ASME Transaction, Volume 107, pp. 110-115.

122. Tekeli, A. & Hazar, S. a. S. A., 2009. Transient Analysis of Engine Parts under Engine Loads and Random Road Vibration for Fatigue Evaluation. SAE Int. J. Commer. Veh., 1(1), pp. 275-283.

123. TMS , 2015. Sound and Vibration Rental Pricelist, Cincinnati OH : s.n.

124. Tong, Z., Zhang, Y., Zhang, Z. & Hua, H., 2007. Dynamic behavior and sound transmission analysis of a fluid–structure coupled system using the direct-BEM/FEM. Journal of Sound and Vibration, 299(3), p. 645.

125. Treloar, L. R. G., 1975. The Physics of Rubber Elasticity. 3rd ed. Oxford: Clarendon Press.

126. University of Birmingham, 2013. Bluebear. [Online] Available at:

https://intranet.birmingham.ac.uk/it/teams/infrastructure/fm/bear/bluebear/index.aspx

[Accessed 24 11 2013].

127. Visakh, P. M., Thomas, S., Chandra, A. K. & Mathew, A. P. eds., 2013. Advances in Elastomers II: Composites and Nanocomposites. Berlin: Springer.

128. Wan-Doo, Kim, W.-S., Woo, C.-S. & Lee, H.-J., 2004. Some Considerations on Mechanical Testing Methods of Rubbery Materials using Nonlinear Finite Element Analysis. Polymer International, 53(7), pp. 850-856.

129. Wang Chung, C. & Lindsay Buist, M., 2012. A novel nonlinear viscoelastic solid model. Nonlinear Analysis: Real World Applications, 13(3), pp. 1480-1488.

130. Wang, M. & Guth, E., 1952. Statistical theory of networks of non-Gaussian flexible chains. The Journal of Chemical Physics, 20(7), p. 1144–1157.

131. Wilkinson, J., 1965. The Algebraic Eigenvalue Problem. Oxford: Oxford University Press.

132. Xiaozhi, Z., Yan, C. & Lili, X., 2002. A New Explicit Solution of Dynamic Response Analysis. Earthquake Engineering and Engineering Vibration, 1(3), pp. 1-8.

133. Xua, M.-R., Xub, S. & Guo, H. Y., 2010. Determination of natural frequencies of fluid-conveying pipes using homotopy perturbation method. Computers and Mathematics with Applications, Volume 60, pp. 520-527.

134. Xueliang, C., Xing, J. & Xianxin, T., 2006. Study on Explicit Integration Formula for Dynamic Acceleration Response. Earthquake Engineering and Engineering Vibration, 5(2), pp. 60-67.

135. Yang, X., 2011. Finite element analysis and experimental investigation of tyre characteristics for developing strain-based intelligent tyre system , PhD Theses, s.l.: University Of Birmingham.

136. Yang, X., 2011. Finite element analysis and experimental investigation of tyre characteristics for developing strain-based intelligent tyre system, Birmingham, UK: University of Birmingham.

137. Yang, X. & Olatunbosun, O., 2012. Optimization of Reinforcement Turn-up Effect on Tyre Durability and Operating Characteristics for Racing Tyre Design. Materials & Design, Volume 35, pp. 798-809.

138. Yang, X., Olatunbosun, O. & and Bolarinwa, E., 2010. Materials Testing for Finite Element Tire Model. SAE Int. J. Mater. Manuf, 3(1), pp. 211-220.

139. Yang, X., Olatunbosun, O. & Bolarinwa, E., 2009. Generation of Tyre Cross-sectional Geometry for FE Tyre Model Using Image Processing Techniques. International Journal of Engineering Simulation., 10(1), pp. 3-10, ISSN 1468-1137.

140. Yehya, B. S., 1976. Tri-Axial Tyre Dynamics, Ph.D. Thesis, s.l.: The University of Birmingham.

141. Yeoh, O. H., 1990. Characterization of Elastic Properties of Carbon-Black-Filled Rubber Vulcanizates. Rubber Chemistry and Technology, 63(5), pp. 792-805.

142. Yeoh, O. H. & Fleming, P. D., 1998. A new attempt to reconcile the statistical and phenomenological theories of rubber elasticity. Journal of Polymer Science Part B: Polymer Physics, 35(12), pp. 1919-1931.

143. Zheng, X., Mao, J. & Hao, Z.-y., 2015. Coupled analysis of engine noise and interior noise of an automobile. Journal of Central South University, 22(2), pp. 753-760.

Appendix A: Scripts for FSI Analysis

A.1. Python script for generating the INP deck file

```
clc
clear
close all
freq = 1:800;
fluid = textread('Co-execution-fluid.inp','%s','delimiter','\n','whitespace','');
for i=1:1:length(freq)
   filename = ['Coexecution_FSI_Fluid_' num2str(i) '.inp'];
   fluid{30964,:} = [num2str((1/17)/freq(i)) ',' num2str(1/freq(i)) ',0.025, 2. , 1'];
   fid = fopen(filename, 'wt');
   fprintf(fid, '%s\n', fluid{:});
   fclose(fid);

end
solid = textread('Co-execution-solid.inp','%s','delimiter','\n','whitespace','');
for i=1:1:length(freq)
   filename = ['Coexecution_FSI_Solid_' num2str(i) '.inp'];
   solid{241388,:} = [num2str((1/17)/freq(i)) ',' num2str(1/freq(i)) ', 1e-12'];
   solid{238784,:} = ['1,' num2str(freq(i)*6.28) ', 0., 0.'];
   fid = fopen(filename, 'wt');
   fprintf(fid, '%s\n', solid{:});
   fclose(fid);

end
cosimjobs={
   'import os'};
   'os.system(''abaqus cosimulation -cosimj Coexecution_FSI_1 -j
Coexecution_FSI_Fluid_1,Coexecution_FSI_Solid_1 inter'')';

v=2;   % The row that submission are started
for h=1:1:length(freq)
   cosimjobs{h+v-1,1}=['os.system(''abaqus cosimulation -cosimj Coexecution_FSI_' num2str(h)
'.inp'   ' -j '   'Coexecution_FSI_Fluid_' num2str(h) '.inp',',' 'Coexecution_FSI_Solid_' num2str(h)
'.inp' ' inter'')'];
end
fid = fopen('MNruncosims.py', 'wt');
fprintf(fid, '%s\n', cosimjobs{:});
fclose(fid);
```

A.2. Python script for Post-Processing

```
from odbAccess import *
from abaqusConstants import *
for i in range(1,800,1):
   odb = openOdb('Coexecution_FSI_Solid_' + str(i) + '.odb')
   myAssembly = odb.rootAssembly
   step1=odb.steps['Step-1']
   region=step1.historyRegions['Node SOLID-1.2892'] # Identify node of interest
   UYData=region.historyOutputs['U2'].data #Only displacement along direction 2
```

```
   dispFile=open('Nset_A_UY' + str(i) + '.csv','w') #create comma separated value file, which can
be read directly into MS Excel
   dispFile.write('Time (sec), Nset_A_UY (m) \n')
   for time, u2Disp in UYData: #Write two columns, time and U2
      dispFile.write('%10.4E, %10.4E\n' % (t , u2 Disp)) #
   disp File. close()
   #-------------------------------------------
   region=step1.historyRegions['Node SOLID-1.2892'] # Identify node of interest
   UXData=region.historyOutputs['U1'].data #Only displacement along direction 1
   dispFile=open('Nset_A_UX' + str(i) + '.csv','w') #create comma separated value file, which can
be read directly into MS Excel
   dispFile.write('Time (sec), Nset_A_UX (m) \n')
   for time, u1Disp in UXData: #Write two columns, time and U1
      dispFile.write('%10.4E, %10.4E\n' % (t , u1Disp))
   disp File. close()
   #-------------------------------------------
   region=step1.historyRegions['Node SOLID-1.2892'] # Identify node of interest
   UZData=region.historyOutputs['U3'].data #Only displacement along direction 3
   dispFile=open('Nset_A_UZ' + str(i) + '.csv','w') #create comma separated value file, which can
be read directly into MS Excel
   dispFile.write('Time (sec), Nset_A_UZ (m) \n')
   for time, u3Disp in UZData: #Write two columns, time and U3
      dispFile.write('%10.4E, %10.4E\n' % (t , u3Disp))
   disp File.c lose()
   #-------------------------------------------
  # Calculate displacement magnitude
   summ = 0
   component Labels = ('U1', 'U2', 'U3')
   for name in component Labels:
      summ = summ + power( region . history Outputs[name], 2.0)
      summ = sqrt (summ)
   # printmagnitude
   #
   dispFile=open('Nset_A_U' + str(i) + '.csv','w')
   dispFile.write('Time (sec), Nset_A_U(m) \n')
   for dataPair in sum.data:
      dispFile.write('%10.4E, %10.4E\n'%(dataPair[0], dataPair[1]))
   dispFile.close()
   odb = openOdb('Coexecution_FSI_Solid_' + str(i) + '.odb') #Write the path to your ODB file
between the ''
   myAssembly = odb.rootAssembly
   step1=odb.steps['Step-1']
   region=step1.historyRegions['Node RIG_PLATE.5308'] # Identify node of interest
   UOOXData=region.historyOutputs['U1'].data #Only displacement along direction 1
   dispFile=open('Nset_OO_UX' + str(i) + '.csv','w') #create comma separated value file, which
can be read directly into MS Excel
   dispFile.write('Time (sec), Nset_OO_UX (m) \n')
   for time, u1Disp in UOOXData: #Write two columns, time and U1
      dispFile.write('%10.4E, %10.4E\n' % (t , u1Disp))
   disp File. close()
   #-------------------------------------------
```

```
   region=step1.historyRegions['Node RIG_PLATE.5308'] # Identify node of interest
   UOOYData=region.historyOutputs['U2'].data #Only displacement along direction 2
   dispFile=open('Nset_OO_UY' + str(i) + '.csv','w') #create comma separated value file, which
can be read directly into MS Excel
   dispFile.write('Time (sec), Nset_OO_UY (m) \n')
   for time, u2Disp in UOOYData: #Write two columns, time and U1
      dispFile.write('%10.4E, %10.4E\n' % (t, u2Disp))
   disp File. close()
   #-----------------------------------------------
   region=step1.historyRegions['Node RIG_PLATE.5308'] # Identify node of interest
   UOOZData=region.historyOutputs['U3'].data #Only displacement along direction 3
   dispFile=open('Nset_OO_UZ' + str(i) + '.csv','w') #create comma separated value file, which
can be read directly into MS Excel
   dispFile.write('Time (sec), Nset_OO_UZ (m) \n')
   for time, u3Disp in UOOZData: #Write two columns, time and U1
      dispFile.write('%10.4E, %10.4E\n' % (t, u3Disp))
   disp File. close()
   #-----------------------------------------------
  # Calculate displacement magnitude
   sum = 0
   componentLabels = ('U1', 'U2', 'U3')
   for name in componentLabels:
      sum = sum + power(region.historyOutputs[name], 2.0)
      sum = sqrt(sum)
   #
   # print magnitude
   #
   dispFile=open('Nset_OO_U' + str(i) + '.csv','w')
   dispFile.write('Time (sec), Nset_OO_U(m) \n')
   for dataPair in sum.data:
      dispFile.write('%10.4E, %10.4E\n'%(dataPair[0], dataPair[1]))
   disp File. close()

   odb = openOdb('Coexecution_FSI_Solid_' + str(i) + '.odb') #Write the path to your ODB file
between the ''
   myAssembly = odb.rootAssembly
   step1=odb.steps['Step-1']
   region=step1.historyRegions['Node SOLID-1.6467'] # Identify node of interest
   VCXData=region.historyOutputs['V1'].data #Only displacement along direction 1
   dispFile=open('Nset_C_VX' + str(i) + '.csv','w') #create comma separated value file, which can
be read directly into MS Excel
   dispFile.write('Time (sec), Nset_C_VX (m) \n')
   for time, v1Disp in VCXData: #Write two columns, time and U1
      dispFile.write('%10.4E, %10.4E\n' % (t, v1Disp))
   disp File.close()
   #-----------------------------------------------
   region=step1.historyRegions['Node SOLID-1.6467'] # Identify node of interest
   VCYData=region.historyOutputs['V2'].data #Only displacement along direction 2
   dispFile=open('Nset_C_VY' + str(i) + '.csv','w') #create comma separated value file, which can
be read directly into MS Excel
   dispFile.write('Time (sec), Nset_C_VY (m) \n')
```

```
   for time, v2Disp in VCYData: #Write two columns, time and U1
      dispFile.write('%10.4E, %10.4E\n' % (t, v2Disp))
   disp File. close()
   #-----------------------------------------------
   region=step1.historyRegions['Node SOLID-1.6467'] # Identify node of interest
   VCZData=region.historyOutputs['V3'].data #Only displacement along direction 3
   dispFile=open('Nset_C_VZ' + str(i) + '.csv','w') #create comma separated value file, which can
be read directly into MS Excel
   dispFile.write('Time (sec), Nset_C_VZ (m) \n')
   for time, v3Disp in VCZData: #Write two columns, time and U1
      dispFile.write('%10.4E, %10.4E\n' % (t, v3Disp))
   disp File. close()
   #-----------------------------------------------
  # Calculate displacement magnitude
   summ = 0
   component Labels = ('V1', 'V2', 'V3')
   for name in component Labels:
      summ = summ + power (region. History Outputs[name], 2.0)
      summ = sqrt (summ)
   #
   # printmagnitude
   #
   dispFile=open('Nset_C_V' + str(i) + '.csv','w')
   dispFile.write('Time (sec), Nset_C_V(m) \n')
   for dataPair in sum.data:
      dispFile.write('%10.4E, %10.4E\n'%(dataPair[0], dataPair[1]))
   dispFile.close()
odb.close
```

A.3. Matlab Script to View/Export results

```
clc
clear all
close all
j=0;
figure(1)
for i=1:1:799
   j=j+1;
   clear U0 UA
   filename_UA = ['D:\writing\CH6\fem\Nset_B_U' num2str(i) '.csv'];
   filename_U0 = ['D:\writing\CH6\fem\Nset_OO_U' num2str(i) '.csv'];
   UA = csvread(filename_UA,1);
   U0 = csvread(filename_U0,1);
   FR(j) = i; % Frequency
   TR(j) = max(abs(UA(:,2)))./max(abs(U0(:,2))); % Transmissibility
end
plot(FR,TR)
figure(2)
n=0;
```

```
for i=1:1:799
   n=n+1;
   clear F0 VA
   filename_VA = ['D:\writing\CH6\fem\Nset_B_V' num2str(i) '.csv'];
   filename_F0 = ['D:\writing\CH6\fem\Nset_OO_F' num2str(i) '.csv'];
   VA = csvread(filename_VA,1);
   F0 = csvread(filename_F0,1);
   FR(j) = i; % Frequency
   MO(j) = max(abs(VA(:,2)))./max(abs(F0(:,2))); % Mobility
end
plot(FR,MO)
```

Appendix B: List of Publications

- S. Arabi, O.R. Olatunbosun, M. Behroozi, “Development of virtual testing of EGR Coolant Rail”, SAE Int. J. Passeng. Cars - Mech. Syst. 6(2):927-936, 2013, doi: 10.4271/2013-01-1373.
- S. Arabi, O.R. Olatunbosun, M. Behroozi, “Equivalent lumped properties of rubber with viscoelastic behaviour in the vibration analysis of EGR coolant rail ”, 2013 JSAE Annual Congress, Japan
- S. Arabi, O.R. Olatunbosun, “Investigation of Vibration Characteristics of EGR Coolant Rail”, Research Poster Conference 2012, University of Birmingham, UK.